ORTA DOĞU TEKNİK ÜNİVERSİTESİ
FEN BİLİMLERİ ENSTİTÜSÜ MÜDÜRLÜĞÜ

TEZ ŞABLONU ONAY FORMU
THESIS TEMPLATE CONFIRMATION FORM

1. Şablonda verilen yerleşim ve boşluklar değiştirilmemelidir.
2. **Jüri tarihi** Başlık Sayfası, İmza Sayfası, Abstract ve Öz'de ilgili yerlere yazılmalıdır.
3. İmza sayfasında jüri üyelerinin unvanları doğru olarak yazılmalıdır. Tüm imzalar **mavi pilot kalemle** atılmalıdır.
4. **Disiplinlerarası** programlarda görevlendirilen öğretim üyeleri için jüri üyeleri kısmında tam zamanlı olarak çalıştıkları anabilim dalı başkanlığının ismi yazılmalıdır. Örneğin: bir öğretim üyesi Biyoteknoloji programında görev yapıyor ve biyoloji bölümünde tam zamanlı çalışıyorsa, İmza sayfasına biyoloji bölümü yazılmalıdır. İstisnai olarak, disiplinler arası program başkanı ve tez danışmanı için disiplinlerarası program adı yazılmalıdır.
5. Tezin **son sayfasının sayfa** numarası Abstract ve Öz'de ilgili yerlere yazılmalıdır.
6. Bütün chapterlar, referanslar, ekler ve CV sağ sayfada başlamalıdır. Bunun için **kesmeler** kullanılmıştır. **Kesmelerin kayması** fazladan boş sayfaların oluşmasına sebep olabilir. Bu gibi durumlarda paragraf (¶) işaretine tıklayarak kesmeleri görünür hale getirin ve yerlerini **kontrol edin**.
7. Figürler ve tablolar kenar boşluklarına taşmamalıdır.
8. Şablonda yorum olarak eklenen uyarılar dikkatle okunmalı ve uygulanmalıdır.
9. Tez yazdırılmadan önce PDF olarak kaydedilmelidir. Şablonda yorum olarak eklenen uyarılar PDF dokümanında yer almamalıdır.
10. Tez taslaklarının kontrol işlemleri tamamlandığında, bu durum öğrencilere METU uzantılı öğrenci e-posta adresleri aracılığıyla duyurulacaktır.
11. Tez yazım süreci ile ilgili herhangi bir sıkıntı yaşarsanız, Sıkça Sorulan Sorular (SSS) sayfamızı ziyaret ederek yaşadığınız sıkıntıyla ilgili bir çözüm bulabilirsiniz.

1. Do not change the spacing and placement in the template.
2. Write **defense date** to the related places given on Title page, Approval page, Abstract and Öz.
3. Write the titles of the examining committee members correctly on Approval Page. **Blue ink** must be used for all signatures.
4. For faculty members working in **interdisciplinary programs**, the name of the department that they work full-time should be written on the Approval page. For example, if a faculty member staffs in the biotechnology program and works full-time in the biology department, the department of biology should be written on the approval page. Exceptionally, for the interdisciplinary program chair and your thesis supervisor, the interdisciplinary program name should be written.
5. Write **the page number of the last page** in the related places given on Abstract and Öz pages.
6. All chapters, references, appendices and CV must be started on the right page. **Section Breaks** were used for this. **Change in the placement** of section breaks can result in extra blank pages. In such cases, make the section breaks visible by clicking paragraph (¶) mark and **check their position.**
7. All figures and tables must be given inside the page. Nothing must appear in the margins.
8. All the warnings given on the comments section through the thesis template must be read and applied.
9. Save your thesis as pdf and Disable all the comments before taking the printout.
10. This will be announced to the students via their METU students e-mail addresses when the control of the thesis drafts has been completed.
11. If you have any problems with the thesis writing process, you may visit our Frequently Asked Questions (FAQ) page and find a solution to your problem.

☒ **Yukarıda bulunan tüm maddeleri okudum, anladım ve kabul ediyorum. / I have read, understand and accept all of the items above.**

Name : Vahit Eren
Surname : Taburoğlu
E-Mail : e120155@metu.edu.tr
Date : 30.05.2024
Signature : _____

CHARACTERIZATION AND ENHANCEMENT OF ANTIBACTERIAL DIAMOND LIKE CARBON (DLC) NANO FILMS AGAINST *MYCOBACTERIUM CHIMAERA*

A THESIS SUBMITTED TO
THE GRADUATE SCHOOL OF NATURAL AND APPLIED SCIENCES
OF
MIDDLE EAST TECHNICAL UNIVERSITY

BY

VAHİT EREN TABUROĞLU

IN PARTIAL FULFILLMENT OF THE REQUIREMENTS
FOR
THE DEGREE OF DOCTOR OF PHILOSOPHY
IN
MICRO AND NANOTECHNOLOGY

MAY 2024

Approval of the thesis:

CHARACTERIZATION AND ENHANCEMENT OF ANTIBACTERIAL DIAMOND LIKE CARBON (DLC) NANO FILMS AGAINST *MYCOBACTERIUM CHIMAERA*

submitted by **VAHİT EREN TABUROĞLU** in partial fulfillment of the requirements for the degree of **Doctor of Philosophy** i**n Micro and Nanotechnology, Middle East Technical University** by,

Prof. Dr. Naci Emre Altun
Dean, **Graduate School of Natural and Applied Sciences** _____

Prof. Dr. Deniz Üner
Head of the Department, **Micro and Nanotechnology** _____

Prof. Dr. Alpan Bek
Supervisor, **Micro and Nanotechnology** _____

Examining Committee Members:

Assoc. Prof. Dr. Hatice Duran
Materials Science & Nanotechnology Eng., TOBB ETU _____

Prof. Dr. Alpan Bek
Physics, METU _____

Assoc. Prof. Dr. Hande Toffoli
Physics, METU _____

Prof. Dr. Çağdaş Devrim Son
Biology, METU _____

Prof. Dr. Mehmet Emre Taşgın
Institute of Nuclear Sciences, Hacettepe Uni. _____

Date: 30.05.2024

I hereby declare that all information in this document has been obtained and presented in accordance with academic rules and ethical conduct. I also declare that, as required by these rules and conduct, I have fully cited and referenced all material and results that are not original to this work.

Name Last name: Vahit Eren Taburoğlu

Signature:

ABSTRACT

CHARACTERIZATION AND ENHANCEMENT OF ANTIBACTERIAL DIAMOND LIKE CARBON (DLC) NANO FILMS AGAINST *MYCOBACTERIUM CHIMAERA*

Vahit Eren Taburoğlu
Doctor of Philosophy, Micro and Nanotechnology
Supervisor: Prof. Dr. Alpan Bek

May 2024, 137 pages

DLC (Diamond-Like Carbon) thin films which are synthesized by RF-PECVD on medical grade steel substrates will be evaluated in terms of its antibacterial properties against to *Mycobacterium chimaera*. In the world of health, cardiac surgery infection caused by the Mycobacterium chimaera is becoming an increasingly important emerging problem. Heater Cooler Units (HCU's) which is an essential tool used for cardiac surgeries and also other issued equipment are contaminated by *Mycobacterium chimaera*. This is one of the critical problems that should be solved with appropriate technics/methods. Diamond Like Carbon (DLC) nano films are good candidates as an antibacterial coating on the critical surfaces. Due to its unique tribological, physical and mechanical surface properties, DLC films can combine three important antibacterial leading characteristics in its body; these are namely anti-adhesive, contact active and biocide release characteristics. One of the aims of this study is to search, characterize and enhance the antibacterial properties of DLC on medical tools and together with optimum surface properties.

Keywords: *Mycobacterium chimaera*, Diamond-Like Carbon, Thin Film, Nano 2-D Structures, Antibacterial

ÖZ

DLC (ELMAS BENZERİ KARBON) FİLMLERİN "*MYCOBACTERIUM CHIMAERA*" BAKTERİSİNE KARŞI ANTİ BAKTERİYEL ÖZELLİKLERİNİN İNCELENMESİ VE GELİŞTİRİLMESİ

Vahit Eren Taburoğlu
Doktora, Mikro ve Nanoteknoloji
Tez Yöneticisi: Prof. Dr. Alpan Bek

Mayıs 2024, 137 sayfa

Bu çalışmanın amacı RF-PECVD tekniği kullanılarak medikal çelik alttaşlar üzerine kaplanan DLC (Elmas Benzeri Karbon) nano filmlerin "*Mycobacterium chimaera*" bakterisine karşı anti bakteriyel özelliklerinin araştırılmasıdır. Yakın geçmişte ortaya çıkan ve günümüzde giderek daha sık rastlanılan "*Mycobacterium chimaera*" bakterisi kaynaklı problemler özellikle kalp/akciğer operasyonlarında önemli bir sorun olmaya başlamıştır. Bu operasyonlarda yardımcı bir araç olarak kullanılan ısıtma soğutma birimi (HCU) yüzeyleri ve bağlı ekipman bu bakterinin etrafa yayılması için uygun birer kuluçka yeri olmaktadır. Bu çalışmada radyo frekans ile oluşturulan plazma destekli CVD tekniği ile medikal çelik yüzeyler üzerine kaplanan DLC ince filmlerin yapışma engelleyici, temas aktif ve biyosit anti bakteriyel özellikleri "*Mycobacterium chimaera*" bakterisine karşı kullanılmış olup, sonuçlar karakterize edilerek ve diğer yüzey özellikleri ile birlikte optimum anti bakteriyel özellikler elde edilmeye çalışılmıştır.

Anahtar Kelimeler: Mykobakteri Kimera, Elmas Benzeri Kaplama, İnce Film, Nano 2-D Yapılar, Anti bakteriyel

To my big family, my wife and my dearie daughter

ACKNOWLEDGMENTS

The author wishes to express his deepest gratitude to his supervisor Prof. Dr. Alpan Bek his guidance, advice, criticism, encouragements and insight throughout the research.

The author would also like to thank Assoc. Prof. Dr. Hatice Durmuş for his critical direction on the tests, suggestions and comments.

The author would also like to thank Assoc. Prof. Dr. Çağdaş Devrim Son for his complete support especially for florescent microscope and also suggestions and comments.

The author would also like to thank Assoc. Prof. Dr. Hande Toffoli for his suggestions, inspiration she gave and comments.

The author would also like to thank for Prof. Dr. Mehmet Emre Taşgın his suggestions and comments.

The author would also like to thank Dr. Sema Doğan Yiğit for her valuable contribution for bacterial tests, and for also all support to complete such a demanding interdisciplinary thesis.

TABLE OF CONTENTS

ABSTRACT v

ÖZ vi

ACKNOWLEDGMENTS viii

TABLE OF CONTENTS ix

LIST OF TABLES xiii

LIST OF FIGURES xiv

LIST OF ABBREVIATIONS xxii

CHAPTERS 1

1. INTRODUCTION 1

2. LITERATURE REVIEW 5

2.1 Bonding Structure in Diamond-Like Character 5

2.2 A General View on Properties of Diamond-like Carbon Film 9

2.3 Growth Mechanisms and Structural Observations on Hydrogenated Amorphous Diamond-Like Carbon Films 12

2.4 Residual Stress in DLC 16

2.5 Tribo-Mechanical View 19

2.5.1 Wear Mechanisms 19

2.5.2 Hardness and Friction 21

2.6 Coating Technique: (PE)CVD 24

2.6.1 General Information on Different Application Methods of CVD 25

2.6.2 Comparison of CVD with Other Applied Techniques 27

2.7 Antimicrobial Coatings 29
2.7.1 Mechanisms 29
2.7.2 Antimicrobial Studies in Literature with DLC 30
2.8 The Problem on HCU Surfaces 32
3. EXPERIMENTAL STUDIES 35
3.1 Revealing the Surface Material 35
3.2 The Base Material (304 Steel) 38
3.3 Cutting the Substrates 39
3.4 Polishing the Substrates 39
3.5 Coating the First Substrates (PVD + PECVD) 43
3.6 Coating the Rest with Different DLC Thicknesses 45
3.7 Adding AgPd to DLC 48
3.8 Measuring Contact Angle 49
3.9 Nano-Indentation (Hardness) Tests 52
3.10 Friction Tests 53
3.11 Deciding on and Designing the Bacterial Experiments 56
3.11.1 The First Trials: Direct Application on the Agar Medium 57
3.11.2 Another Trial with the Kirby-Bauer Test Method 58
3.11.3 Test in Liquid Medium with Bacteria 59
3.11.4 Test on the Bacteria which are Directly Planted on the Samples 60
3.12 Procuring the *Mycobacterium chimera* 63
3.13 Preparation of Bacteria, Agar and Fluidic Feeding Mediums 63
3.13.1 Middlebrook 7H9 Broth Base 63
3.13.2 Middlebrook 7H10 Agar Base 64
3.13.3 Activating *Mycobacterium chimaera* Strain 65

3.13.4 Preparation of *Mycobacterium chimaera* for the Tests 66
3.13.5 Preparation of Samples for the Tests 67
3.13.6 Incubation of Bacteria on the Samples 67
3.14 Applying Different Test Methods on *Mycobacterium chimaera* and Analyzing the Results 68
3.14.1 Pressing Samples Directly to Agar 68
3.14.2 Bacteria from Fluid on the Samples to Fluidic Feeding Medium 69
3.14.3 Bacteria Taken Directly from the Samples to Agar 70
3.14.4 Bacteria Obtained by Sonication from the Samples to Agar 71
3.15 *Mycobacterium chimaera* under Field Emission Scanning Electron Microscope (FESEM or SEM) 73
3.15.1 The Fixation and Coating Procedure for the FESEM Measurements 73
3.15.2 The SEM Measurements 74
3.16 The Florescence Microscope Measurements of *Mycobacterium chimaera* 81
3.16.1 Florescent microscope results for the uncoated steel (Control) sample: 83
3.16.2 Florescent microscope results for the 100 nm DLC coated sample: . 85
3.16.3 Florescent microscope results for the 200 nm DLC coated sample: . 87
3.17 The FTIR & ATR Measurements of *Mycobacterium chimaera* 90
3.17.1 The ATR Measurements for the Band of 1500-1750 cm^{-1} wavenumber 93
4. CONCLUSION & DISCUSSIONS 95
REFERENCES 97
APPENDICES 105

A. Roughness Measurements 105
B. Friction Measurements 113
C. Florescent Microscope Measurement 115
D. FESEM Measurements 121
CURRICULUM VITAE 137

LIST OF TABLES

TABLES

Table 2.1. XPS results for DLC coated samples [58] 9
Table 2.2. Comparison of properties of diamond, ta-C, a-C:H and graphite [11] .. 10
Table 2.3. Characteristics of DLC coatings and aluminum [13], [4], [14], [15] 11
Table 2.4. Dominant wear mechanisms for various contact modes [22] 20
Table 2.5. Contact mechanisms for practical applications [22] 21
Table 2.6. Hardness (H), Young's modulus (E), and H/E ratio of the different families of DLC films (a = amorphous; ta = tetrahedral amorphous) [14] 24
Table 2.7. The properties of films (at 25°C) coated by CVD [4] 28
Table 3.1. Handheld XRF Measurement Results 37
Table 3.2. TiO_2 and 150 nm DLC Coated Polished/Not polished Samples 46
Table 3.3. Samples Coated for Different DLC Thicknesses 47
Table 3.4. Samples which are coated 3 nm AgPd 49
Table 3.5. Samples which are exposed to Contact Angle measurement 50
Table 3.6. Contact Angle Measurements 51
Table 3.7. Nano Indentation Test Results 52
Table 3.8. Friction (Slip) SP-2100 Slip/Peel Test Results 56
Table 3.9. Inhibition rates for S. aureus on the sample surfaces 61
Table 3.10. number of the red & green stained bacteria for the samples 89

LIST OF FIGURES

FIGURES

Figure 1.1. Family of Human Pathogenic Mycobacteria [37].....2
Figure 1.2. M. chimaera was the name selected since a chimera in Anatolian/Greek mythology is a mixture of 3 different animals and M. chimaera is a genetic mix between different MAC strains. 2
Figure 1.3. Distribution of Nontuberculous Mycobacteria Strains throughout the Turkey [38].....3
Figure 2.1. Three hybridization configurations of carbon atom with possible σ and π bond structures [5] 5
Figure 2.2. Schematic variation of fractional diamond-like character of (a) a-C and (b) a-C:H with deposition ion energy [6].....7
Figure 2.3. A sample XPS monitoring DLC on Si substrate [10] 8
Figure 2.4. Ternary phase diagram for various DLC films with respect to their sp^2, sp^3 and hydrogen contents [11]. 9
Figure 2.5. Molecular Dynamic (MD) Simulation model: Final configurations of deposited films derived from 1000 incident C_2H_2 molecules at different incident energies. Yellow balls represent one-fold carbon atoms, red balls are two-fold (sp^1) atoms, white balls are three-fold (sp^2) atoms, cyan ones are four-fold (sp^3) atoms, and blue ones are hydrogen atoms. [16] 14
Figure 2.6. Atomic structures and depth profiles obtained at 30 eV C_2H_2 incidence. [16].....15
Figure 2.7. Incident energy vs relative density, hydrogen content, sp^3 fraction [16] 16
Figure 2.8. Idealized intrinsic stress versus impact energy per atom [20].....18
Figure 2.9. Relationship between stress and change of surface geometry [12] 19
Figure 2.10. Classification of coatings with respect to hardness and coefficient of friction, highlighting the special case of carbon-based coatings [14] 22
Figure 2.11. Schematic diagram of the three main fundamental contributions to friction (or tangential) force F_t with a normal force F_n [14] 23

Figure 2.12. Schematics of Anti-microbial Strategy 29
Figure 2.13. Different Defense Mechanisms on Bacteria. 30
Figure 2.14. Typical Heating-Cooler Unit of a Heart-Lung Bypass Device 32
Figure 2.15. Typical Heater Cooler Unit (HCU) 33
Figure 2.16. A Surgical Room with the Heating-Cooler Unit of a Heart-Lung Bypass Device [44] 33
Figure 3.1. Inside (top) view of the HCU 36
Figure 3.2. Top surface of the HCU 36
Figure 3.3. The handheld XRF Device Showing the Measurement Result 37
Figure 3.4. 304 Steel Plate 38
Figure 3.5. 304 Steel Substrates Cut by a Water Jet Device 39
Figure 3.6. The Polishing Device Respective Sandpapers in Terms of Particle Thicknesses 40
Figure 3.7. Carbide Dremel Tip 40
Figure 3.8. Polishing Setup 41
Figure 3.9. Sample#13: 8 nm rough 42
Figure 3.10. Sample#13: 216 nm rough 42
Figure 3.11. Sample#16: 566 nm rough 43
Figure 3.12. TiO_2 PVD Coated Samples 44
Figure 3.13. Sample #2 PVD Coating of TiO_2 44
Figure 3.14. TiO_2 (25 nm) + DLC (150 nm) Coated 304 Steel Samples 45
Figure 3.15. Samples Successfully Coated with 15 nm TiO_2 and Different Thicknesses (50/100/200 nm) of DLC 48
Figure 3.16. Contact angle Measurements 51
Figure 3.17. SP-2100 Slip/Peel Tester Used for Friction Coefficient Measurement Test 53
Figure 3.18. Samples prepared for Friction (Slip) SP-2100 Slip/Peel Tester 54
Figure 3.19. Samples tested on the Friction (Slip) SP-2100 Slip/Peel Tester 55
Figure 3.20. Bacteria studied; S. aureus: Staphylococcus aureus (ATCC 25923), E. coli: Escherichia coli (ATCC25922) 57

Figure 3.21. Bacteria studied under the Kirby-Bauer Test; S. aureus : Staphylococcus aureus (ATCC 25923), E. coli : Escherichia coli (ATCC25922).. 58
Figure 3.22. Test of the Samples in Bacteria Enriched Liquid Medium; E. coli : Escherichia coli (ATCC25922) 59
Figure 3.23. Addition of bacteria to samples 60
Figure 3.24. Densities of growing bacteria (from left to right: 50 nm-100 nm-200 nm-the thick sample) 62
Figure 3.25. The materials used for preparation of 7H10 Agar feeding medium ... 64
Figure 3.26. Activating the Mycobacterium intracellular subsp. *Chimaera* strain . 65
Figure 3.27. Developed fluidic and agar feeding mediums after 8 days 65
Figure 3.28. The other developed fluidic and agar feeding mediums after 8 days . 66
Figure 3.29. The samples in bacteria are incubated for the 1st method 67
Figure 3.30. The samples on which 0.5 McFarland density bacteria added in six welled plates 68
Figure 3.31. Result of the first test/method in which samples are directly pressed on the agar medium 69
Figure 3.32. The density difference results obtained by UV-Spectrophotometer... 70
Figure 3.33. Agar plates on which bacteria are seeded taken directly from the samples 70
Figure 3.34. The inhibition rate of mycobacteria chimaera for different thicknesses 71
Figure 3.35. Removal process of bacteria form the surface by sonication 72
Figure 3.36. The agar mediums to which the bacteria which could attach to surface are seeded 72
Figure 3.37. Counting the bacterial colonies (cfu/ml) which were formerly attach to surface are seeded and adhesion rates 73
Figure 3.38. *Mycobacterium chimaera* on the substrate which is uncoated and very rough. 75
Figure 3.39. SEM image of 5 *Mycobacterium chimaera* (1 alive, 2 start to die, and 3 dead) on the 100 nm DLC coated sample 76

Figure 3.40. *Mycobacterium chimaera* newly copied themselves on substrate which is coated with 200 nm DLC thin film. 77
Figure 3.41. *Mycobacterium chimaera* copied themselves on substrate which is coated with 200 nm DLC thin film. One of them in three chain group is dead and denatured after the division. 78
Figure 3.42. *Mycobacterium chimaera* on substrate which is coated with 100 nm DLC thin film. 79
Figure 3.43. *Mycobacterium chimaera* on substrate which is coated with 100 nm DLC thin film. 80
Figure 3.44. *Mycobacterium chimaera* on substrate which is coated with 200 nm DLC thin film. 81
Figure 3.45. Florescent image of mixed (colored as Red & Green) double staining on SH-SY5Y human cells under fluorescent microscope [59] 82
Figure 3.46. Florescent image of mixed (colored as Red & Green) *Mycobacterium chimaera* on lamella which is taken from the uncoated Control sample 84
Figure 3.47. Florescent image of mixed (colored as Red & Green) *Mycobacterium chimaera* on substrate which is the uncoated control sample 85
Figure 3.48. Florescent image of live & dead (mixed) *Mycobacterium chimaera* on lamella which is taken from the 100 nm DLC coated sample 86
Figure 3.49. Florescent image of live & dead (mixed) *Mycobacterium chimaera* on substrate which is the 100 nm DLC coated sample 87
Figure 3.50. Florescent image of live & dead (mixed) *Mycobacterium chimaera* on lamella which is taken from the 200 nm DLC coated sample 88
Figure 3.51. Florescent image of live & dead (mixed) *Mycobacterium chimaera* which is taken from the 200 nm DLC coated sample 89
Figure 3.52. The comparative graph for live/dead percentages for each sample 90
Figure 3.53. FTIR (in reflection mode) measurements before and after the film developed on the samples 91

Figure 3.54. Characteristic IR spectra of a biofilm the spectral regions representative for lipids, proteins, nucleic acids, and carbohydrates are shown [56]. 92
Figure 3.55. The 1500-1750 cm^{-1} wavenumber ATR absorbance results of the samples 93
Figure A.1. Roughness Measurement by a Zygo Roughness Measuring Device for Sample #1 105
Figure A.2. Roughness Measurement by a Zygo Roughness Measuring Device for Sample #2 105
Figure A.3. Roughness Measurement by a Zygo Roughness Measuring Device for Sample #3 106
Figure A.4. Roughness Measurement by a Zygo Roughness Measuring Device for Sample #4 106
Figure A.5. Roughness Measurement by a Zygo Roughness Measuring Device for Sample #5 107
Figure A.6. Roughness Measurement by a Zygo Roughness Measuring Device for Sample #6 107
Figure A.7. Roughness Measurement by a Zygo Roughness Measuring Device for Sample #7 108
Figure A.8. Roughness Measurement by a Zygo Roughness Measuring Device for Sample #8 108
Figure A.9. Roughness Measurement by a Zygo Roughness Measuring Device for Sample #9 109
Figure A.10. Roughness Measurement by a Zygo Roughness Measuring Device for Sample #10 109
Figure A.11. Roughness Measurement by a Zygo Roughness Measuring Device for Sample #11 110
Figure A.12. Roughness Measurement by a Zygo Roughness Measuring Device for Sample #12 110

Figure A.13. Roughness Measurement by a Zygo Roughness Measuring Device for Sample #13 111
Figure A.14. Roughness Measurement by a Zygo Roughness Measuring Device for Sample #14 111
Figure A.15. Roughness Measurement by a Zygo Roughness Measuring Device for Sample #15 112
Figure A.16. Roughness Measurement by a Zygo Roughness Measuring Device for Sample #16 112
Figure B.17. Friction (Slip) SP-2100 Slip/Peel Test Results for the Sample #30. 113
Figure B.18. Friction (Slip) SP-2100 Slip/Peel Test Results for the Sample #5... 113
Figure B.19. Friction (Slip) SP-2100 Slip/Peel Test Results for the Sample #7... 114
Figure B.20. Friction (Slip) SP-2100 Slip/Peel Test Results for the Sample #23. 114
Figure C.21. Florescent image of live *Mycobacterium chimaera* on lamella which is taken from the uncoated control sample 115
Figure C.22. Florescent image of dead *Mycobacterium chimaera* on lamella which is taken from the uncoated control sample 115
Figure C.23. Florescent image of live *Mycobacterium chimaera* on substrate which is the uncoated control sample 116
Figure C.24. Florescent image of dead *Mycobacterium chimaera* on substrate which is the uncoated control sample 116
Figure C.25. Florescent image of live *Mycobacterium chimaera* on lamella which is taken from the 100 nm DLC coated sample 117
Figure C.26. Florescent image of dead *Mycobacterium chimaera* on lamella which is taken from the 100 nm DLC coated sample 117
Figure C.27. Florescent image of live *Mycobacterium chimaera* on substrate which is the 100 nm DLC coated sample 118
Figure C.28. Florescent image of dead *Mycobacterium chimaera* on substrate which is the 100 nm DLC coated sample 118
Figure C.29. Florescent image of live *Mycobacterium chimaera* on lamella which is taken from the 200 nm DLC coated sample 119

Figure C.30. Florescent image of dead *Mycobacterium chimaera* on lamella which is taken from the 200 nm DLC coated sample 119
Figure C.31. Florescent image of live *Mycobacterium chimaera* which is taken from the 200 nm DLC coated sample 120
Figure C.32. Florescent image of dead *Mycobacterium chimaera* which is taken from the 200 nm DLC coated sample 120
Figure D.33. FESEM image of *Mycobacterium chimaera* which is taken from the Control sample 121
Figure D.34. FESEM image of *Mycobacterium chimaera* which is taken from the 100 nm DLC coated sample 122
Figure D.35. FESEM image of *Mycobacterium chimaera* which is taken from the 100 nm DLC coated sample 123
Figure D.36. FESEM image of *Mycobacterium chimaera* which is taken from the 100 nm DLC coated sample 124
Figure D.37. FESEM image of *Mycobacterium chimaera* which is taken from the 100 nm DLC coated sample 125
Figure D.38. FESEM image of *Mycobacterium chimaera* which is taken from the 100 nm DLC coated sample 126
Figure D.39. FESEM image of *Mycobacterium chimaera* which is taken from the 200 nm DLC coated sample 127
Figure D.40. FESEM image of *Mycobacterium chimaera* which is taken from the 200 nm DLC coated sample 128
Figure D.41. FESEM image of *Mycobacterium chimaera* which is taken from the 200 nm DLC coated sample 129
Figure D.42. FESEM image of *Mycobacterium chimaera* which is taken from the 200 nm DLC coated sample 130
Figure D.43. FESEM image of *Mycobacterium chimaera* which is taken from the 200 nm DLC coated sample 131
Figure D.44. FESEM image of *Mycobacterium chimaera* which is taken from the 200 nm DLC coated sample 132

Figure D.45. FESEM image of *Mycobacterium chimaera* which is taken from the 200 nm DLC coated sample 133
Figure D.46. FESEM image of *Mycobacterium chimaera* which is taken from the 200 nm DLC coated sample 134
Figure D.47. FESEM image of *Mycobacterium chimaera* which is taken from the 200 nm DLC coated sample 135

LIST OF ABBREVIATIONS

ABBREVIATIONS

BHI: Brain Heart Infusion

DLC: Diamond-Like Carbon

EPS: Extracellular Polymeric Substance

HCU: Heating Cooling Unit

MAC: Mycobacterium Avium Complex

NTM: Non-Tuberculous Bacterium

OADC: Oleic Albumin Dextrose Catalase

FESEM: Field Emission Scanning Electron Microscope

PBS: Phosphate Buffered Saline

PECVD: Plasma Enhanced Chemical Vapor Deposition

PEPVD: Plasma Enhanced Physical Vapor Deposition

QWOT: Quarter Wave Optical Thickness

UV: Ultra Violet

CHAPTERS

CHAPTER 1

INTRODUCTION

Infections in cardiac surgery caused by the bacteria Mycobacterium chimaera are becoming increasingly important in the field of health. Heater Cooler Units (HCU's), which are crucial tools used in cardiac surgeries and other medical equipment, are being contaminated by *Mycobacterium chimaera*. This is a significant issue that must be addressed with proper techniques and methods.

Mycobacterium chimaera was identified as a separate species in 2004. It is a member of the *Mycobacterium Avium Complex* (MAC) and belongs to the family of NTM (Non-Tuberculous Bacterium). NTMs are environmental organisms commonly found in soil and water sources. They have been linked to many cases of device-related and post-surgical infections and outbreaks, and they are resistant to disinfection. NTM biofilms can survive in various temperatures, pH levels, and low-nutrient conditions, making them difficult to eradicate. Bacteria within a biofilm are protected by an extracellular polymeric substance (EPS) that acts as a barrier against disinfectants. *Mycobacterium chimaera* 's ability to form biofilms may contribute to its resistance to disinfectants.

There are reports the ability of *Mycobacterium chimaera* to attach and accumulate on a panel of commonly used medical device materials including stainless steel, titanium, silicone and polystyrene surfaces [9]. Founding in hospital and household water sources they are very dangerous for especially open and deep surgical wounds. *Mycobacterium chimaera* infections are slow-growing. Because of this it can take

from several months to six years for an infection to develop. Signs of a possible *Mycobacterium chimaera* infection may include persistent fevers, increasing or unusual shortness of breath, fatigue, unexplained weight loss, nausea, persistent cough or cough with blood, redness, heat, pus at the surgical site, night sweats, joint pain, muscle pain, vomiting, and abdominal pain.

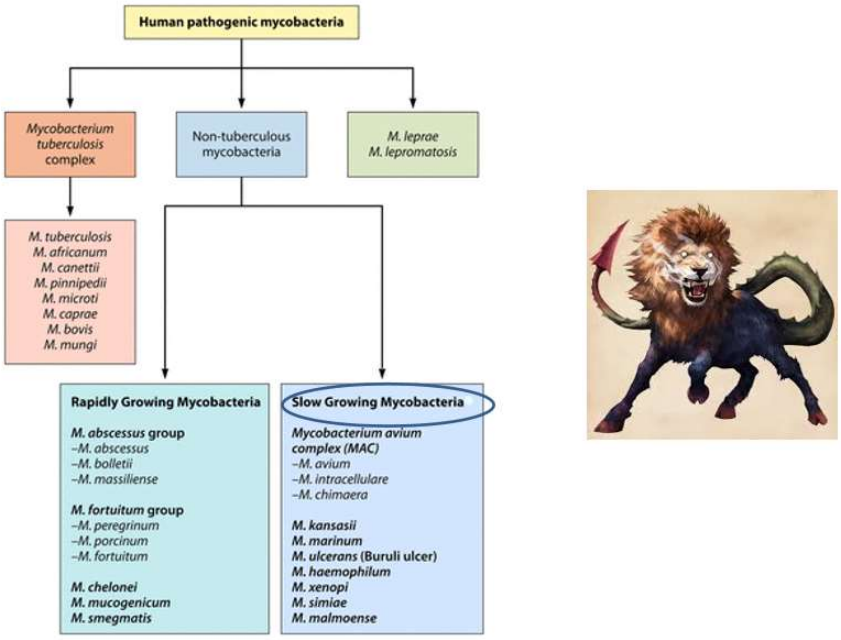

Figure 1.1. Family of Human Pathogenic Mycobacteria [37]

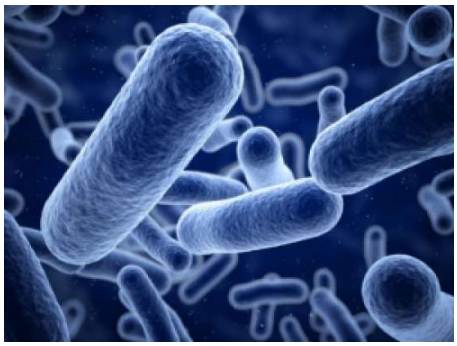

Figure 1.2. M. chimaera was the name selected since a chimera in Anatolian/Greek mythology is a mixture of 3 different animals and M. chimaera is a genetic mix between different MAC strains.

Although it is a new branch among the nontuberculous strains it has been started to be isolated in different cities of Turkey (Figure 1.3.).

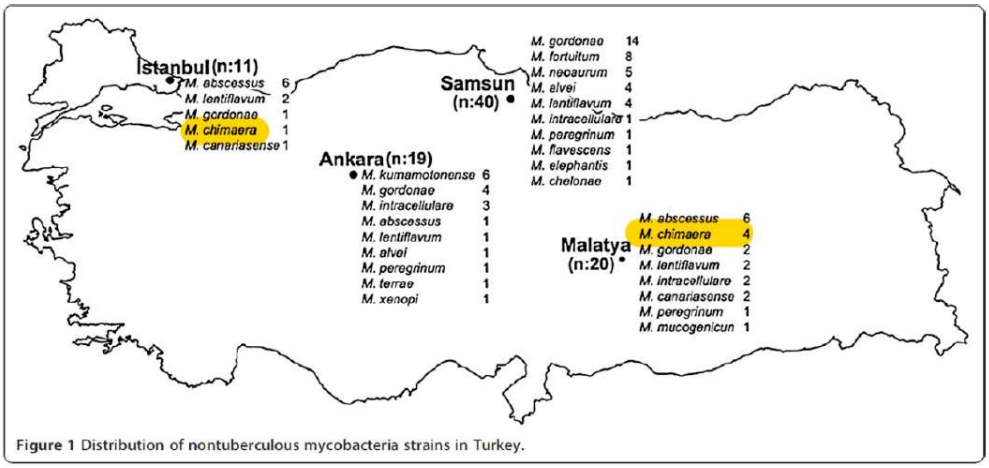

Figure 1.3. Distribution of Nontuberculous Mycobacteria Strains throughout the Turkey [38]

There are already clinical cases, as well as academic research conducted globally and domestically on this hot topic. Furthermore, there has been an increasing academic interest in Turkey with the rise of cases, though limited in number. For example, in July of 2019 Serap Şimşek published an article named as "Açık Kalp Cerrahisi Uygulanmış Hastalarda Kontamine Isıtıcı-Soğutucu Cihazlarla İlişkili *Mycobacterium chimaera* İnfeksiyonları: Küresel Bir Salgın" [39] in Istanbul University. Moreover, in January of 2017 Haluk Eraksoy released another article on the bacterium "*Mycobacterium chimaera* ya da Likya'nın Sönmeyen Ateşi", 2017 January [40].

Furthermore, other types of bacteria also can incubate on the surfaces of any HCU. Even the HCU is clean before the first use; different microbial growth (Fusarium solani, Sphingomonas paucimobilis, Pseudomonas aeruginosa, *Mycobacterium* chelonae, and gordonae) can be identified over time and could not be permanently eliminated. Four of these microorganisms were also found in tap water. [41]

Although there are many different techniques to solve bacterial problems, only a few of them are sustainable and applicable without causing harm or disruption to the environment. Coating the surface with appropriate antibacterial layers is one of the most promising techniques. In many cases, Diamond-Like Carbon (DLC) nanofilms are good candidates for antibacterial coating on critical surfaces.

CHAPTER 2

LITERATURE REVIEW

2.1 Bonding Structure in Diamond-Like Character

Diamond is a carbon allotrope, meaning it is a formation of carbon atoms bonded in a specific order with covalent bonds. Carbon is a unique and versatile element due to the various configurations it can form with itself and other elements. A neutral carbon atom has six electrons surrounding its nucleus. The electron orbitals in the ground state of a carbon atom are arranged in the $1s^2 2s^2 2p^2$ configuration [4]. During the bonding process with other atoms, the four valence electrons are transformed into one of three basic hybridization configurations: sp^1, sp^2, and sp^3 (Figure 2.1.).

In a sp^1 configuration, two of the valence electrons enter σ orbitals and form σ bonds directed along the x-axis, while the other two form weaker π bonds. In a sp^2 configuration, carbon forms graphite, which is a stable carbon allotrope with sp^2 trigonal bonding. In a sp^3 configuration, diamond is formed, an allotrope with sp^3 tetragonal bonding (4 σ bonds with 109.5-degree angles). The extreme physical properties of diamond are a result of its strong, directional σ bonds [5].

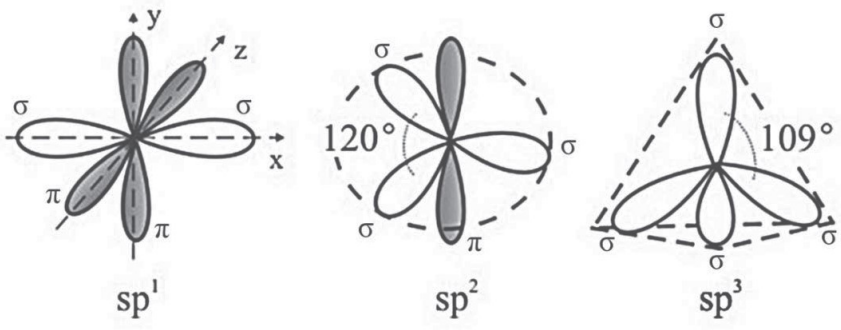

Figure 2.1. Three hybridization configurations of carbon atom with possible σ and π bond structures [5]

Although diamond-like carbon (DLC) gets its unique properties from the presence of C-C sp^3 bonds in the film, for a film to be classified as DLC, it must also contain other types of bonds and atoms. Otherwise, it would simply be considered diamond, as diamond is almost entirely made up of C-C sp^3 bonds. According to literature, a film with less than 70% sp^3 fraction may be classified as amorphous DLC [5].

DLC films exhibit a meta-stable mixed phase that can consist of various types of bonds, including C-C sp^3, C-C sp^2, and C-H bonds. The mechanical properties such as Young's modulus and hardness are primarily influenced by C-C sp^3 bonds, while C-C sp^2 bonds have minimal impact. Additionally, C-H bonds do not contribute to the bonding network but can actually enhance the elasticity of the film by promoting relaxation throughout the material. This allows for the creation of conformal DLC coatings on complex geometries [6].

In summary, the presence of C-C sp^3 bonds gives DLC its diamond-like properties, while the inclusion of C-C sp^2 and C-H bonds adds elasticity and flexibility to the film, making it suitable for various applications.

Hydrogen atoms typically form covalent bonds with carbon (C-H) when participating in film formation. These bonds are incredibly strong, even stronger than C-C bonds, making them difficult to remove from the carbon surface. This bond gives the film an inert character, protecting it from various chemicals, including acids and bases, and contributing to its durability. However, some hydrogen atoms can be trapped within the film and may be lost when heated. These free hydrogen atoms can act as a reservoir and replace any lost or removed hydrogen atoms, particularly from the surface [7].

The energy of ions plays a crucial role in bond formation. In both hydrogen-free and hydrogenated DLC films, the optimal ion energy is around 100 eV. Beyond this point in hydrogenated DLC films, the sp^2 fraction increases, making the film more graphitic. Conversely, in hydrogen-free DLCs, as the energy decreases below 100 eV (Figure 2.2.), the film becomes more graphitic with a higher sp^2 fraction. In

hydrogenated DLC films, as the ion energy drops below 100 eV, the C(sp^3)-H bond fraction increases, leading to a more polymeric film [6].

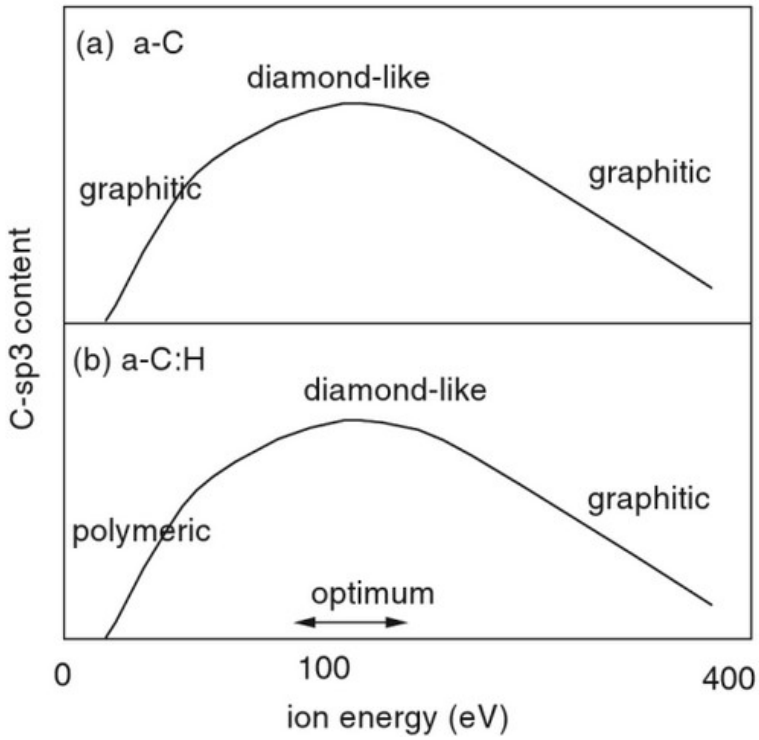

Figure 2.2. Schematic variation of fractional diamond-like character of (a) a-C and (b) a-C:H with deposition ion energy [6]

The binding energies of sp^2, sp^3, and other types of bonds can be distinguished using techniques like X-ray photoelectron spectroscopy (XPS) (Figure 2.3.). The characteristic carbon C peak 1s appears in the range of 283 eV to 290 eV and can be broken down into several components based on the carbon structure and other possible elements. The fitted peaks within the C 1s peak may correspond to C-C bonds. C-C bonds can be identified by three peaks: one from sp^2 hybridized atoms appearing at 284.25 ± 0.30 eV known as C 1s-2, another from sp^3 hybridized atoms appearing at 285.33 ± 0.38 eV known as C 1s-3, and lastly a peak from sp^1 appearing at 283 eV. Peaks representing carbon-oxygen bonding can appear at higher binding energies than the C-C peaks, each indicating a different bonding state. In the

identified peaks, C 1s-4 for (C-O) appears around 285.5 eV, C 1s-5 for (C=O) appears around 287.7 eV, and C 1s-6 for the carboxylic (O=C-O) group appears around 290 eV. These peaks are referred to as satellite peaks in DLC samples as they are not used in sample analysis [8]. The C 1s-3 peak can also correspond to C-H bonding, reported to appear at the same position as sp^3-connected carbon atoms (C-C). Using only XPS makes it difficult to differentiate between C-C and C-H bonds [9].

We have also conducted XPS measurements on the DLC films that we had previously developed (Table 2.1.). We used the same technique, precursor gases, parameters, and PECVD machine as in our previous studies [58]. The results presented in Table 2.1. align with the literature and the values depicted in Figure 2.3.

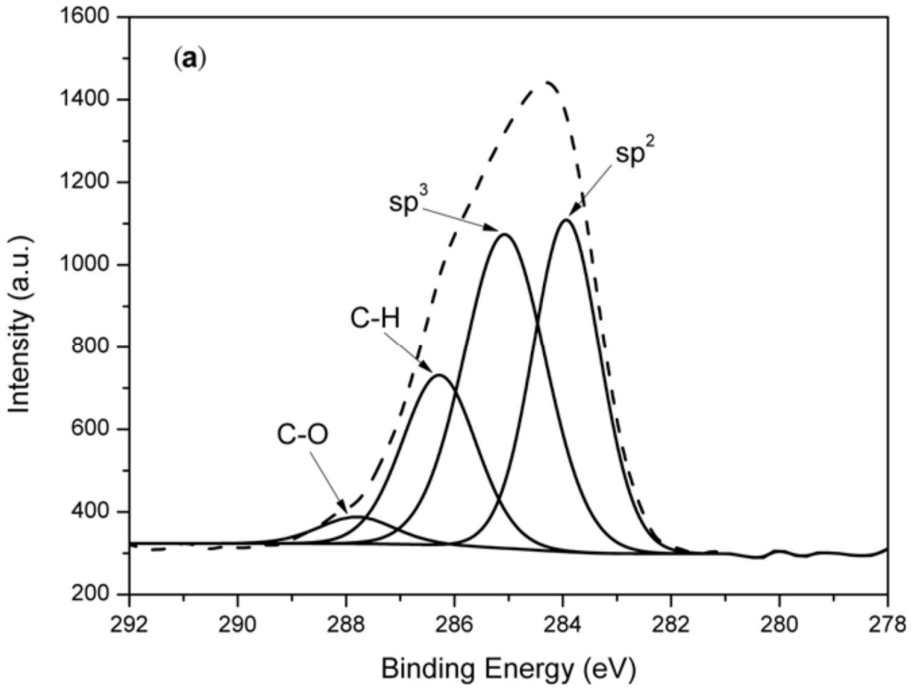

Figure 2.3. A sample XPS monitoring DLC on Si substrate [10]

Table 2.1. XPS results for DLC coated samples [58]

Sample No	sp^3 ~@285.20 eV (%)	sp^2 ~@284.55 eV (%)	C-O ~@287 eV (%)	sp^3/sp^2
5	55.09	37.59	7.33	1.47
7	49.11	36.39	14.50	1.35
15	54.78	37.55	7.67	1.46
18	63.15	26.66	10.18	2.37

2.2 A General View on Properties of Diamond-like Carbon Film

Typically, DLC thin films are composed of sp^3 and sp^2 bonds. The third defining factor is hydrogen content. In Figure 2.4., the ternary diagram shows that film composition depends on the structure. Therefore, as the sp^3 concentration increases, the film characteristics exhibit more diamond-like properties, known as tetrahedral amorphous (ta) carbon. On the other hand, sp^2 is graphitic and mechanically soft.

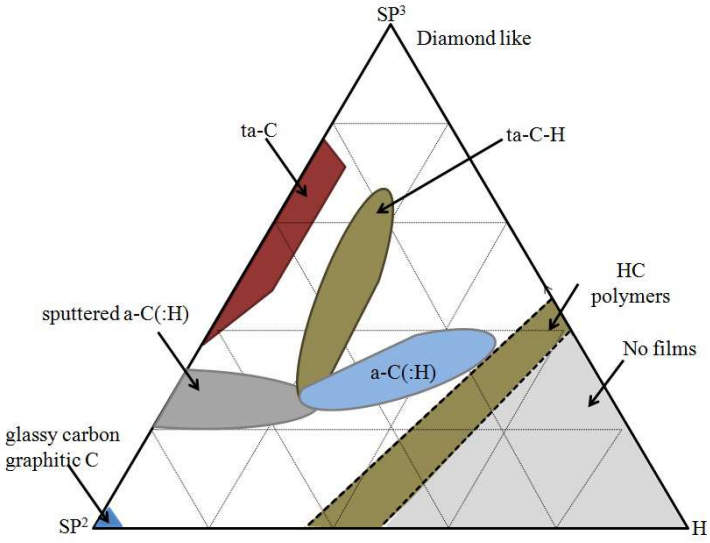

Figure 2.4. Ternary phase diagram for various DLC films with respect to their sp^2, sp^3 and hydrogen contents [11].

Diamond is the hardest material ever known in nature. DLC film, as the name suggests, has similar characteristics to diamond. It has superior hardness values and a very low coefficient of friction, making its wear resistance comparatively better than other known hard thin films. Table 2.2. compares some properties of diamond, ta-C (tetrahedral amorphous carbon), DLC, a-C:H (hydrogenated amorphous carbon) DLC, and graphite.

A high sp^3 to sp^2 ratio not only increases hardness but also intrinsic stresses. The hydrogen percentage is less than 1% for a-C films, and if the hydrogen concentration exceeds 1%, the film is then called a-C: H. Additionally, hydrogen in plasma etches sp^2 bonds, favoring the formation of sp^3. It has been shown that as the DC bias voltage in a PECVD chamber increases, the H-to-C ratio increases with an increasing sp^3 to sp^2 ratio [12]. Generally speaking, in hydrogenated DLC films, the H content is more than 30%, and commercially available DLC films predominantly consist of sp^3 bonds compared to sp^2.

Table 2.2. Comparison of properties of diamond, ta-C, a-C:H and graphite [11]

	Diamond	DLC (ta-C)	DLC(a-C:H)	Graphite
Crystal system	Diamond cubic	Amorphous	Amorphous	Hexagonal
Mass density (g/cm^3)	3.51	2.5-3.3	1.5-2.4	2.26
sp^3 Content (%)	100	50-90	20-60	0
Hydrogen content (%)	0	0-10	10-50	0
Hardness (GPa)	100	50-80	10-45	<5
Friction coefficients in humid air	0.1	0.05-0.25	0.02-0.3	0.1-0.2
Friction coefficients in dry air	0.1	0.6	0.02-0.2	>0.6
Band gap (eV)	5.5	1-2.5	1-4	-0.04

Table 2.3. Characteristics of DLC coatings and aluminum [13], [4], [14], [15]

Chemical properties	DLC
Composition	Carbon, hydrogen
Structure	Mixture of sp^3 (tetrahedral diamond type) and sp^2 (trigonal graphitic) and amorphous
Reactivity	Generally inert to acids, alkalis, solvents, salts, water, and other reagents at ambient temperature
Physical properties	
Density	1.8-2.1 g/cm^3
Thermal conductivity	10 W/cm x K
Coefficient of expansion	9 x 10^{-6}/C
Electrical resistance	Several MΩ x cm
Adhesion	34.473 MPa std. pull strength
Permeability	Barrier to hydrogen and other gases

The precursor gases can include some well-known hydrocarbons, specifically CH_4 (methane), C_2H_2 (acetylene), C_2H_6 (ethane), C_2H_4 (ethylene), and C_6H_{12} (cyclohexane). In addition to hydrocarbon precursor gases, it is not uncommon to use molecular hydrogen (H_2) in the literature.

DLC films can be deposited using a variety of methods, such as filtered cathodic vacuum arc (FCVA), ion beam assisted deposition, DC- and RF-plasma-assisted chemical vapor deposition, and sputtering. Among these methods, plasma-enhanced (RF-assisted [13,56mHz]) vapor deposition (PECVD) is a highly reliable and repeatable one. Although most CVD techniques require high temperatures, DLC can be deposited using PECVD at relatively low temperatures, around 100-150°C. In addition to creating a plasma from which the film is constructed, the RF source used in this technique also generates activated species in the plasma, including ions, excited species, and electrons, making the process more energetic.

It is also possible to increase the durability of the film by using argon as a plasma etching agent. Ar+ preferential etching of weaker bonds reduces the concentration of sp^2 bonds, increases stable sp^3 bonds, and enhances the film's "diamond-like" properties.

2.3 Growth Mechanisms and Structural Observations on Hydrogenated Amorphous Diamond-Like Carbon Films

Due to the amorphous structure of hydrogenated diamond-like films, there is a variety of structural diversity and the growth mechanism responsible for this diversity is primarily influenced by the energies of incoming ions or molecules, the abundance of precursor gases, and other factors. In other words, there are no distinct growth mechanisms or structural models.

In literature, one can find studies that use molecular dynamic (MD) simulations to analyze the microstructure and growth mechanism of hydrogenated amorphous carbon films. One such study was published on 8 May 2014 [16]. The substrate in the study is diamond, and the precursor gas used is C_2H_2.

One key finding of the study is that at low energies, molecular adsorption plays a dominant role in the film growth process, causing incident molecules to maintain their original molecular structures [17]. When incident energy increases, film density initially increases and then stabilizes, while hydrogen content decreases due to molecular fragmentation [18].

Moreover, hydrogen atoms are crucial in the development of hydrogenated amorphous carbon films. There was a nearly linear relationship between the amount of hydrogen flowing and its incorporation into the film. Additionally, low energies are conducive to hydrogen adsorption, the creation of C–H bonds, and the formation of sp^3 structure. Conversely, at higher energies, the sub-plantation of carbon atoms and the formation of C–C bonds are mainly responsible for the creation of sp^3

structures. Furthermore, a rise in hydrogen content or flow rate in the source gas leads to a decrease in film density and an increase in the proportion of sp^3.

In the molecular dynamics (MD) study, researchers also investigated the impact of the incident energy of deposited agents. They observed the behavior of C_2H_2 molecules when the incident energy ranged from 5 to 150 electron volts (eV) per carbon atom. The substrate used was once again diamond. It was observed that below 20 eV, dense, thick, and homogeneous films could not be obtained due to the high hydrogen content, as shown in Figure 2.5. The reason for this is that at energies below 20 eV, there is a high hydrogen content on the surface, resulting in a high rebound ratio and low deposition yield.

Furthermore, the results also indicated that at low energy levels, there is no intermixing with the film due to the soft landing of the incident atoms. Additionally, at higher energies, such as 80 eV and above, long monoatomic carbon chains and rings made up of sp1-C atoms start to appear on the surface with very few hydrogen atoms. These films containing sp1-C atoms and low hydrogen content are very unstable and can easily be etched by oxygen in the air.

On the other hand, as the energy increases, the intermixing of the film with the substrate becomes more apparent, as shown in Figure 2.5.

This study specifically presents the atomic structures and depth profiles obtained at an incidence of 30 eV C_2H_2. Relative densities, sp^3 fractions, and hydrogen contents are calculated from the substrate surface to the very top surface of the film. The sp^3 fraction is defined as the number of sp^3 bonded carbon atoms divided by the total number of carbon atoms. Hydrogen content is defined as the ratio of the number of hydrogen atoms to the total number of atoms. As a result, three distinct regions can be observed in Figure 2.6. These regions are the transition region, intrinsic region, and surface region.

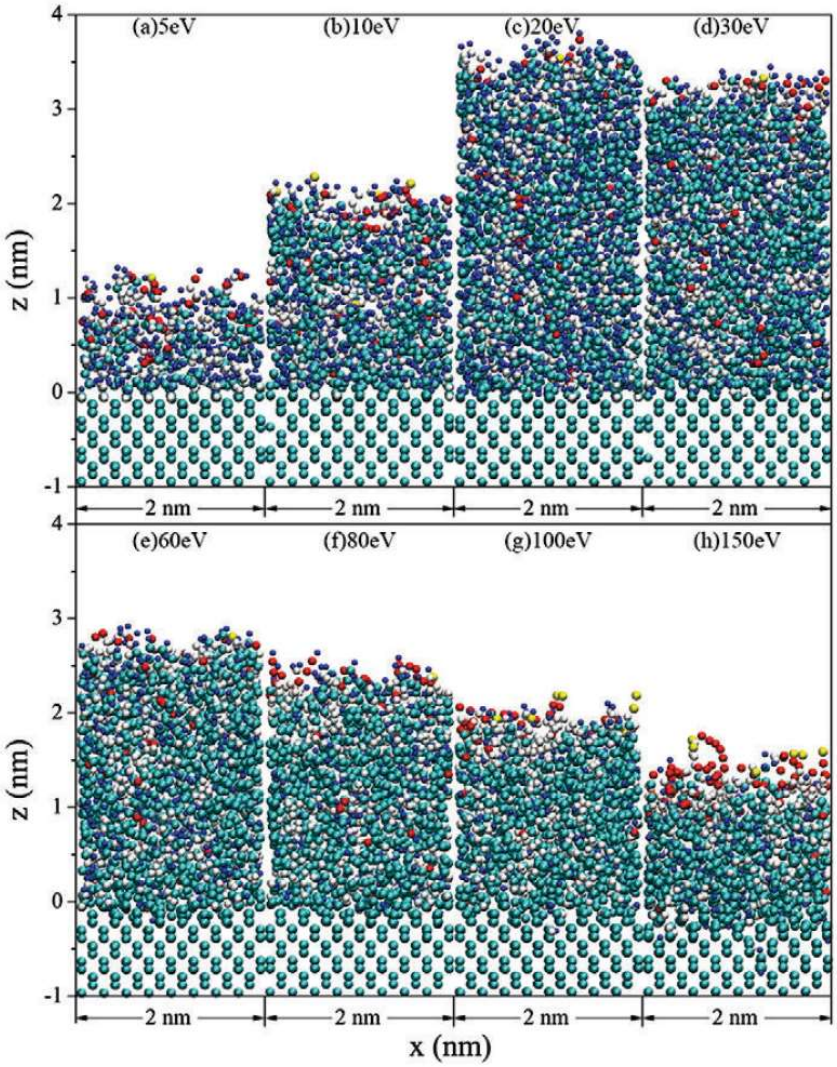

Figure 2.5. Molecular Dynamic (MD) Simulation model: Final configurations of deposited films derived from 1000 incident C_2H_2 molecules at different incident energies. Yellow balls represent one-fold carbon atoms, red balls are two-fold (sp^1) atoms, white balls are three-fold (sp^2) atoms, cyan ones are four-fold (sp^3) atoms, and blue ones are hydrogen atoms. [16]

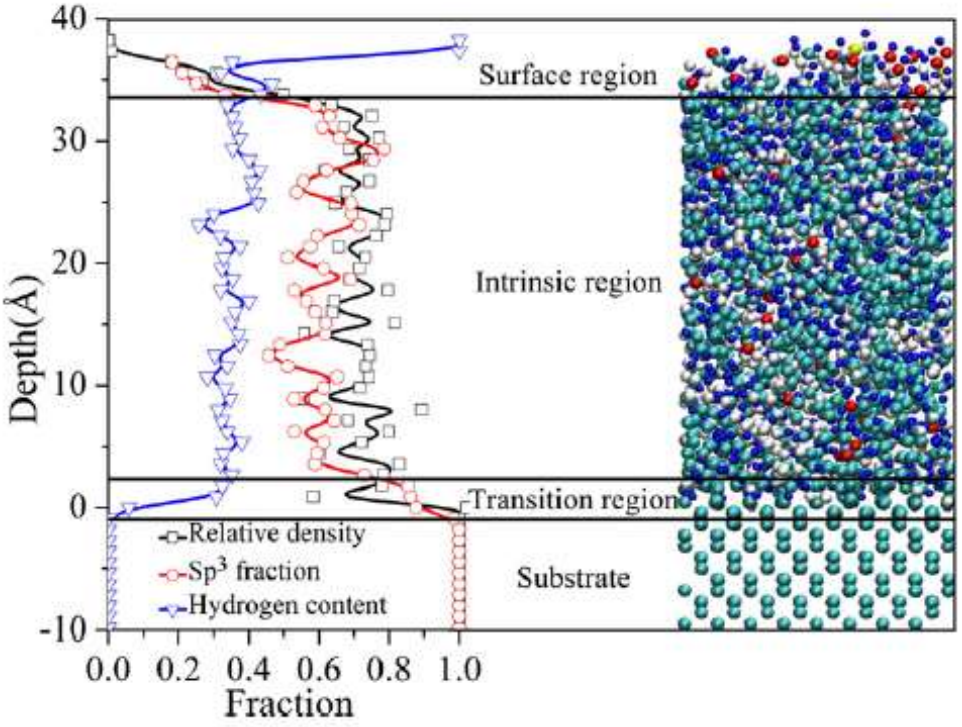

Figure 2.6. Atomic structures and depth profiles obtained at 30 eV C_2H_2 incidence. [16]

Generally, the film properties in the intrinsic region represent the properties of the entire film. Despite small fluctuations, structural parameters remain mostly constant. In other words, the sp^3 fraction is approximately 60% and the hydrogen content is around 35%. The hydrogen content in the surface region shows a quick increase, indicating that hydrogen atoms tend to cluster in the surface region [16]. The high hydrogen content near or on the surface leads to the super-low friction properties of a-C:H films through surface passivation. Additionally, the effects of incident energy are also examined, and the results are shown in Figure 2.7.

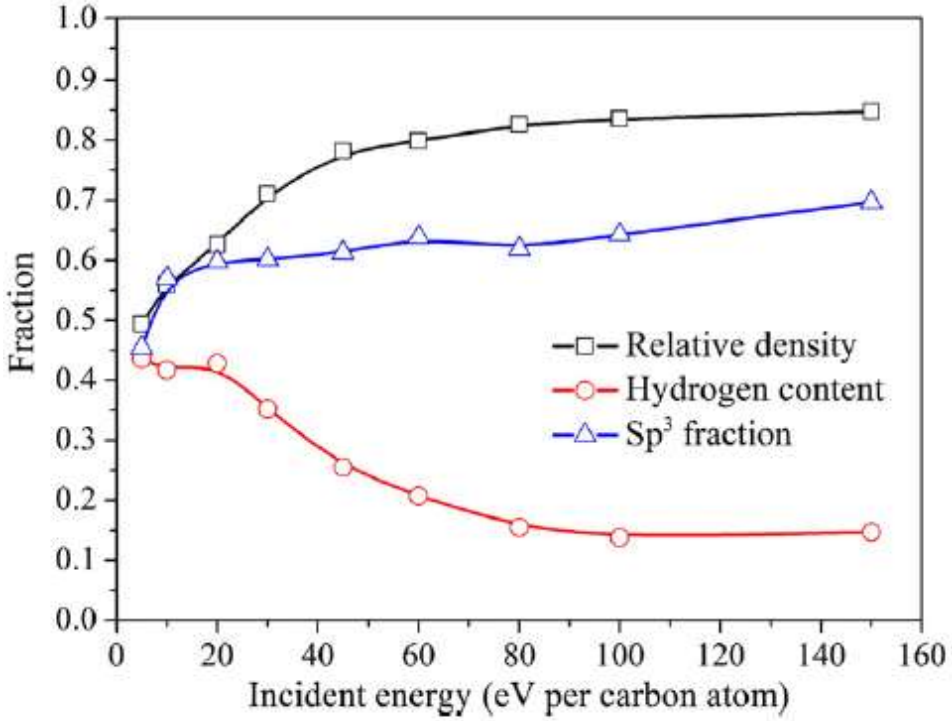

Figure 2.7. Incident energy vs relative density, hydrogen content, sp^3 fraction [16]

Regarding the sp^3 fraction, there is a gradual increase noted, from 45% at 5 eV to 70% at 150 eV, indicating a more diamond-like quality and improved mechanical properties. Additionally, the hydrogen content decreases as the energy increases, as mentioned previously, and this is referred to as dehydrogenation [16].

2.4 Residual Stress in DLC

In order to achieve good adhesion to the substrate surface, the stress developed in the film is a crucial factor. In film technology, stresses are classified as either intrinsic or extrinsic [19]. CVD allows for films to be deposited slowly and conformally onto the surface, thereby minimizing temperature differences that could create residual thermal stress during deposition. However, if there is a difference in thermal expansion coefficient between the film and the substrate, stress can develop in the film when there are changes in temperature.

As an extrinsic type, stress due to thermal expansion can be formulated as:

$$S_{TCE} = Y_f (\alpha_f - \alpha_s) (T_d - T_m) \qquad \text{(Equation 2.1)}$$

where "f" is film, "s" is substrate, Y_f is film's yield strength, $\alpha_{f\ and}$ α_s are thermal expansion coefficients of film and substrate respectively, "T_d" means temperature during deposition, "T_m" means temperature after the run and during measurement [12].

On the other hand, intrinsic stresses result from compressive or tensile forces built into the film layer. Origins of intrinsic stress can be complicated and can be due to:

- Material properties
- Deposition process
- Growth method of nano-structure
- Defects and contamination.

In general, thin films develop compressive intrinsic stress when particles with high energies are present, resulting from energetic deposition processes. According to Y. Pauleau, these energetic particles can include atoms, molecules, ions, and radicals that are either condensed on the film surface and integrated into the film, or reflected off the film surface and backscattered into the gas phase. Energetic particles typically have an average energy above 0.5 eV, while particles below this value are considered non-energetic [20]. Additionally, carbon species with high kinetic energies (ranging from 2.5 to 25 eV) tend to form sp^3 configurations, which contribute to diamond-like properties in the film. Therefore, a balance must be struck between high sp^3 content and compressive stress in the film.

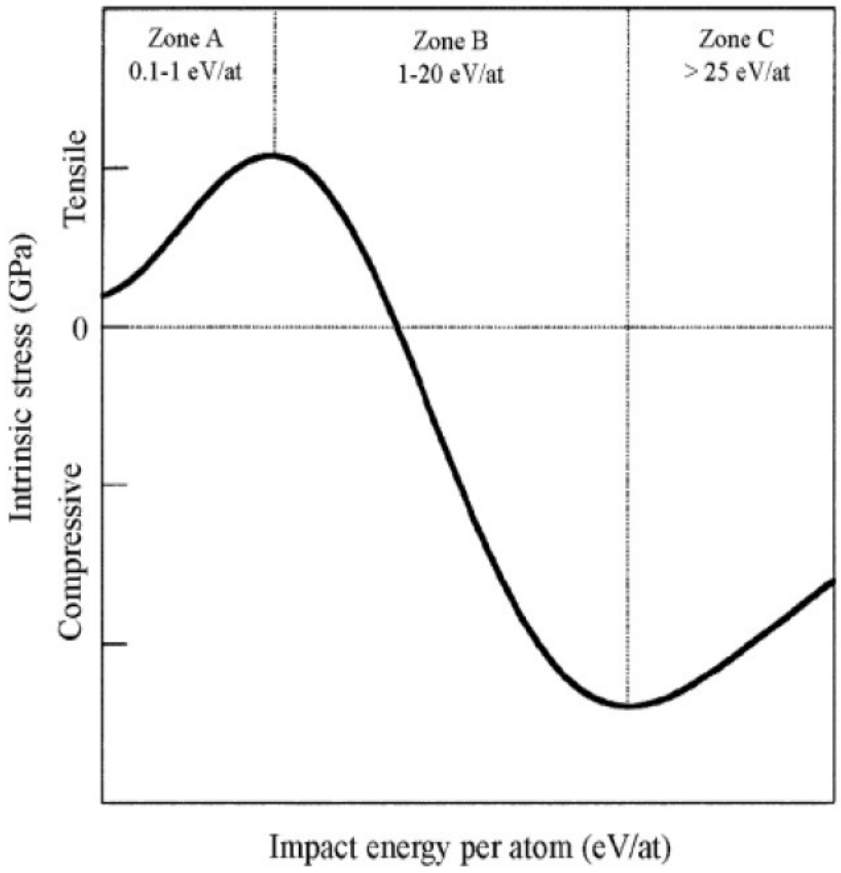

Figure 2.8. Idealized intrinsic stress versus impact energy per atom [20]

On the other hand, tensile stresses develop and increase in films because of non-energetic particles and micro voids which are generated in the film due to these non-energetic particles. Figure 2.8. shows the relation between impact energy and intrinsic stress.

Additionally, when the film is convex on the surface, the stress is compressive in the substrate and tensile in the film. Conversely, if the film contracts parallel to the surface, the stress becomes tensile in the substrate and compressive in the film, leading to the film becoming concave (Figure 2.9.).

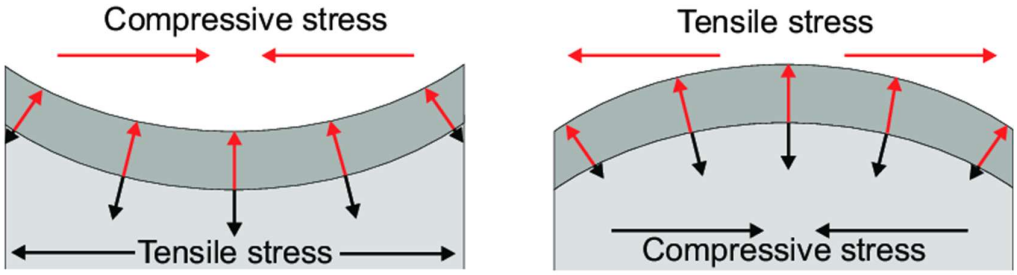

Figure 2.9. Relationship between stress and change of surface geometry [12]

Additionally, tension T (rather than stress) rises as the thickness increases: T = S x t, where "S" represents stress and "t" represents thickness. As a result, shear stress is created between the coating and the substrate. DLC thin films typically have inherent compressive stress. If this stress surpasses the adhesive force, the film will fail [12].

2.5 Tribo-Mechanical View

2.5.1 Wear Mechanisms

In most industrial applications, such as plastic injection molding, and for various components like valves and cylinders, the main cause of wear is related to the interfaces between the fluid and the body. However, the majority of identified wear mechanisms are related to the contact interfaces between solid bodies [21].

Naturally, the specific wear mechanism depends on the contact mode. Contact modes [22] for various body-to-body interactions can be due to:

- Purely sliding mode
- Purely rolling mode
- Mixed mode: a combination of rolling and sliding
- Purely impact mode

- Mixed impact and sliding mode

The most dominant wear mechanisms occurring in well-designed coating systems are:

- Abrasive wear
- Adhesive wear
- Fatigue wear
- Erosive wear
- Corrosive wear
- Impact wear

Improperly designed coating systems can experience one of the key wear mechanisms related to load carrying capacity. Excessive loading can lead to cohesive failure, resulting in delamination of the film, or adhesive failure caused by the film flaking off from the substrates or components.

In Table 2.4. various contact modes and wear mechanisms are grouped for 2-body interactions [22].

Table 2.4. Dominant wear mechanisms for various contact modes [22]

	Abrasive wear	Adhesive wear	Fatigue wear
Sliding mode	x	x	
Rolling mode	x		x
Mixed mode	x	x	x
Impact mode			x
Impact + sliding	x		x

For the majority of industrial applications, a combination of sliding and impact wear may occur. In these cases, the contact loads are as high as possible and very close to the yield point of the base materials. As a result, the near-surface regions of these

materials need to be designed and optimized in order to counteract abrasive, impact, and fatigue wear by increasing the load-carrying capacity.

Multiple contact methods are provided, which include different contact modes listed in Table 2.5.

Table 2.5. Contact mechanisms for practical applications [22]

	Sliding	Rolling	Sliding + rolling	Impact	Impact + sliding
Roller bearing		x	x		
Plunger	x			x	
Sliding bearing	x				
Piston pin	x				
Valve				x	x
Tappet	x				x
Gear			x		x
Camshaft	x				x
Ejector pin	x				

2.5.2 Hardness and Friction

Hardness and friction are key topics when discussing surfaces, particularly those of moving parts or surfaces that are exposed to harsh environmental conditions. This is crucial for durability and efficiency.

In industries where liquid lubricants are not feasible or are insufficient in reducing friction, solid lubricant coatings and super hard coatings are becoming more common [14]. There are two main categories of coatings: "soft coatings" (solid lubricants) which have low friction coefficients, and "hard coatings" which are effective for wear resistance and long-term durability. Soft coatings typically include soft metals, polymers, and lamellar solids like graphite, while hard coatings consist of hard ceramics, nitrides, carbides, borides, and oxides. In research, a hardness threshold of

10 GPa is used to determine whether a coating is considered hard or soft. Additionally, a friction coefficient of 0.3 is the dividing line between solid lubricants and anti-wear coatings [14]. Figure 2.10. illustrates this distinction clearly.

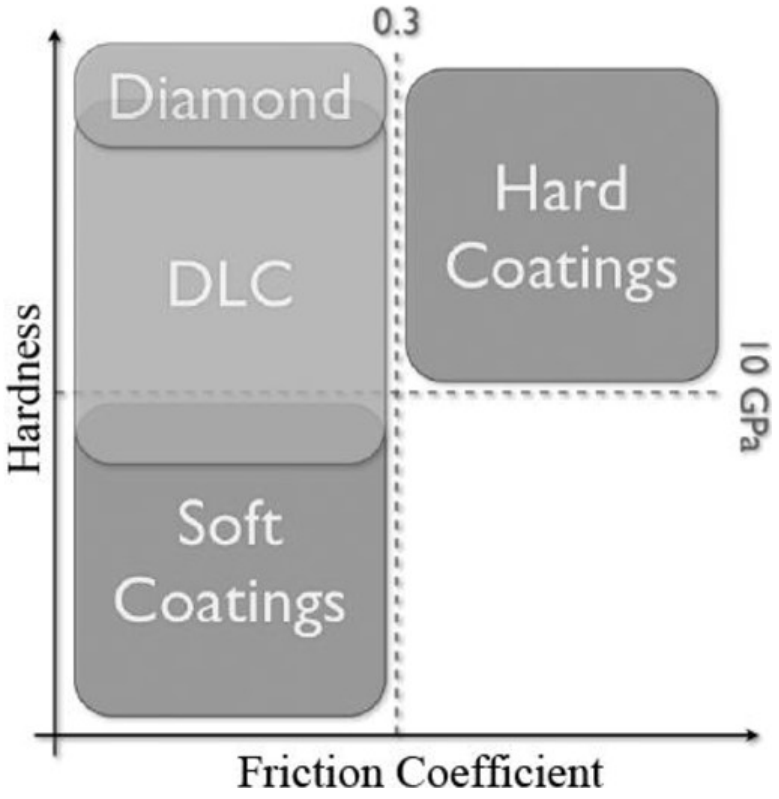

Figure 2.10. Classification of coatings with respect to hardness and coefficient of friction, highlighting the special case of carbon-based coatings [14]

Although it is challenging to achieve high wear resistance and low friction values simultaneously, there is an exceptional solution: DLC coating. DLC coatings can provide both low coefficient of friction and low wear rates at the same time. Compared to other CVD films, DLC has the highest hardness values, which is crucial for improving wear resistance. The friction force between solid bodies is the result of three phenomena: abrasion, shearing, and adhesion forces (Figure 2.11.).

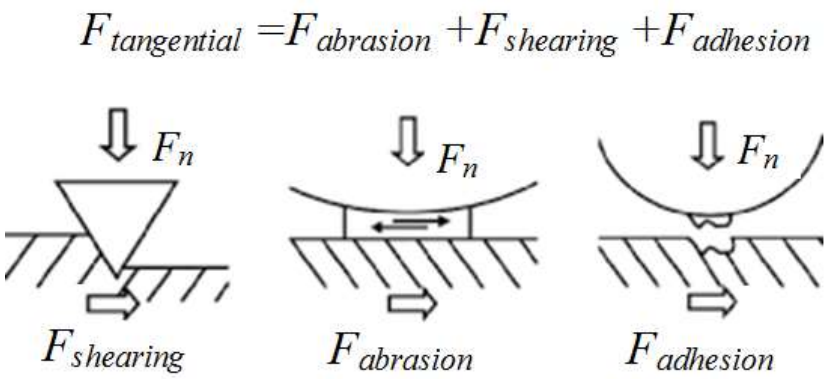

Figure 2.11. Schematic diagram of the three main fundamental contributions to friction (or tangential) force F_t with a normal force F_n [14]

Abrasive force arises from debris or rough surfaces and becomes apparent when one body is harder than the other [23]. Shearing force occurs as a result of plastic or viscous flow. Additionally, adhesive force can be caused by electrostatic force, capillary force, polarization forces (van der Waals), and bonding forces (covalent, ionic, metallic, or hydrogen bonding) [14].

For a protective coating which designed to reduce wear, wear-volume (V) can be calculated using F_N (normal force), k (wear coefficient), H (hardness) and L (sliding distance) by Archard's law [14]:

$$V = (k/H)LF_N \qquad \text{(Equation 2.2)}$$

There wear coefficient (k) depends on mainly on the materials and wear regime.

In addition, hardness (H) and elastic modulus (E) are key parameters in the tribological behavior of the film. For a wear-resistant hard coating, the plastic deformation during indentation, or in other words the ratio of hardness (H) to Young's modulus (E) - known as H/E - determines the film's ability to tolerate strain. Higher H/E ratios also lead to greater elastic recovery rates. For instance, the highest achievable value with heat-treated tool steel is approximately 0.04, while ceramics such as Al_2O_3, ZrO_2, Si_3N_4, and SiC have values around 0.06. Nitride-based coatings

like TiN and CrN typically have values around 0.08. However, DLC films can have values as high as 0.2.

Table 2.6. Hardness (H), Young's modulus (E), and H/E ratio of the different families of DLC films (a = amorphous; ta = tetrahedral amorphous) [14]

	a-C	a-C:H	ta-C	ta-C:H
Hardness (GPa)	12-18	7-30	28-65	28-60
Elastic modulus (GPa)	160-190	60-210	210-650	175-290
H/E ratio	0.08	0.1-0.16	0.1-0.2	0.16-0.21

Moreover, increasing the hydrogen content tends to decrease both hardness and Young's modulus, but it also increases the sp^3 fraction, which improves these mechanical properties (H, E).

In reality, a coating must be hard in order to avoid abrasive or adhesive wear, but it also needs to be strain tolerant and tough to prevent crack propagation and follow substrate deformations. This is especially important when there are large differences in elastic modulus between the coatings and their substrates. This can be a significant limitation in some cases, so it should be taken into consideration when designing the coating procedure.

2.6 Coating Technique: (PE)CVD

CVD coatings are widely used in applications that require resistance to wear, often across a wide range of temperatures. In fact, coatings and their substrates can be thought of as composites that offer unique combinations of properties.

In most cases, achieving the best possible solution with a basic substrate or bulk material is very difficult, if not completely impossible. For example, when coating a cutting tool like a twist drill, the drill must be made of a tough and strong material, such as high-speed tool steel, that can endure the stresses of drilling. At the same time, its surface must be very hard and chemically resistant to withstand abrasion and corrosion. However, hardness and toughness are usually opposing properties and

it can be rare for a single material to have both. One solution is to coat the steel body with a refractory metal carbide or nitride, or another appropriate hard coating material that protects the steel from high temperature oxidation and reactions with the material being cut. This coating provides the necessary hardness and wear resistance.

2.6.1 General Information on Different Application Methods of CVD

Generally speaking, chemical vapor deposition (CVD) involves the creation of a thin solid film on a substrate material through a chemical reaction with vapor phase precursors [26]. This process is different from physical vapor deposition (PVD) methods such as evaporation and reactive sputtering, which primarily involve the adsorption of atomic or molecular species onto the substrate in a physical manner (physisorption). The chemical reactions of the precursor species take place both in the gas phase and on the substrate. These reactions can be stimulated or initiated by heat (thermal CVD), high-frequency radiation such as UV (photo-assisted CVD), and low-frequency radiation such as RF (radio frequency). Regardless of the specific sub-method used, the surface reaction primarily falls under the category of chemisorption [27].

There are various acronyms for different types of CVD techniques [27]. The most commonly used ones are listed below.

MOCVD stands for metal-organic chemical vapor deposition, which uses metal-organic precursors. This can also include precursors containing metal-oxygen or metal-nitrogen bonds, and even metal-hydrides.

There are also MOCVD processes known as MOVPE, which stands for metal-organic vapor phase epitaxy, or OMVPE, which stands for organometallic vapor phase epitaxy. In all of these methods, single crystal (epitaxial) films are created on single crystal substrates using metal-organic precursors [27].

Plasma-assisted or plasma-enhanced CVD (PECVD) is a technique in which electrical energy, rather than thermal energy, is used to start reactions for the production of chemically active ions and radicals that can take part in reactions on a surface. These reactions lead to the formation of a layer on the substrate. One major advantage of PECVD over thermal CVD processes is that deposition can happen at very low temperatures, even near room temperature, allowing for the use of temperature-sensitive substrates.

Another derivative of the chemical vapor deposition (CVD) process is atomic layer deposition (ALD) or atomic layer epitaxy (ALE). It is also referred to as pulsed CVD or atomic layer chemical vapor deposition (ALCVD). In ALD, gaseous precursors are introduced sequentially onto the substrate surface, and the reactor is purged with an inert gas or evacuated between the precursor pulses. The chemical reactions that lead to film deposition in ALD occur only on the substrate at temperatures below the thermal decomposition temperature of the metal-containing precursor, and gas-phase reactions are not significant [27].

There are other derivatives of chemical vapor deposition (CVD), such as chemical beam epitaxy (CBE) in which volatile metal-organic precursors and gaseous co-precursors are utilized. Another closely related technique is metal-organic molecular beam epitaxy (MOMBE) which uses volatile metal-organic precursors and co-precursor vapor derived from the solid element. In both CBE and MOMBE, the chemical reactions occur solely on the substrate resulting in single crystal films, therefore gas phase reactions do not play a significant role in film growth.

These are some of the main types of CVD techniques. In this study, DLC (diamond-like carbon) coating is introduced as a coating material. Although there may be different alternatives, plasma-assisted or plasma-enhanced CVD (PECVD) technique, in which electrical energy or electrical potential difference is used to generate plasma, is one of the suitable techniques for DLC.

In a conventional CVD process, the steps are summarized as follows:

1- Evaporation and transportation of reagents (precursors) in the bulk gas flow region into the reactor;

2- Gas phase reactions of precursors in the reaction zone to produce reactive intermediates and gaseous by-products;

3- Mass transport of reactants to the substrate surface;

4- Adsorption of the reactants on the substrate surface;

5- Surface diffusion to growth sites, nucleation, and surface chemical reactions leading to film formation;

6- Desorption and mass transfer of remaining fragments of the decomposition away from the reaction zone [27].

2.6.2 Comparison of CVD with Other Applied Techniques

Wear and corrosion protection can be achieved through established techniques like hard-facing and plating, or through surface modification processes such as boriding, nitriding, carburizing, and ion implantation. While these techniques offer sufficient protection in most environments, they may become inadequate over time if conditions are too harsh.

Another useful and common technique is plasma spraying, but it has the drawback of needing thick deposits to provide sufficient protection. Often, extensive grinding and polishing are required. Other techniques, like sputtering, offer excellent protection but are restricted by their line-of-sight characteristics. This includes difficulty coating deep holes and trenches, as well as low deposition rates. However, the use of magnetron sputtering with multiple targets helps to partially overcome this limitation.

Chemical vapor deposition (CVD) has fewer limitations and is therefore increasingly utilized in numerous industrial applications, especially those involving extreme conditions. It is often the most effective solution for severe issues such as erosion,

friction, or hot corrosion. Additionally, CVD is considered one of the most conformal coating methods, as the coatings closely adhere to and mimic the surface morphology and intricacies. A variety of CVD coated films are presented in Table 2.7.

Table 2.7. The properties of films (at 25°C) coated by CVD [4]

Material	Hardness kg/mm^2	Thermal conductivity W/cm.K	Coefficient of thermal expansion m/m.°C 10^{-6}	Notes/Comments
TiC	3200	0.17	7.6	high wear and abrasion resistance low friction
TiN	2100	0.33	9.5	high lubricity stable and inert
Ti(CN)	2500 - 3000	0.2 - 0.3	0.8	stable lubricant
Cr_7C_3	2250	0.11	10	resist oxidation to 900°C
SiC	2800	1.25	3.9	high conductivity shock resistance
TiB_2	3370	0.25	6.6	high hardness and wear resistance
Al_2O_3	1910	0.34	8.3	oxidation resistant high stability
DLC	3000 - 5000	2.0	9.0	high hardness high thermal conductivity

2.7 Antimicrobial Coatings

2.7.1 Mechanisms

Due to its unique tribological, physical and mechanical surface properties, DLC films can combine three important antibacterial leading characteristics in its body; these are namely anti-adhesive, contact active and biocide release characteristics. One of the aims of this study is to search, characterize and enhance the antibacterial properties of DLC on medical tools and together with optimum surface properties.

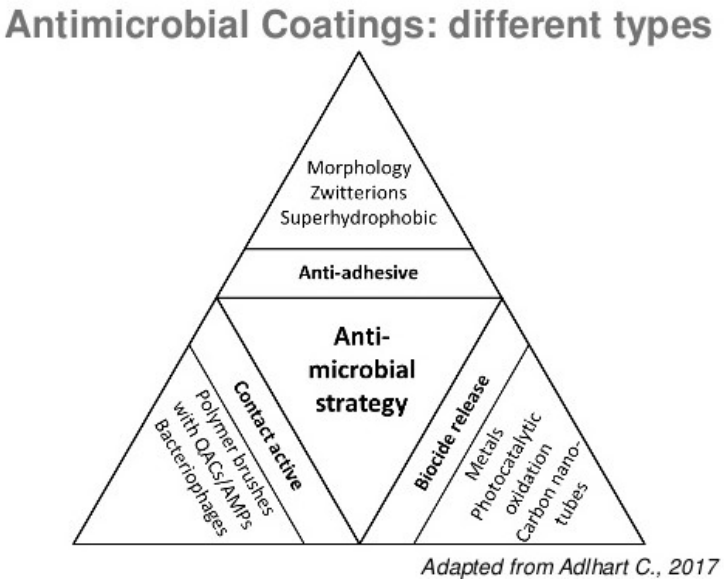

Figure 2.12. Schematics of Anti-microbial Strategy

In Figure 2.12. these three mechanisms are shown schematically. Due to its intrinsic characteristics DLC films can show these properties on its bare surface. First, DLC has one of the known lowest friction coefficients and has hydrophobic character.

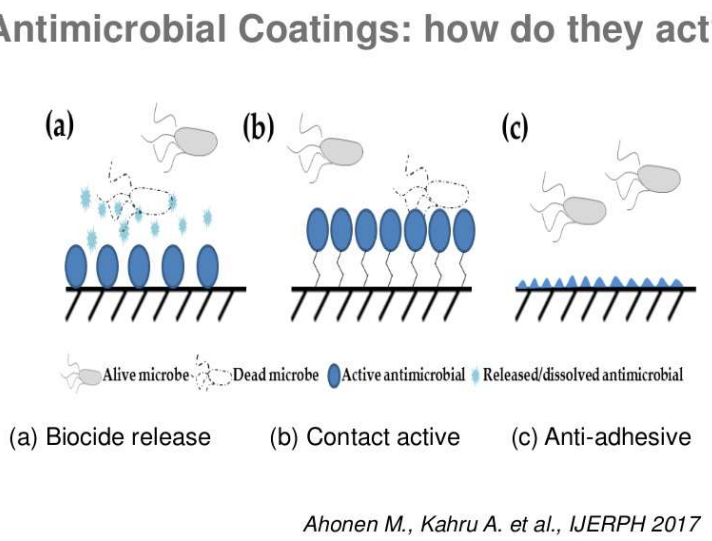

Figure 2.13. Different Defense Mechanisms on Bacteria.

2.7.2 Antimicrobial Studies in Literature with DLC

There already carbon incorporated trials to solve some bacterial problems with different film and substrate configuration [42], [43]. However, uniqueness of this study is that it will be the first trial with DLC on the steel against to a new species called as *Mycobacterium chimera*.

Diamond-like carbon (DLC) films exhibit antibacterial properties by creating a physical barrier that prevents bacterial adhesion and proliferation on the surface. The unique chemical inertness and high hydrophobicity of DLC hinder bacterial growth by reducing nutrient availability and promoting a hostile environment for bacterial survival. DLC's nanostructured surface can disrupt bacterial cell membranes, leading to bacterial cell death. These antibacterial mechanisms make DLC a promising material for healthcare applications. These findings are supported by various studies in the literature, highlighting the effectiveness of DLC in preventing bacterial colonization on medical devices and disrupting bacterial cell walls to cause cell death.

In a study published in the Journal of Materials Chemistry B, researchers found that diamond-like carbon film exhibits strong antibacterial properties due to its unique surface characteristics [60]. The film's hardness and low friction make it difficult for bacteria to adhere to its surface, preventing their growth and proliferation. Additionally, the film's chemical composition enables it to interact with bacterial cell membranes, disrupting their function and ultimately leading to their death. This information is supported by a research article published in the Journal of Physics D: Applied Physics, which highlights the antibacterial mechanisms of diamond-like carbon film through a comprehensive analysis of its surface properties and bacterial interactions. Overall, the antibacterial properties of diamond-like carbon film make it a promising material for various biomedical applications.

In a current scientific research, a novel antibacterial bandage design has been introduced utilizing diamond-like carbon with silver nanoparticle (DLC:Ag) coatings on synthetic materials [61]. The antibacterial mechanisms at play in this diamond-like carbon film involve the release of silver ions, known for their potent antibacterial properties, when in contact with bacteria. This release of silver ions disrupts the bacterial cell membrane, inhibiting essential cell functions and ultimately leading to bacterial cell death.

Furthermore, DLC films exhibit potent antibacterial properties due to their unique surface structure and chemical composition. Specifically, the sp^3 hybridized carbon atoms in the DLC film have been found to disrupt bacterial cell walls, leading to cell death. This mechanism of action has been supported by various articles in the literature [62].

Studies have demonstrated the effectiveness of DLC in preventing bacterial colonization on medical devices. Furthermore, the nanostructured surface of DLC can disrupt bacterial cell membranes upon contact, leading to bacterial cell death. This multifaceted antibacterial mechanism of DLC makes it a promising material for various applications in healthcare and beyond.

2.8 The Problem on HCU Surfaces

There are many different application fields of antibacterial coatings. Medical tools, food conservation, equipment open to public are among the most popular ones. In this study, inner surfaces and the other auxiliary equipment of the heart-lung bypass device is considered as to be coated by DLC. Especially heating-cooling tanks which are the main functional parts of a heart-lung bypass device, are good candidates to work on. In other words, heating-cooling tanks' surfaces are good incubation places for the bacteria.

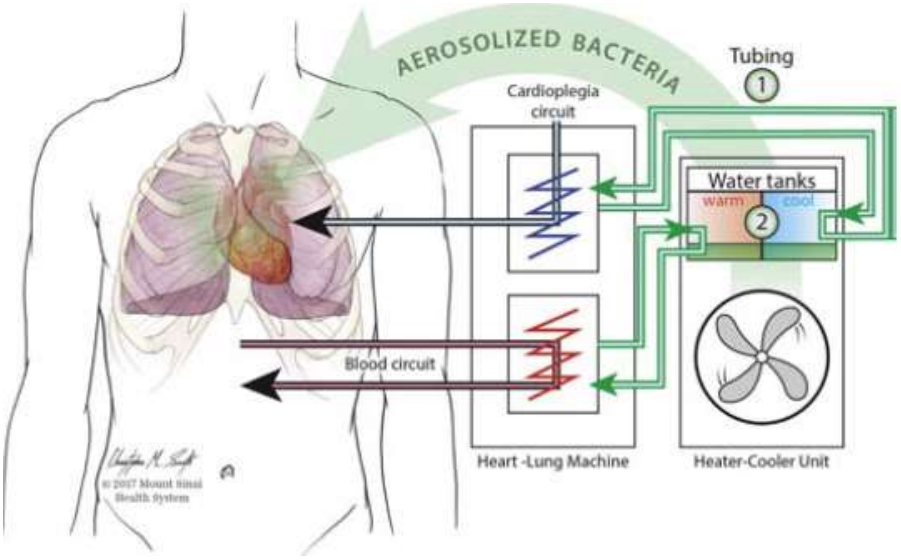

Figure 2.14. Typical Heating-Cooler Unit of a Heart-Lung Bypass Device

Figure 2.15. Typical Heater Cooler Unit (HCU)

Figure 2.16. A Surgical Room with the Heating-Cooler Unit of a Heart-Lung Bypass Device [44]

Although there is an ultraclean ventilation system, *Mycobacterium chimera* can incubate and reach the critical places in a surgical room. The best and ultimate

solution is to stop it at the very source. Hence if appropriate coating can be applied on the surfaces, it is going to be one of the best solutions.

CHAPTER 3

EXPERIMENTAL STUDIES

3.1 Revealing the Surface Material

We conducted a measurement session on the Heater Cooler Unit (HCU) in the Hearth Center at the Faculty of Medicine of Ankara University. We took multiple measurements from various locations inside the device. Analysis carried out using the Thermo Fisher Scientific XL5 800 handheld XRF device on the surfaces of the walls surrounding the tanks revealed that the walls are made of steel (SS-304), with the material content results provided in Table 3.1. Unfortunately, we were unable to measure some surfaces of the tank (the yellow surface shown in the picture below). These yellow surfaces are composed of a type of heat insulator and are considered non-condensing surfaces due to the low temperature gradient across the material, resulting in a low probability of condensation occurring there.

On top of the tanks, there are electrical components that prevent us from taking measurements with the device. The probability of condensation on these sides is also very low, making these surfaces less than ideal for incubation.

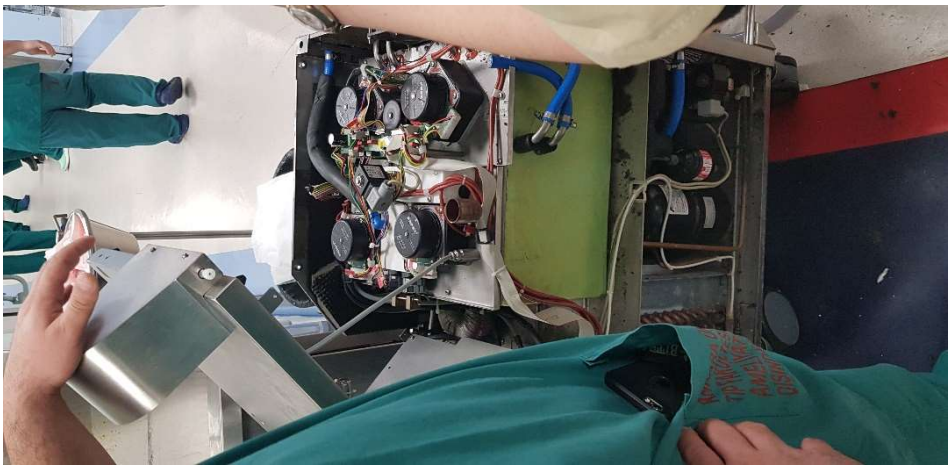

Figure 3.1. Inside (top) view of the HCU

Figure 3.2. Top surface of the HCU

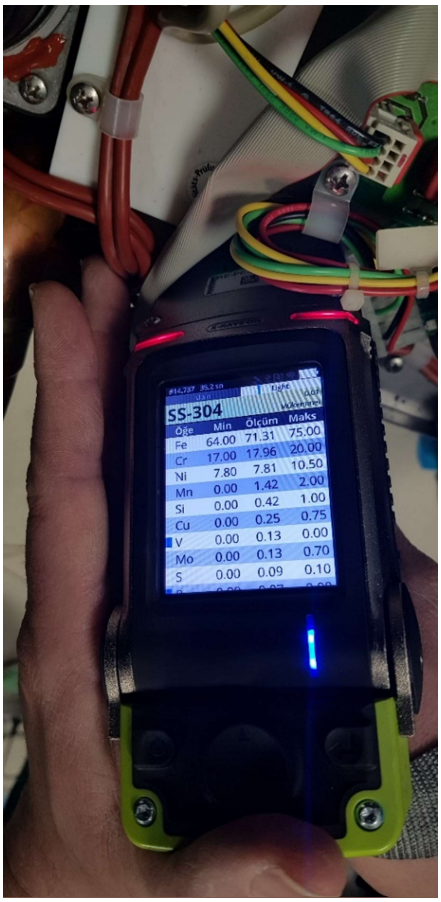

Figure 3.3. The handheld XRF Device Showing the Measurement Result

Table 3.1. Handheld XRF Measurement Results

SS - 304 STEEL	
Fe	71.31%
Cr	17.00%
Ni	7.81%
Mn	1.42%
Si	0.42%
Cu	0.25%
V	0.13%
Mo	0.13%
S	0.10%

3.2 The Base Material (304 Steel)

After revealing that the surfaces are made of 304 steel, the next step is to find appropriate 304 steel samples to cut, shape, and polish before coating and further characterizing the samples. To this end, we conducted a comprehensive search within the industry to identify the most suitable substrates for coating. As a result, we identified steel plates that are commonly used as connection parts, one of which is displayed in the Figure 3.4. Analyses performed using the handheld XRF device, which is also utilized to determine the material composition of the HCU surfaces, confirmed that these plates are indeed 304 steel.

Figure 3.4. 304 Steel Plate

The plates are about 15 cm in length and 3 cm width, and the thickness is about 3 mm.

3.3 Cutting the Substrates

The next step is to cut them in order to obtain cylinders of 8 mm in diameter and 3 mm in thickness. We used a water jet cutting device and get the substrate with rough surfaces.

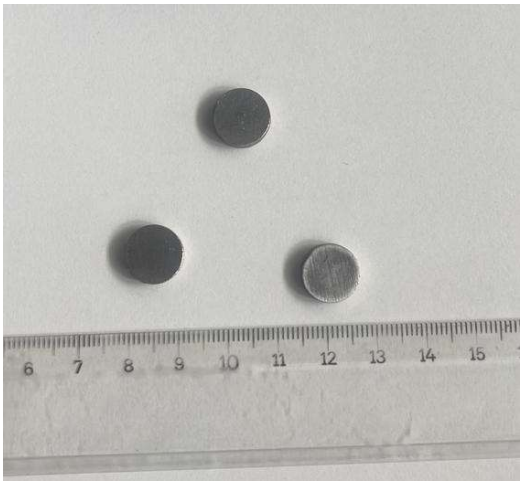

Figure 3.5. 304 Steel Substrates Cut by a Water Jet Device

3.4 Polishing the Substrates

We have 39 cylindrical substrates made of 304 steel after the water jet cutting process. However, in order to properly characterize and coat the surfaces, at least one of the substrates should be polished. There is a polishing device available in the METU Physics Lab. We conducted a trial and were able to achieve a nearly optical grade polished sample, referred to as Sample #1. Although we were successful in achieving a very good polished surface, the process involved three very challenging polishing steps. Firstly, we used 30 micron polishing sandpaper, followed by 6 micron sandpaper, and finally 0.5 micron sandpaper. The surface of the substrate material (304 steel) is hard and tough, resulting in the sandpaper being worn out by the end of the final polishing step. Additionally, we had to use wax to secure the substrate on the rotating table, but encountered difficulty in completely removing the

wax. Even a small amount of remaining wax on the surface poses a significant issue for the subsequent vacuum coating processes of PVD and PECVD.

Figure 3.6. The Polishing Device Respective Sandpapers in Terms of Particle Thicknesses

Due to the problems mentioned above, we began to look for another method to polish the surfaces. We attempted to polish the surfaces manually, so we obtained a dremel tool and bought a couple of fine/finish carbide dremel tips.

Figure 3.7. Carbide Dremel Tip

Figure 3.8. Polishing Setup

Although the resulting surface quality achieved with this technique is not as refined as with the first polishing device, it is believed that the surface quality is still adequate for coating. Both PVD and PECVD methods are preferred for coating "semi-rough" surfaces that are not polished to optical grade. We polished approximately 15 samples using this method. To compare the roughness values, the surface was measured using a Zygo interferometer. The first sample polished with the device had a surface roughness value of about 6-8 nm. In contrast, the other 15 samples had roughness values ranging from 80 nm to 566 nm.

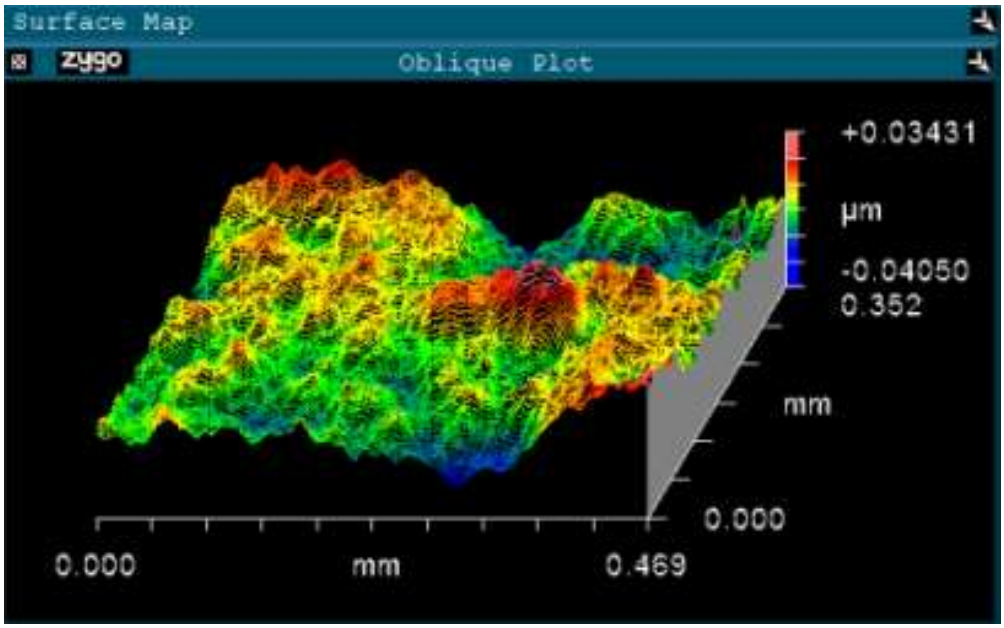

Figure 3.9. Sample#13: 8 nm rough

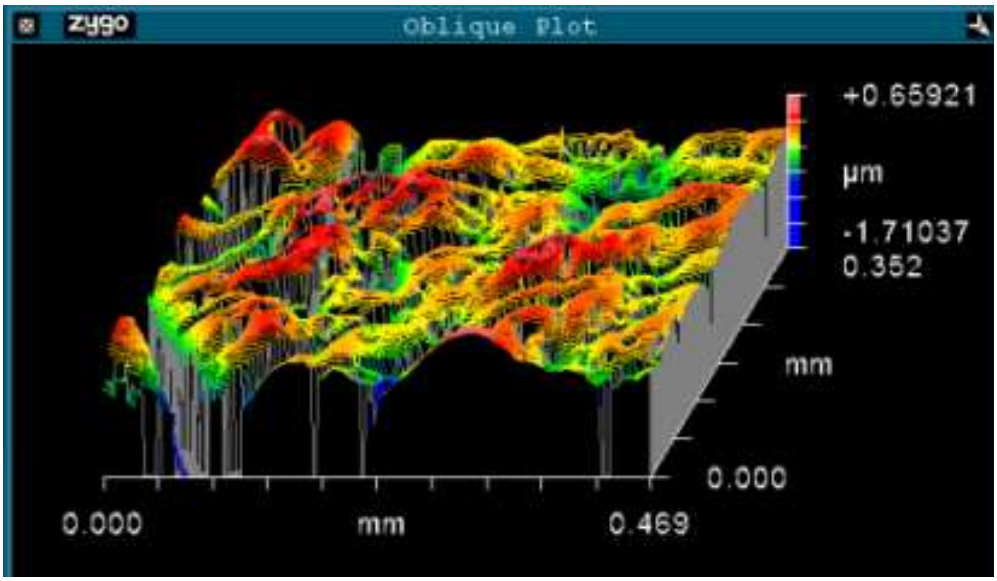

Figure 3.10. Sample#13: 216 nm rough

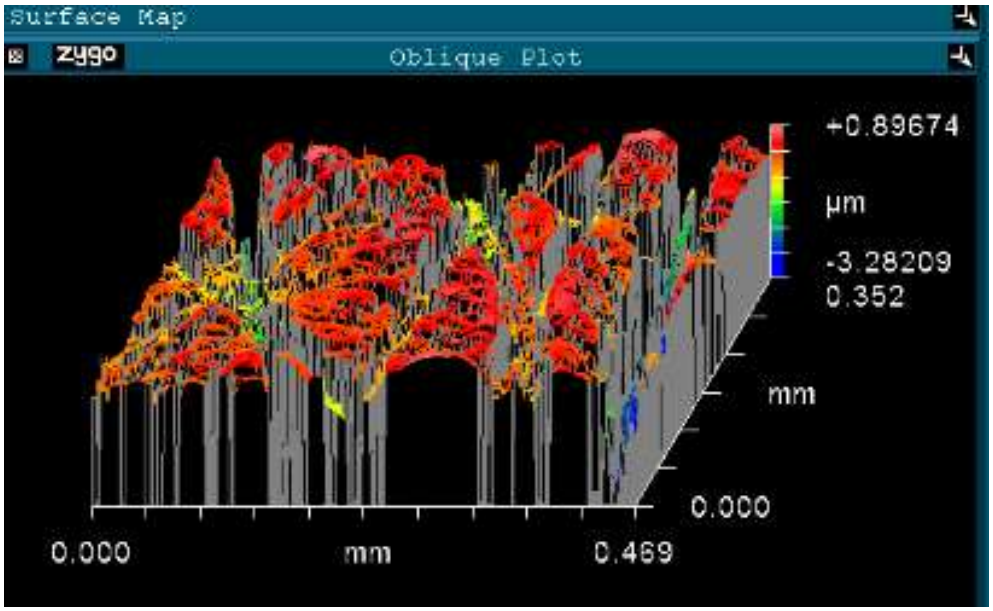

Figure 3.11. Sample#16: 566 nm rough

3.5 Coating the First Substrates (PVD + PECVD)

After polishing the surfaces, the next step is to coat some surfaces in order to see if there will be a successive layer of DLC. Furthermore, as an experimental trial we chose Sample#1 (the best surface polished by device, rms = 8 nm), Sample#2 (polished by hand to a good degree of roughness: rms = 81 nm) and Sample #3 (polished by hand, rms = 500 nm). Hence, we will obtain results with different surface roughness values to compare.

From the literature and past experiences, we know that it is very improbable to coat the bare steel surface with DLC. Hence, we need an intercalating layer. The intercalating layer must accommodate and conformal to both substrate surface (in our case 304 steel) and outer layer of DLC. There are three source-material options in our case for the intercalating layer: 1st AgPd, 2nd TiO_2 and 3rd SiO_2. One of the best matching material in terms of its intrinsic lattice structure is titanium and also its compounds are still good for both steel and DLC to adhere.

Therefore, we decided to first coat TiO_2 as an intercalating layer using the PVD technique with a Leybold PVD coating machine. Prior to the coating step, we heated up the chamber to approximately 130 ºC and performed an Argon plasma etching step before coating with 25 nm of TiO_2. All three samples were coated in the same run. The results were quite satisfactory as we achieved a golden-like yellowish appearance of TiO_2 on the steel surfaces. This golden-like color is a result of the Quarter Wave Optical Thickness (QWOT) Rule.

Figure 3.12. TiO_2 PVD Coated Samples

Figure 3.13. Sample #2 PVD Coating of TiO_2

The final step is to coat all three samples with DLC (Diamond Like Carbon) in order to see if they are accepting the DLC on top of them properly. We coat all three sample

in a PECVD chamber at the same time and run (a cycle in which all pre-coating and coating steps are done). As a conditioning step, we first apply Argon plasma etching for the 100 seconds and then we coat about 150 nm DLC on top of them. We chose methane (CH_4) as the precursor gas for CVD.

Figure 3.14. TiO_2 (25 nm) + DLC (150 nm) Coated 304 Steel Samples

3.6 Coating the Rest with Different DLC Thicknesses

After proving that on the first layer of 25 nm TiO_2, the second 150 nm thick DLC layer sequentially and successfully coated, we observe that both layers remain constant on the steel substrate for months, hence we decide on to try different thicknesses of DLC. Besides, we decide on a thinner intercalating layer to keep the effect of it on the total film performance as far as it accommodates the second layer namely DLC on itself. Hence, we try 15 nm coating layer instead of 25 nm TiO_2 as a first coating layer. We observe that 15 nm TiO_2 layer is successfully coated and kept on the surfaces then we coat rest of the samples apart from the samples #13, #15, #20 and #26 which are assigned for other surfaces characterization procedures.

Table 3.2. TiO_2 and 150 nm DLC Coated Polished/Not polished Samples

		TiO2 (25 nm)	DLC (150 nm)	TiO2 (15 nm)
1	polished	done	done	
2	polished	done	done	
3	polished	done	done	
4	polished			done
5	polished			done
6	polished			done
7	polished			done
8	polished			done
9	polished			done
10	polished			done
11	polished			done
12	polished			done
13	polished			
14	polished			done
16	not polished			done
17	not polished			done
18	not polished			done
19	not polished			done
20	not polished			
21	not polished			done
22	not polished			done
23	not polished			done
24	not polished			done
25	not polished			done
26	not polished			

The next step is to decide on the thicknesses DLC layers. Since we are going to search the effect of different thicknesses of DLC layers as an antibacterial coating, we should properly decide on the film thicknesses. As we choose thin DLC layers, as a matter of concept of this study, we avoid thick DLC layer and keep the thicknesses about a few hundred nm or thinner. Hence, as it given in the table we decided and applied 50 nm, 100 nm, 200 nm and 500 nm DLC layers and we run different sessions on the machine.

Table 3.3. Samples Coated for Different DLC Thicknesses

		TiO2 (25 nm)	DLC (150 nm)	TiO2 (15 nm)	DLC (50 nm) (50 s DLC Tip3 7.6-10.6)	DLC (100 nm) (100 s DLC Tip3 7.6-10.6)	DLC (200 nm) (200 s DLC Tip3 7.6-10.6)	DLC (500 nm) (500 s DLC Tip3 7.6-10.6)	DLC (1500 nm) (1500 s DLC Tip3 7.6-10.6)
1	polished	done	done						
2	polished	done	done						
3	polished	done	done						
4	polished			done	x				
5	polished			done	done				
6	polished			done	done				
7	polished			done		done			
8	polished			done		done			
9	polished			done		done			
10	polished			done			done		
11	polished			done			done		
12	polished			done				x	
13	polished							x	
14	polished			done				x	
16	not polished			done				x	
17	not polished			done			done		
18	not polished			done	done				
19	not polished			done	done				
20	not polished								
21	not polished			done		done			
22	not polished			done			done		
23	not polished			done			done		
24	not polished			done				x	
25	not polished			done					
26	not polished								
30	polished								done
31	polished								done

We choose four substrates for each session to be coated with DLC for each different thickness (namely 50, 100, 150, 200 and 500 nm). We know that the machine is calibrated so that every process second makes almost 1 nm thick DLC layer, we conduct the runs based on this assumption. As a result, we obtain DLC coated

substrates which have thicknesses of 50 nm (50 s), 100 nm (50 s) and 200 (200 s). Unfortunately, 500 (500 s) nm thick layer cannot accommodate on the surface and destructed in seconds. The most probable reason is that the DLC layers are too thick and create too much intrinsic compressive stress in the films. Films cannot carry these stresses and destructed. On the other hand, other reasons like cleanliness of the surface and the chamber could play some critical roles in the destruction.

Figure 3.15. Samples Successfully Coated with 15 nm TiO_2 and Different Thicknesses (50/100/200 nm) of DLC

Moreover, in order to replace the destructed 500 nm on steel substrates we decide to coat another process in which 1500 nm thick DLC films coated on Si substrates. Moreover, these 1500 nm thick DLC coated substrates are used in friction test later. We already have experiences of this 1500 nm thick DLC coating on Si substrates and we know that that much thick DLC on Si quite stable and not self-destroyed.

3.7 Adding AgPd to DLC

We have planned to conduct test on DLC coated samples and also on control samples. We chose bare steel surfaces as control samples. Besides, it is beneficial and can enhance our vision to add/dope agents into the some chosen samples

surfaces. For this purpose, two different samples namely sample #23 (coated 200 nm DLC) and one of the Si samples which are coated thick DLC on them are selected. Then by using the PEPVD coating chamber they were first pre-bombarded with Ar plasma in order to prepare surfaces. Followingly only 3 nm AgPd is added/coated onto the surfaces. Although Ag is well known and extensively used antibacterial material, there is no study with AgPd as antibacterial solution to *Mycobacterium chimera* in the literature. Hence it will be the first trial to add AgPd molecules onto DLC films and conduct antibacterial tests against to *Mycobacterium* c*himera*.

The samples which are AgPd coated are listed table below:

Table 3.4. Samples which are coated 3 nm AgPd

		TiO2 (15nm)	DLC (200 nm) (200 s DLC Tip3 7.6-10.6)	DLC (1500 nm) (1500 s DLC Tip3 7.6-10.6)	AgPd (3 nm by PEPVD)	
23	Not-polished 304 Steel	done	done		done	
30	Optical Grade polished Silicon			done	done	

3.8 Measuring Contact Angle

Contact angle is a good measure whether the surface is hydrophobic or hydrophilic. As the contact angle increases hydrophobicity also increases. Hydrophobic surfaces are naturally better surfaces in terms of antibacterial properties. Generally, they give less chance to incubate bacteria on the surfaces, because they are also unwilling to accommodate water on the surface. Consequently, they are better antibacterial surfaces compared to hydrophilic surfaces.

We reserved 5 samples, 2 of them are polished, TiO_2 and 150 nm DLC coated. 1 of them is polished and only 25 nm TiO_2 coated, 1 of them is just polished bare steel surface and 1 of them is unpolished, rough bare steel surface.

Table 3.5. Samples which are exposed to Contact Angle measurement

Sample #	**SURFACE**		
1	**Polished**	TiO_2 (25 nm)	DLC (150 nm)
3	**Polished**	TiO_2 (25 nm)	DLC (150 nm)
4	**Polished**	TiO_2 (15 nm)	No DLC
13	**Polished**	Uncoated	Uncoated
20	**Not-Polished**	Uncoated	Uncoated

We observe that samples coated with 150 nm DLC film are more hydrophobic than uncoated bare 304 steel surfaces. Furthermore, tough its antibacterial character TiO_2 is worst in terms of hydrophobicity. Although it is difficult to decide by only two samples, it is observed that uncoated and unpolished bare steel surface is more hydrophobic than uncoated but polished one. That is most probably because of deep and uneven/random scratch on the rough surface.

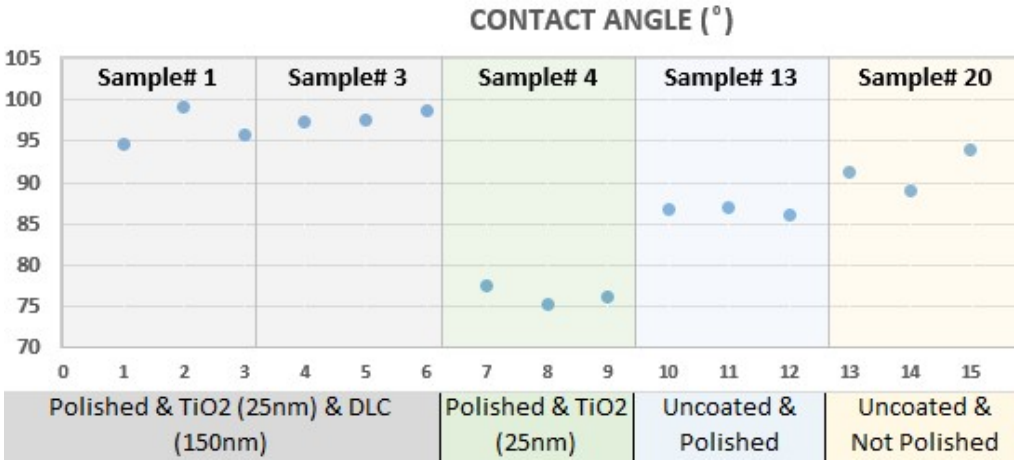

Figure 3.16. Contact angle Measurements

Table 3.6. Contact Angle Measurements

Sample #	Measurement #	(CA) Contact angle (degree)	SURFACE			MEAN CA
1	1	94.6	**Polished**	TiO_2 (25nm)	DLC (150nm)	**96.5**
	2	99.1				
	3	95.8				
3	4	97.4	**Polished**	TiO_2 (25nm)	DLC (150nm)	**97.9**
	5	97.6				
	6	98.8				
4	7	77.5	**Polished**	TiO_2 (15nm)	No DLC	**76.3**
	8	75.1				
	9	76.2				
13	10	86.8	**Polished**	Uncoated	Uncoated	**86.6**
	11	86.9				
	12	86.1				
20	13	91.2	**Not-Polished**	Uncoated	Uncoated	**91.4**
	14	88.9				
	15	94.1				

3.9 Nano-Indentation (Hardness) Tests

For the four samples, indentation test was conducted in Central Lab at METU. These samples are:

Sample #1 (Polished & DLC Coated)

Sample #3 (Polished & DLC Coated)

Sample #13 (Polished Only)

Sample #20 (Not-polished)

It is shown at the that surface hardness values of DLC coated samples are the highest ones as expected (on the order of 10 GPa). Elastic of modulus (EIT) values are very similar for these two samples. On the other hand, both hardness and elastic of modulus values are lowest (polished one is slightly higher than the not-polished one as may be expected) for the bare steel surfaces of sample #13 and sample #20.

Table 3.7. Nano Indentation Test Results

Sample #	Surface Condition	TiO_2 (25 nm)	DLC (150 nm)	Nano Indentation (Destructive)	Hardness HIT [Mpa]	Elastic Modulus EIT [Gpa]
1	Polished & DLC Coated	done	done	done	9893	193
3	Polished & DLC Coated	done	done	done	10495	227
13	Polished Only			done	678	81
20	Not-polished			done	406	49

3.10 Friction Tests

Further characterization of surfaces can be achieved by comparing the friction coefficients of different samples. It is widely recognized that DLC possesses one of the lowest surface friction values or coefficients. Along with its high surface hardness, low friction can contribute to enhancing the film's resilience against external factors. Additionally, low friction, combined with hydrophobicity, is a desirable property to support antibacterial characteristics.

Figure 3.17. SP-2100 Slip/Peel Tester Used for Friction Coefficient Measurement Test

In order to perform the test, we require two samples for each test. One sample must slide over the other for a few seconds, and then we can calculate the comparative friction coefficient. Therefore, we need to coat one of the surfaces of two Silicon samples that are 35 mm in diameter with a 1.5 micron DLC coating. The other samples we will be using are thin film DLC coated test samples, specifically samples numbered #5, #7, and #23. Additionally, we have included an uncoated 304 steel sample (#26) as a control sample.

Figure 3.18. Samples prepared for Friction (Slip) SP-2100 Slip/Peel Tester

The bigger sample (35 mm DLC coated Si) is put on the small one (8 mm steel sample) and the bigger sample is pulled slowly and continuously by the mechanism inside the test machine.

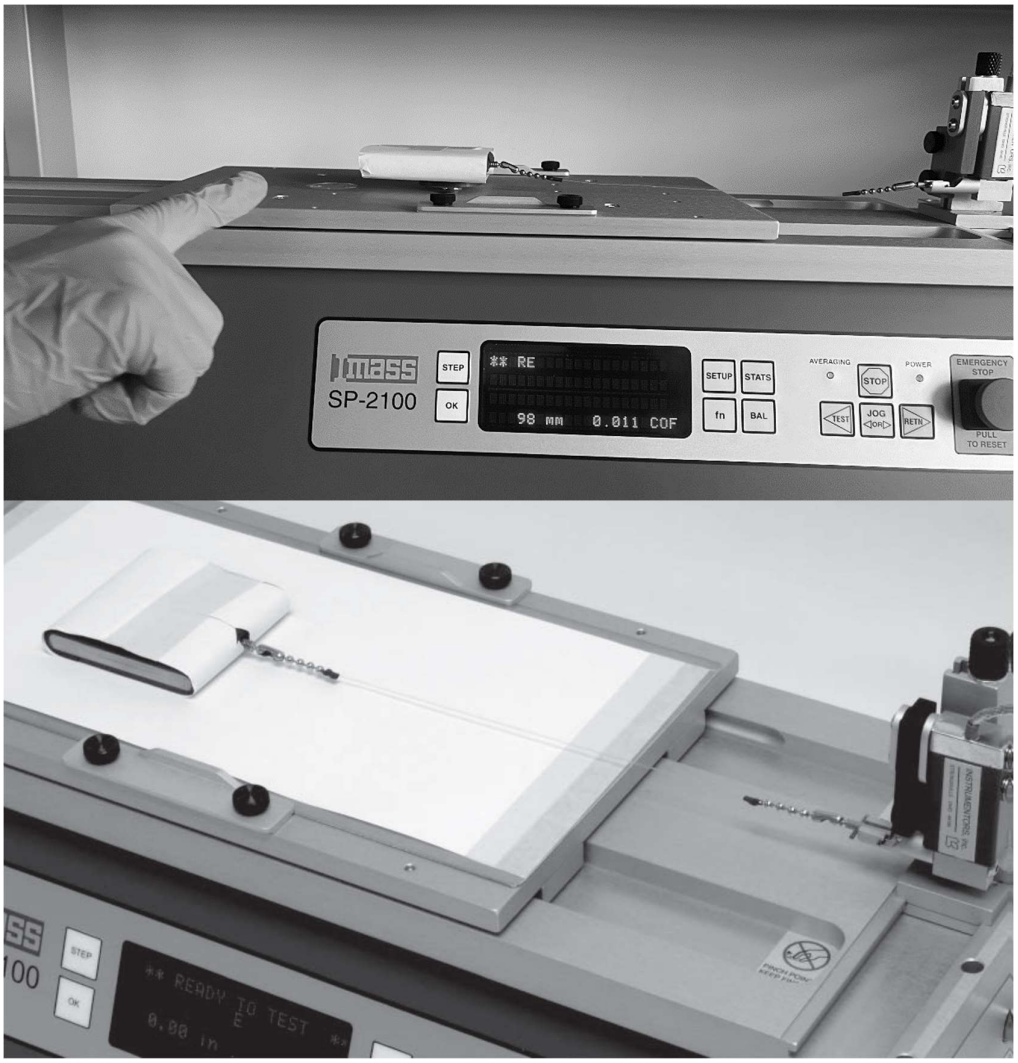

Figure 3.19. Samples tested on the Friction (Slip) SP-2100 Slip/Peel Tester

SP-2000 Slip/Peel Tester is the widely-used instrument for friction measurements. There is a pulling mechanism which pull slowly the sample over another respective surface.

The final results are tabulated below.

Table 3.8. Friction (Slip) SP-2100 Slip/Peel Test Results

Sample #	Surface	Number of Measurements	Mean Peak Static Coefficient	Peak Static Coefficient Standart Deviation	Mean Peak Dynamic Coefficient	Peak Dynamic Coefficient Standart Deviation	Mean Average Dynamic Coefficient	Average Dynamic Coefficient Standart Deviation
26	Bare steel	9	0,208	0,005	0,211	0,004	0,183	0,005
5	50 nm DLC	5	0,172	0,004	0,177	0,004	0,155	0,003
7	100 nm DLC	6	0,223	0,005	0,233	0,006	0,205	0,004
23	200 nm DLC	5	0,193	0,006	0,214	0,006	0,197	0,005

In the literature Carbon-Carbon, Diamond-Diamond and also Carbon/Diamond-Steel static and dynamic friction coefficients are between 0.05 and 0.20. [49]. Hence our test results confirm this knowledge and as it can be seen on the Table 3.8. there is only slight difference between Carbon-Carbon and also Diamond-Steel/Metal surface friction coefficients provided that one surface is carbon, diamond or DLC.

3.11 Deciding on and Designing the Bacterial Experiments

Before beginning the bacterial test, it is crucial to determine the methods to be used. Additionally, we needed to design how the tests would be conducted, so we decided to collaborate with a professional. We reached out to Dr. Sema Yiyit DOĞAN, a professional at Gazi University.

In order to design the tests, first we conduct tests on different bacteria just prior to *Mycobacterium chimera* [45]. Although we did a detailed research, unfortunately there is no institution or firm to supply *Mycobacterium chimera* bacterial samples in Turkey. Nonetheless starting with the other pathogens seems a good model in terms of two aspects. First, we would have chance to see the anti-bacterial effects of our DLC films on these pathogens. Secondly, these tests could give us the idea of most appropriate test method and also can help us to architect the test in a more efficient way. Furthermore, these tests will enhance our understanding of the effect of DLC films on pathogens in a comparative way. Those pathogens are also hospital pathogens; namely, these are E. coli ATCC 25922, S. aureus ATCC 25923, P.

aureginosa, K. pneumoni, S.enterica, B. subtilis, E. aerogenes, L. monocytogenes, S. infantis ve C. albicans ATCC 10231.

3.11.1 The First Trials: Direct Application on the Agar Medium

Double-activated bacterial cultures (S. aureus and E. coli) were inoculated on Brain Heart Infusion (BHI) agar medium, adjusted to McFarland 0.5 density. The samples to be analyzed were sterilized by UV and placed on agars planted with bacteria and incubated for 24 hours at 37 ˚C. The same experimental procedure was applied with antibiotic discs. At the end of incubation, the zones around the samples were evaluated.

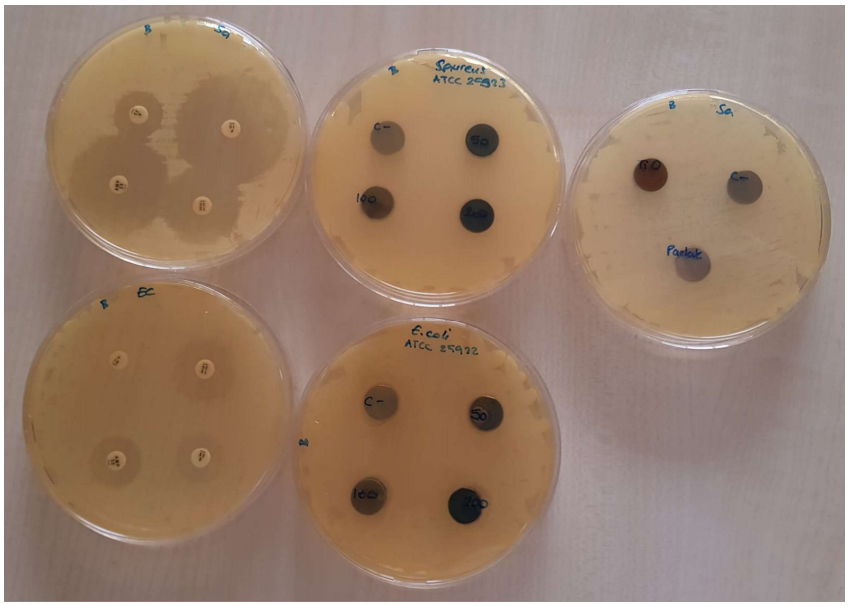

Figure 3.20. Bacteria studied; S. aureus: Staphylococcus aureus (ATCC 25923), E. coli: Escherichia coli (ATCC25922)

Antibiotic discs; Penicillin, Tetracycline, Ampicillin, Streptomycin. used for control. Worked examples; Untreated (C-: negative control), 50 nm DLC-100 nm DLC -200 nm DLC

After one day (24 hours) of observation, the study required us to observe the formation of zones, specifically transparent areas where bacteria cannot grow, similar to antibiotic discs around our samples. However, we were unable to find such results. While we did not anticipate a significantly dramatic effect like antibiotics typically have, this experiment provided an opportunity to demonstrate and progress to the next step, understanding the sole effect of the film.

3.11.2 Another Trial with the Kirby-Bauer Test Method

The Kirby-Bauer test is a bacterial test method in which a bacterial culture is spread evenly on a solid growth medium such as agar. Small paper discs containing different antibiotics are placed on the agar surface and the plates are then incubated to allow bacterial growth.

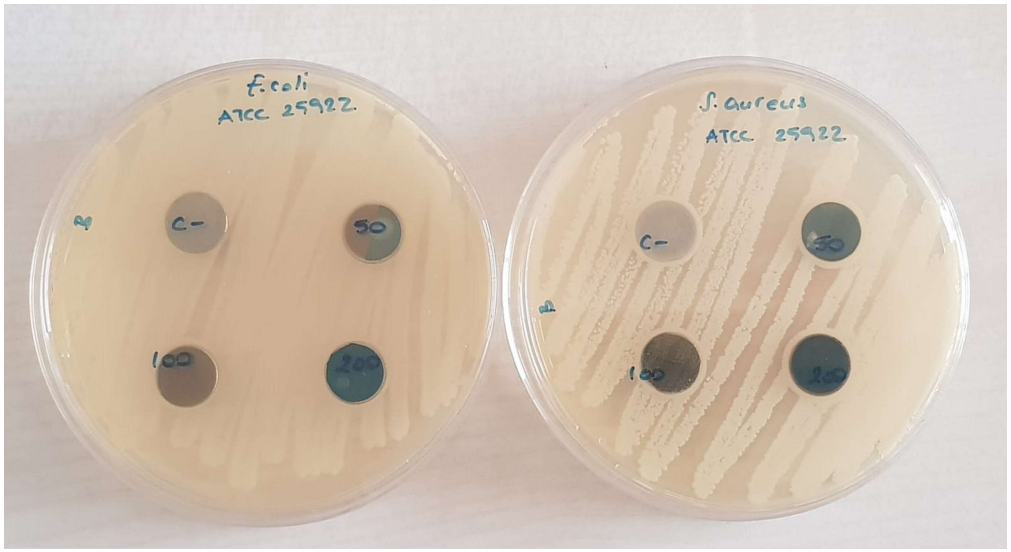

Figure 3.21. Bacteria studied under the Kirby-Bauer Test; S. aureus : Staphylococcus aureus (ATCC 25923), E. coli : Escherichia coli (ATCC25922)

Worked examples; Untreated (C-: negative control), 50 nm DLC-100 nm DLC -200 nm DLC

The study was repeated with the same set of DLC thin film coated samples according to the Kirby-Bauer Test method, but the zone was not observed again.

3.11.3 Test in Liquid Medium with Bacteria

The samples were incubated for 24 hours in broth supplemented with bacteria. Turbidity in the medium indicates bacterial growth. If the density was different between the control and the other samples, we would inoculate on agar medium and count the growing bacterial colonies and show the value in cfu/ml (the number of bacteria per milliliter) and the % viability values. However, we did not continue the study because there was no difference.

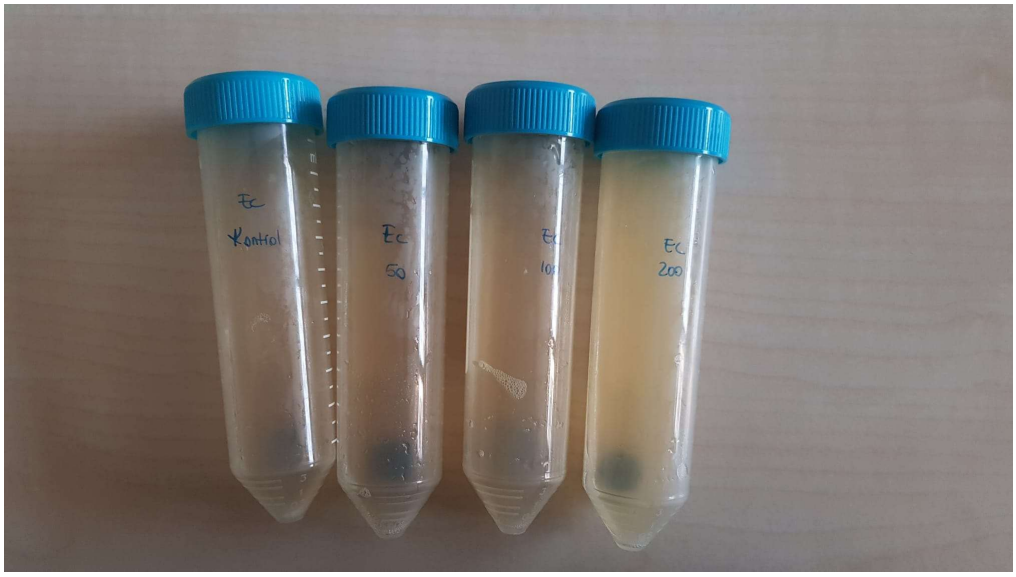

Figure 3.22. Test of the Samples in Bacteria Enriched Liquid Medium; E. coli : Escherichia coli (ATCC25922)

Worked examples; Untreated (C-: negative control), 50 nm DLC-100 nm DLC -200 nm DLC

3.11.4 Test on the Bacteria which are Directly Planted on the Samples

When we search more into the literature to see if there are different methods, we came across that it is possible incubate bacteria directly on the sample and count the viability [46], [47], [48].

Hence, E. coli ATCC 25922 and S. aureus ATCC 25923 bacteria (50) adjusted to McFarland 0.5 density were added to the UV sterilized DLC samples and incubated for 2 hours and 18 hours at 37 ˚C. At the end of the incubation, the bacteria that did not adhere were removed with PBS (Phosphate Buffered Saline), and the remaining bacteria were taken into BHI (Brain Heart Infusion) medium and allowed to grow. The concentrations of bacteria growing in the control and samples were measured with a UV spectrophotometer and the % mortality was calculated according to the formula:

$$\text{Death \%} = ((\text{Control}-\text{Sample})/\text{Control}) \times 100 \qquad \text{(Equation 3.1)}$$

Figure 3.23. Addition of bacteria to samples

After the process, we realized that there is no meaningful activity in terms of E. coli evaluation is done only on S. aureus which are listed the table below:

Table 3.9. Inhibition rates for S. aureus on the sample surfaces

Inhibition % = ((Control-Sample)/Control) x100			
Sample ID (DLC Thickness)	2 hours		18 hours
	Waiting bacteria*	After washing**	
50 nm	5.31	4.88	13.15
100 nm	3.15	3.12	8.08
200 nm	6.29	3.22	9.62
Thick sample (>1000 nm)	-	-	7.21

As it can be readily observed from the table, DLC thin films have clear antibacterial effect as the time pass. In this experiment, we also add a new member into the sample pool, namely the Thick Sample. This Thick Sample has over 1000 nm DLC thick film on the substrate. The aim of using a thick film sample is to observe the effect if we have an execrated thick DLC film on the surface. Unfortunately, 2 hours records are missing; nevertheless, as it can be seen on the right side of the table there is no positive effect of increasing the thickness more. In order to obtain more trustable results, the experiment can be repeated or multiplied with more thick samples but we can assume that in our case study it is enough for the time being.

Moreover, the bacteria placed on the sample were drawn with a pipette and allowed to grow in BHI medium, and the effectiveness of the sample was investigated. For this purpose, at the end of the incubation, the metal samples were washed in PBS to remove the non-adherent bacteria. Afterwards, the metal samples were shaken rapidly in the liquid medium and it was aimed that the adherent bacteria passed into the liquid medium to grow.

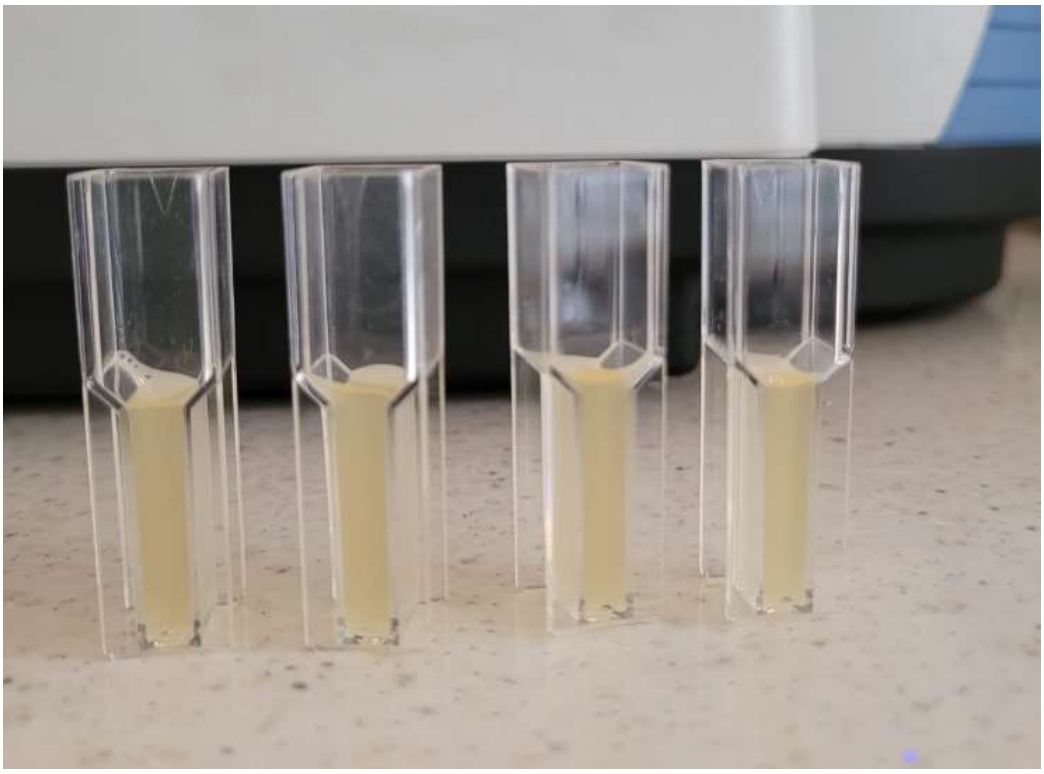

Figure 3.24. Densities of growing bacteria (from left to right: 50 nm-100 nm-200 nm-the thick sample)

This is another method to visualize the rate of vivid bacteria in the solution.

Among the methods the test on the bacteria directly planted on the samples is the best suited test. We try to enhance and characterize the anti-bacterial surface on the so to say medical grade steel, and we know the literature that recent research revealed that *Mycobacterium chimera* is a slow growing type. They can be carried by aerosols from the surfaces where it has incubated for long times to the open deep wounds which are inevitably made during the hearth-lung surgeries. Hence for a slow growing bacterium, the best tests are the long-term observation tests in which bacteria grow directly on the surface with a very slow pace.

3.12 Procuring the *Mycobacterium chimera*

We perform and completed almost what was planned at end of the last term apart from the clinical tests on *Mycobacterium chimera*. Unfortunately, there is no institution which can produce live *Mycobacterium chimera* bacteria to us in Turkey tough our deep and persistent researches. On the other hand, we found alternatives abroad. One is the Culture Collections, UK Health Security Agency in Britain. We got contact with them and ask for bid. They offer each one ampoule of any of the strain's costs £179 per ampoule and shipping costs £95 per shipment. Besides the price, we should also keep the waiting time at minimum when they are in the customs, because of the critically short living life in relatively improper conditions. Another demand from the institution is that the business or institute that is applying for purchase must holds an account with the NCTC / UKHSA Culture Collections. As far as we know neither METU nor ASELSAN has the membership

Fortunately, we came across a supplier in TURKEY which can import live *Mycobacterium chimaera* with appropriate feeding medium for the bacteria. On the other hand, because of the supply chain it will take time to get them. Nevertheless, we started the purchasing procedures by the help of ASELSAN's related project. We got in hand the bacteria and feeding medium in 4 months and then completed the tests in the remaining time given for the thesis completion.

3.13 Preparation of Bacteria, Agar and Fluidic Feeding Mediums

3.13.1 Middlebrook 7H9 Broth Base

We purchase the feeding particles for Middlebrook 7H9 Broth Base, which is suitable for *Mycobacterium chimaera*, along with the bacteria.

4.7 g feeding particle is solved in 900 ml distillated water and 2 m glycerol is added to the solution. The suspension is taken into autoclave and waited 10 minutes at

121˚C for sterilization. After sterilization the temperature falls below 55˚C then 100 ml ADC Enrichment added to it and poured into tubes.

3.13.2 Middlebrook 7H10 Agar Base

The 19-gram Middlebrook 7H9 Broth Base is diluted in 900 ml of pure water and then 5 ml of glycerol is added to it. The suspension is then placed into an autoclave at 121 ˚C for 10 minutes for sterilization. After sterilization, OADC is added to the feeding medium, which is at a temperature of about 50-55˚C. The mixture is then poured into petri dishes to cool down and solidify.

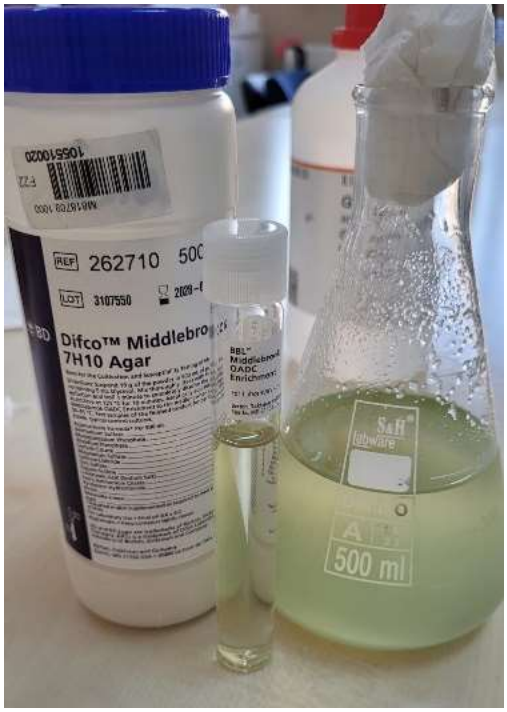

Figure 3.25. The materials used for preparation of 7H10 Agar feeding medium

3.13.3 Activating *Mycobacterium chimaera* Strain

The strains of DSM 44623 *Mycobacterium* intracellular subsp. chimaera which came as lyophilized form in the glass ampoules is activated according to DSMZ protocol. The protocol can be summarized as:

- ❖ Carefully break the ampule which is heated on burner flame by the help of forceps.
- ❖ Pour 0.5 ml feeding medium on the lyophilized culture and wait 30 minutes to solve the pellets.
- ❖ Gently mix it then carry the half of it into fluidic feeding medium and half of it into agar feeding medium wait for incubation at 37˚C in the oven for 8 days.

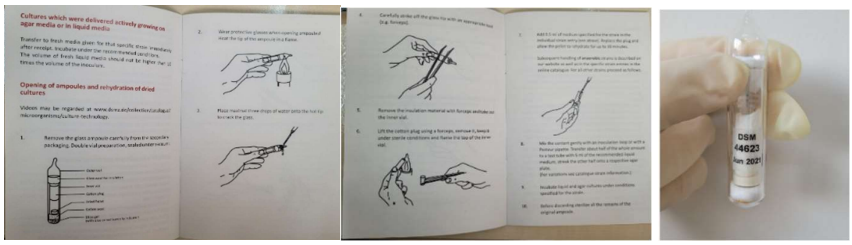

Figure 3.26. Activating the Mycobacterium intracellular subsp. *Chimaera* strain

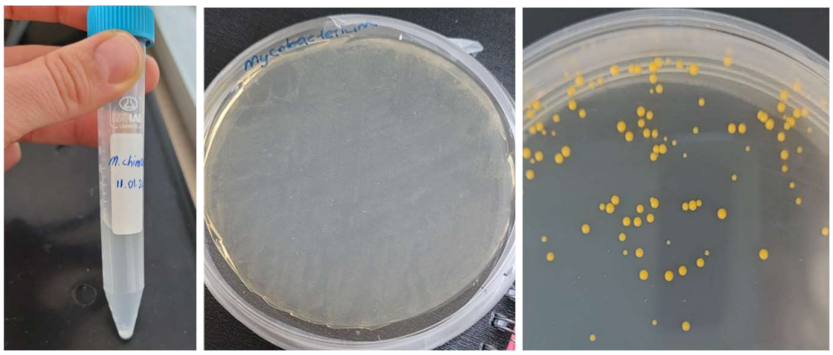

Figure 3.27. Developed fluidic and agar feeding mediums after 8 days

3.13.4 Preparation of *Mycobacterium chimaera* for the Tests

Further development of bacteria for the bacterial tests is done by taking 1% from the first fluidic feeding medium into in the second fluidic environment. Developed bacteria in the fluid are exposed centrifuge at 6000 rpm and 10 minutes in order to remove the supernatant. The remaining bacterial accumulation is called as pellet. In order to obtain pure bacteria, PBS is added to pellet, then it is centrifuged twice at 6000 rpm for 10 minutes to remove remaining particles. After washing with diluted water pellets are arranged to 0.5 McFarland density and pure bacteria solution is ready.

Furthermore, line seeding on the agar plate is completed by using the first activated bacteria. The development on agar and in the fluidic medium is observed and verified.

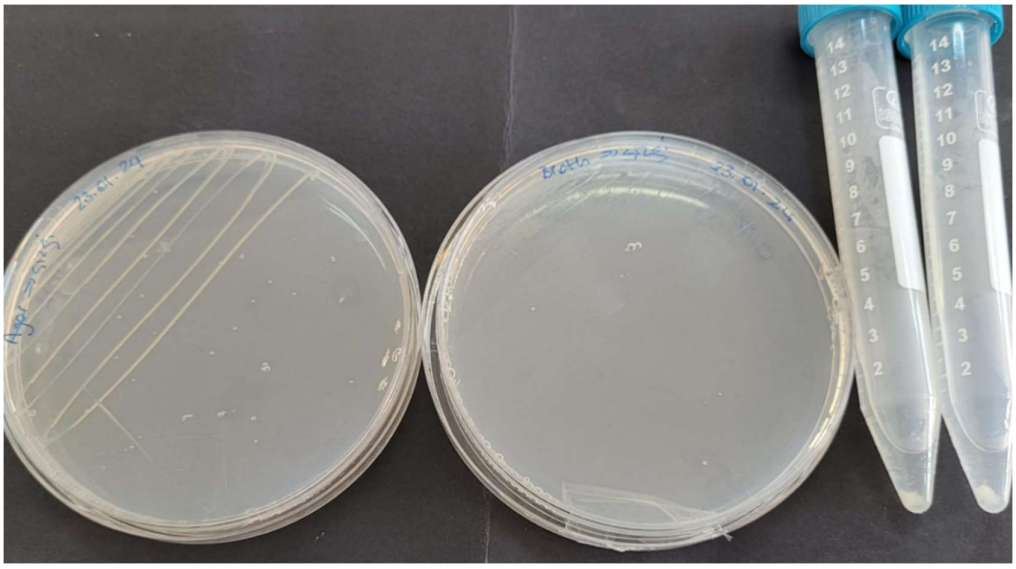

Figure 3.28. The other developed fluidic and agar feeding mediums after 8 days

3.13.5 Preparation of Samples for the Tests

Samples are dipped into ethanol of 70% purity. Then samples are washed with distilled water and dried. As last step of sterilization, all the samples are exposed to UV.

3.13.6 Incubation of Bacteria on the Samples

There are 2 different methods applied in order to incubate bacteria.

In the first method, bacteria are carried into fluidic feeding medium, percentage of the bacteria in the fluid arranged as 1%. Then this fluidic feeding medium is poured into petri dishes. Samples are put into the petri dishes upside down, that means the coated surfaces are facing the fluid at the bottom. Then they are kept at 37˚C for 3 days for incubation.

Figure 3.29. The samples in bacteria are incubated for the 1st method

In the second method, samples are taken into the 6 welled plates, the coated surfaces are facing up. Then bacteria culture which is in 0.5 McFarland density is added on the surface of the samples in the wells. The samples kept at 37˚C for 3 days.

Figure 3.30. The samples on which 0.5 McFarland density bacteria added in six welled plates

3.14 Applying Different Test Methods on *Mycobacterium chimaera* and Analyzing the Results

There are different tests/methods tried in order to analyze anti-adhesion and anti-bacterial character of the films on the samples.

3.14.1 Pressing Samples Directly to Agar

In the first test/method, samples incubated in petri dishes (Figure 3.29.) are directly pushed on the agar medium. Then the agar is waited for 14 days in order to observe development of bacteria.

After 14 days, there are high bacterial growth observed on all the respective surfaces of the agar for samples (Figure 3.31.), hence at the end of this method, there is no distinctive result obtained.

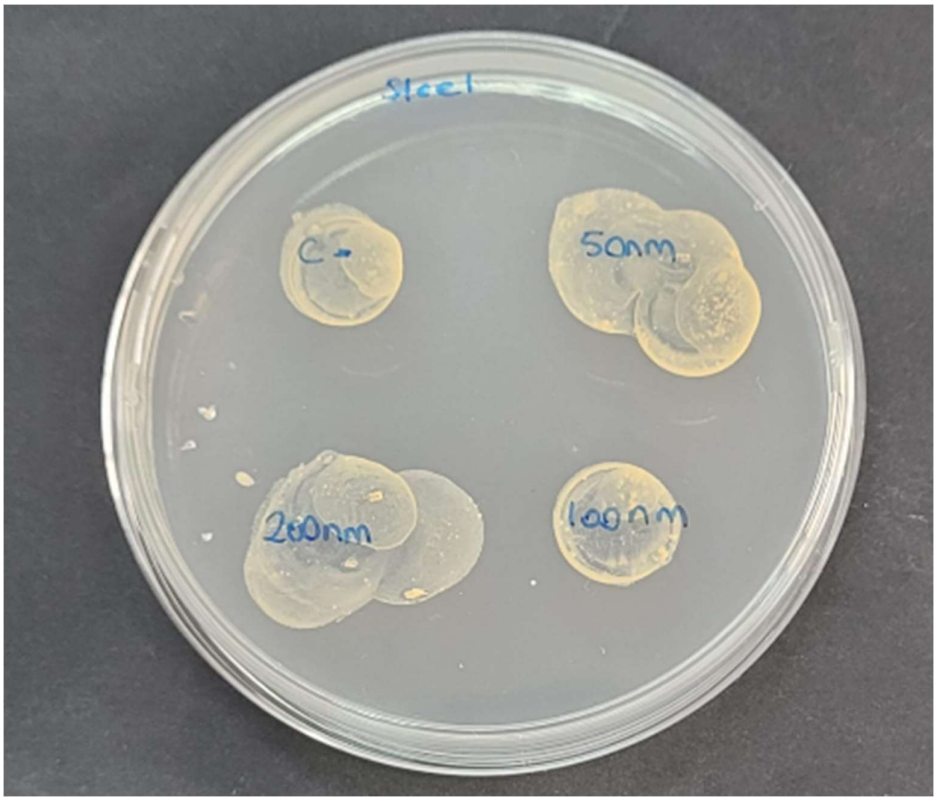

Figure 3.31. Result of the first test/method in which samples are directly pressed on the agar medium

3.14.2 Bacteria from Fluid on the Samples to Fluidic Feeding Medium

Bacteria incubated on the samples (Figure 3.30.) are taken and diluted as 1/10, then they are conveyed into fluidic feeding medium in tubes. Then these tubes are measured by an UV-Spectrophotometer at 600 nm wavelength and classified according to their density differences.

This method gives us bacterial density in a comparative manner. The results are distinctive for the samples. In other words, compared to control sample, DLC coated samples' anti-microbial characteristics are very different. The results are shown in the Figure 3.32. As we expected, there is a gradual increase in antibacterial character with increasing DLC thickness compared to uncoated steel sample.

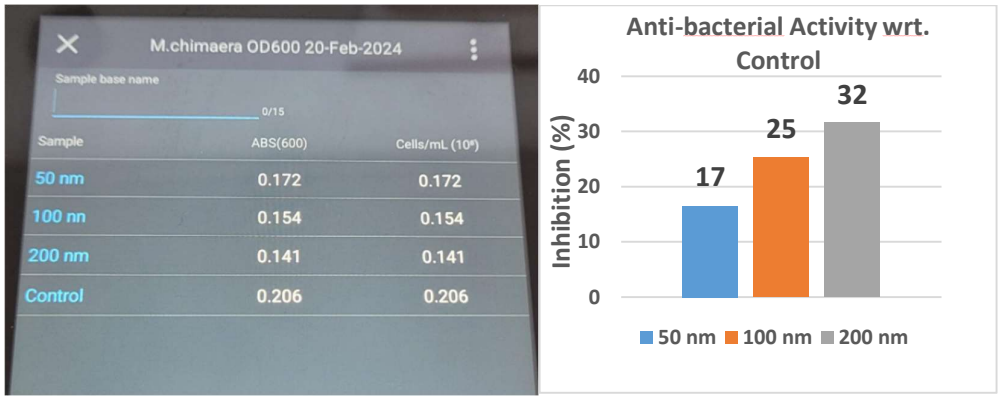

Figure 3.32. The density difference results obtained by UV-Spectrophotometer

3.14.3 Bacteria Taken Directly from the Samples to Agar

Bacteria incubated on the samples (Figure 3.30.) are directly taken, diluted by 1/10 and seeded on the agar. Then, we count the colonies on the agars in order to compare the numbers of live/dead bacteria for each sample. The results are very instructive. We observe that the most successful sample is 200 nm DLC coated one as the Figure 3.34. suggests, the inhibition rate is about 92%.

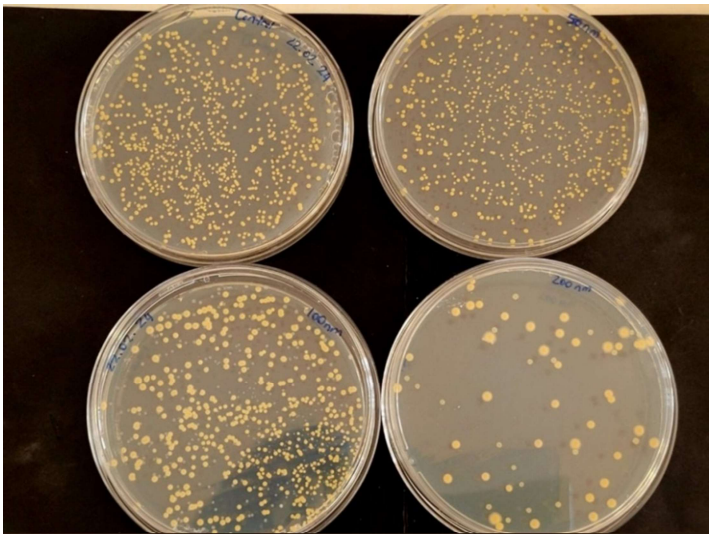

Figure 3.33. Agar plates on which bacteria are seeded taken directly from the samples

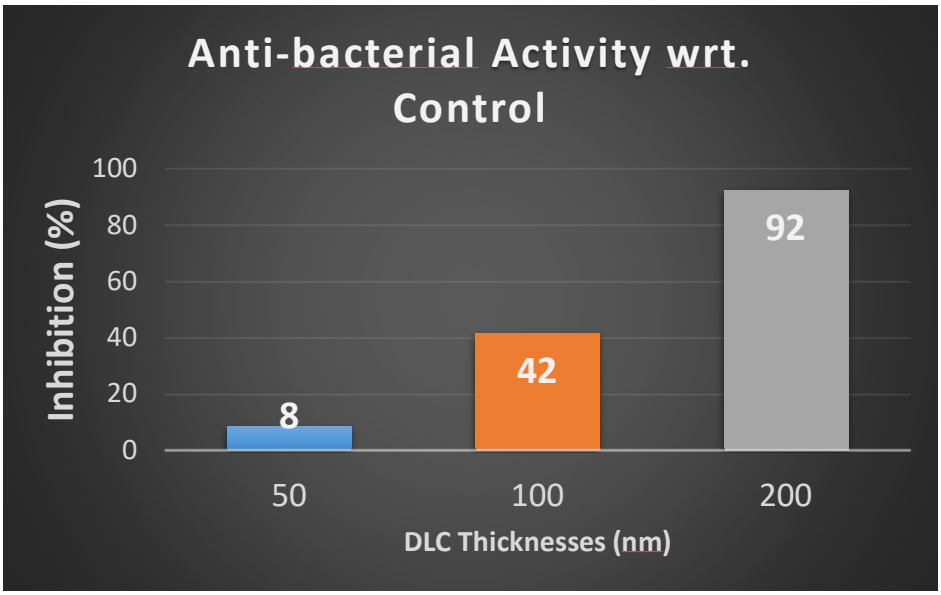

Figure 3.34. The inhibition rate of mycobacteria chimaera for different thicknesses

3.14.4 Bacteria Obtained by Sonication from the Samples to Agar

As a last test, in order to remove the unattached bacteria, samples (Figure 3.30.) are taken into PBS and vortexed for 3 seconds in order to remove unattached bacteria from the surfaces. Then the samples are taken into the tubes containing 10 ml PBS. They are exposed to ultrasonic bath (sonication at 50 Hz) for 30 seconds in order to pull off the attached bacteria to solution (Figure 3.35.). After completing the sonication, 100 µl the solution containing bacteria taken and seeded into the agar medium. After 14 days of incubation, we observe that compared to control sample, DLC coated samples are quite successful to impede the attachment of the bacteria to the surfaces. Figure 3.37. shows the adhesion rates of the DLC coated samples compared to uncoated control sample. The best sample in terms of the anti-adhesion is 200 nm DLC coated sample, then 100 nm DLC coated sample is the second, 50 nm DLC coated one is better than the uncoated control sample but worse than 100 nm DLC coated sample.

Figure 3.35. Removal process of bacteria form the surface by sonication

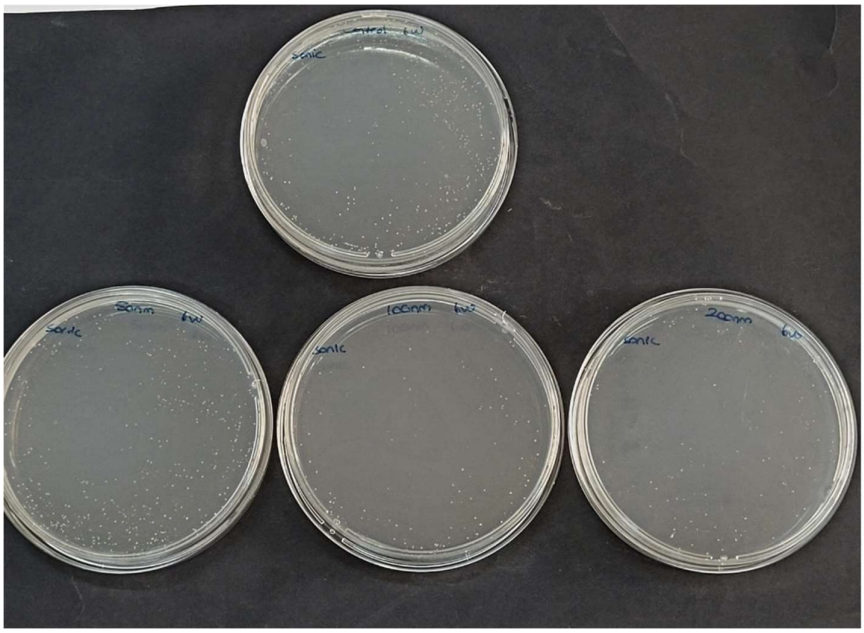

Figure 3.36. The agar mediums to which the bacteria which could attach to surface are seeded

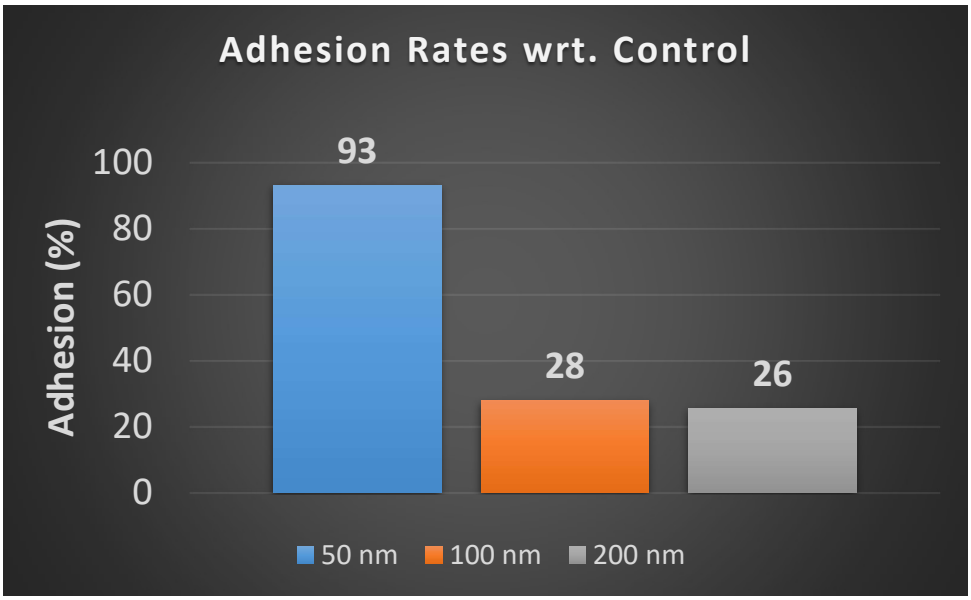

Figure 3.37. Counting the bacterial colonies (cfu/ml) which were formerly attach to surface are seeded and adhesion rates

3.15 *Mycobacterium chimaera* under Field Emission Scanning Electron Microscope (FESEM or SEM)

3.15.1 The Fixation and Coating Procedure for the FESEM Measurements

Before placing the samples into the FESEM an appropriate procedure should be applied to each sample to be observed. The procedure consists of the following steps:

a. All the samples should be cleaned properly with PBS. The aim of this step is to remove all residuals except bacteria from the surface.
b. All the samples should be kept in a solution of 2.5% Glutaraldehyde for 4 hours.
c. The samples should be taken off from the solution without touching the surface which is going to be observed.
d. The samples should be kept in a desiccator without dust or particles for about 1 hour.

e. In order to dehydrate (dry) the samples are put into the solutions of ethanol with the ethanol percentages of 10%, 20%, 30%, 50%, 70%, 85%, 95% and 100% for 10 minutes respectively. There should be 5 minutes between each dip cycle.
f. The sample should be kept in a dry and calm desiccator for 12 hours for further drying.
g. All the sample properly packaged and fixed at the bottom, the surface that is to be observed must be kept untouched in the package.
h. Before the FESEM measurement session the surfaces those are observed should be coat 3 nm AuPd in order to gain conductive character in a proper and clean coating chamber under vacuum.

3.15.2 The SEM Measurements

After 5 days incubation in the fluidic environment enriched with *Mycobacterium chimaera* 3 samples which are 8 mm in diameter are taken for FESEM measurement at METU Central Lab. These three samples are:

1- Control sample: Bare SS-304 sample without any coating
2- A sample coated with 100 nm DLC on 15 nm TiO_2 coated SS-304 Steel sample
3- A sample coated with 200 nm DLC on 15 nm TiO_2 coated SS-304 Steel sample.

Since the bacteria grow at a very slow pace and the biofilm is established about six weeks later than the first attachment after only five days of the incubation period, we observe a very rare bacterial population. Another reason for this rarity is that the DLC films, as expected, slow down the growth. According to the literature, we can see rod-like mycobacteria after five days on the samples, with lengths ranging from 0.5 microns to 3 microns. The variation in length is attributed to the folding of bacteria or the angle at which they are positioned on the surface of the sample. Before

conducting SEM measurements, we follow a fixation procedure, during which we form a glutaraldehyde film in which the bacteria are embedded. This may lead to skewed bacteria in the film.

For the uncoated and not-polished steel sample surface, it is very hard to differentiate bacteria because of the surface very rough topography (Figure 3.38.).

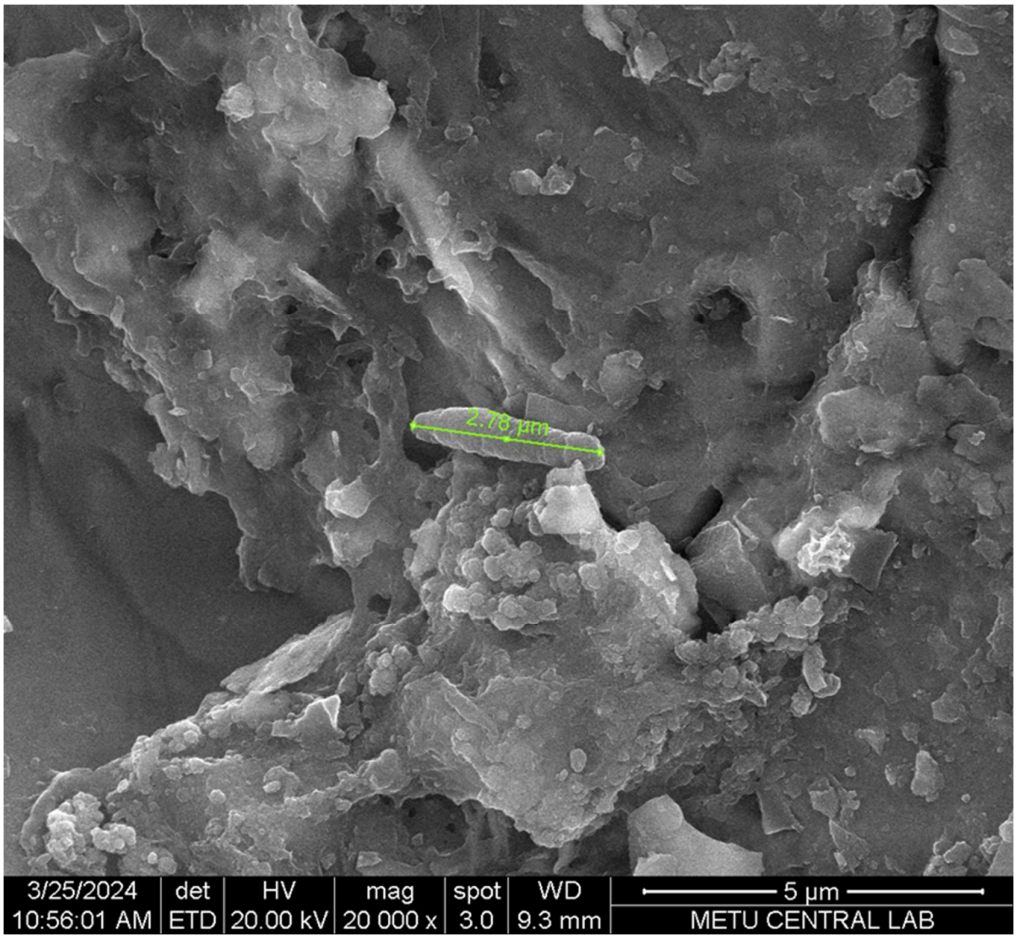

Figure 3.38. *Mycobacterium chimaera* on the substrate which is uncoated and very rough.

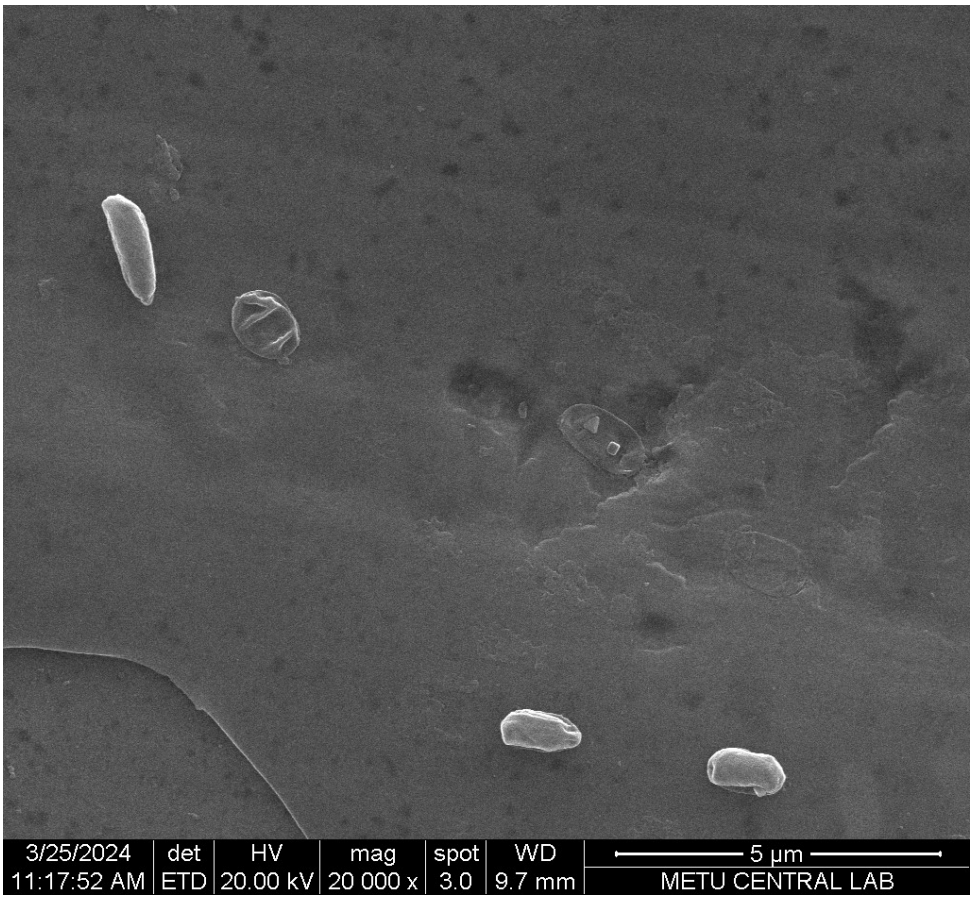

Figure 3.39. SEM image of 5 *Mycobacterium chimaera* (1 alive, 2 start to die, and 3 dead) on the 100 nm DLC coated sample

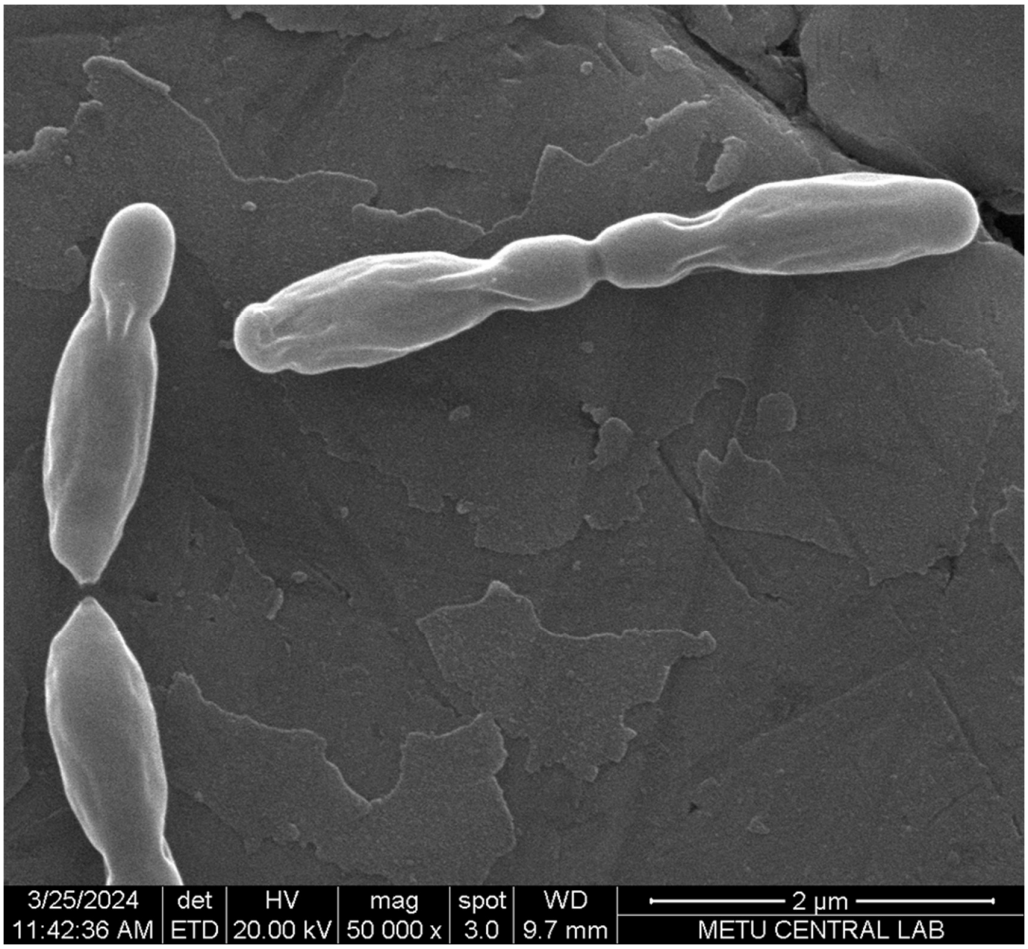

Figure 3.40. *Mycobacterium chimaera* newly copied themselves on substrate which is coated with 200 nm DLC thin film.

As it can observed from the Figure 3.41. some bacteria can die after bacterial cell division.

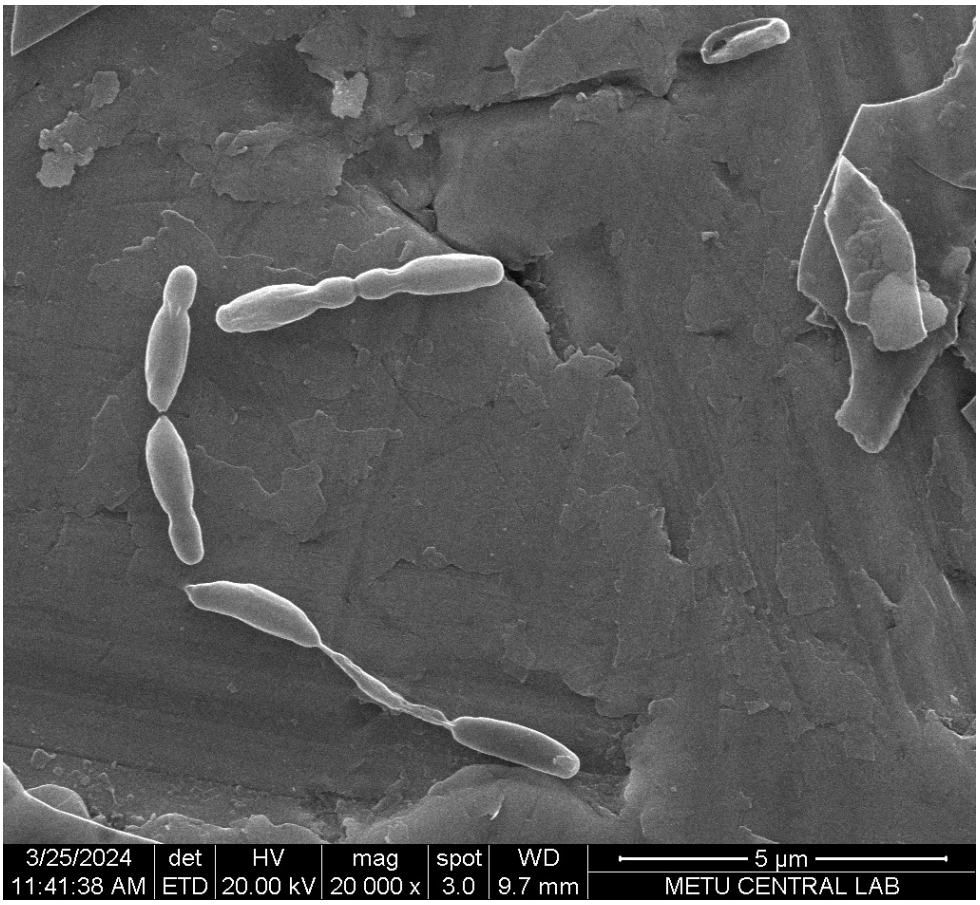

Figure 3.41. *Mycobacterium chimaera* copied themselves on substrate which is coated with 200 nm DLC thin film. One of them in three chain group is dead and denatured after the division.

Furthermore, dying or dead bacteria can be seen on the Figure 3.42., Figure 3.43. and Figure 3.44. Bacteria which are about to die start to collapse inside the membrane of the cell. The membrane outside the cell seems transparent and cell loses its form apparently. Figure 3.44 shows one healthy and two dying *Mycobacterium chimaeras.*

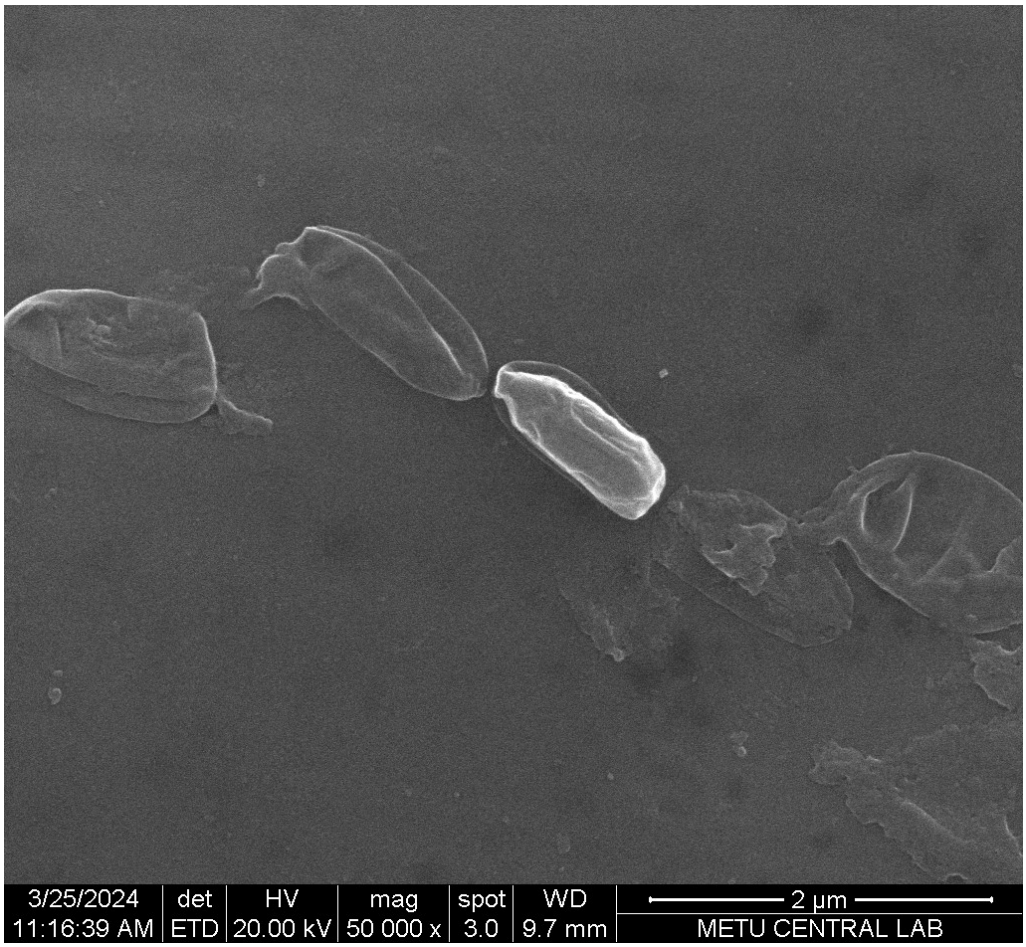

Figure 3.42. *Mycobacterium chimaera* on substrate which is coated with 100 nm DLC thin film.

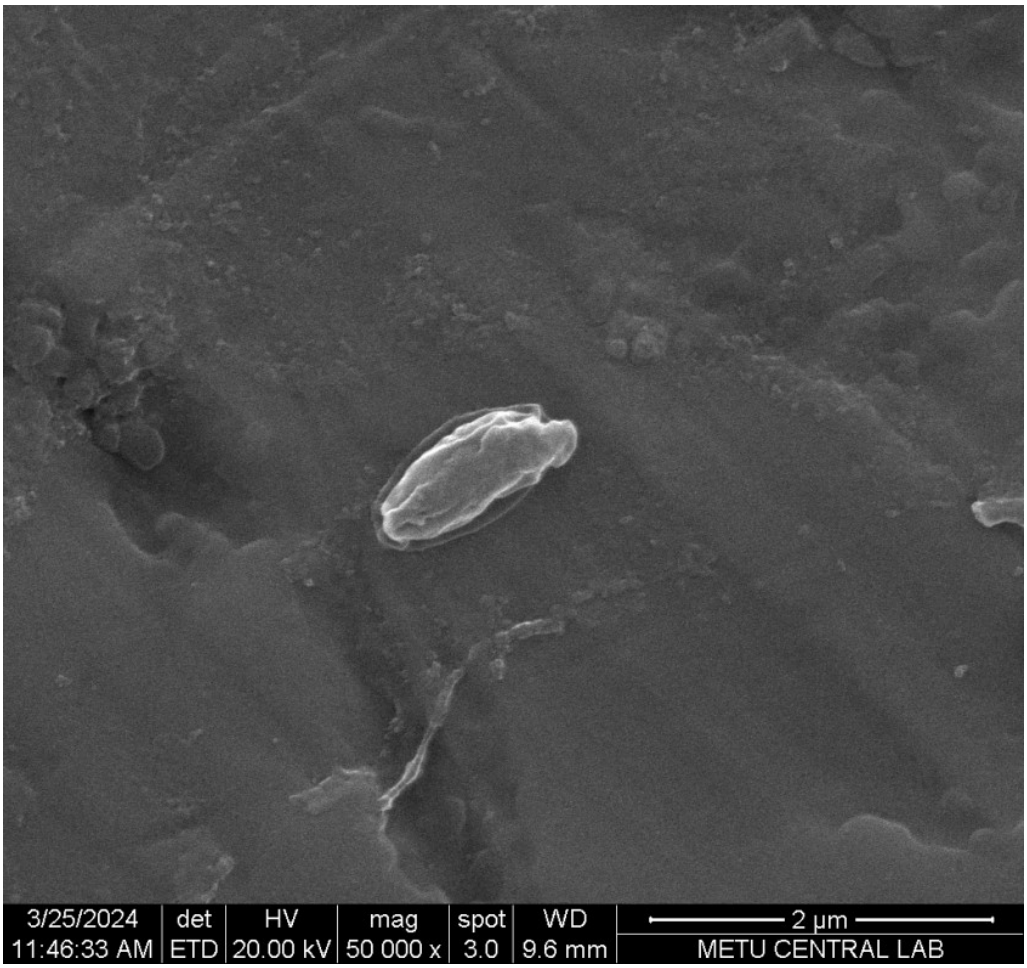

Figure 3.43. *Mycobacterium chimaera* on substrate which is coated with 100 nm DLC thin film.

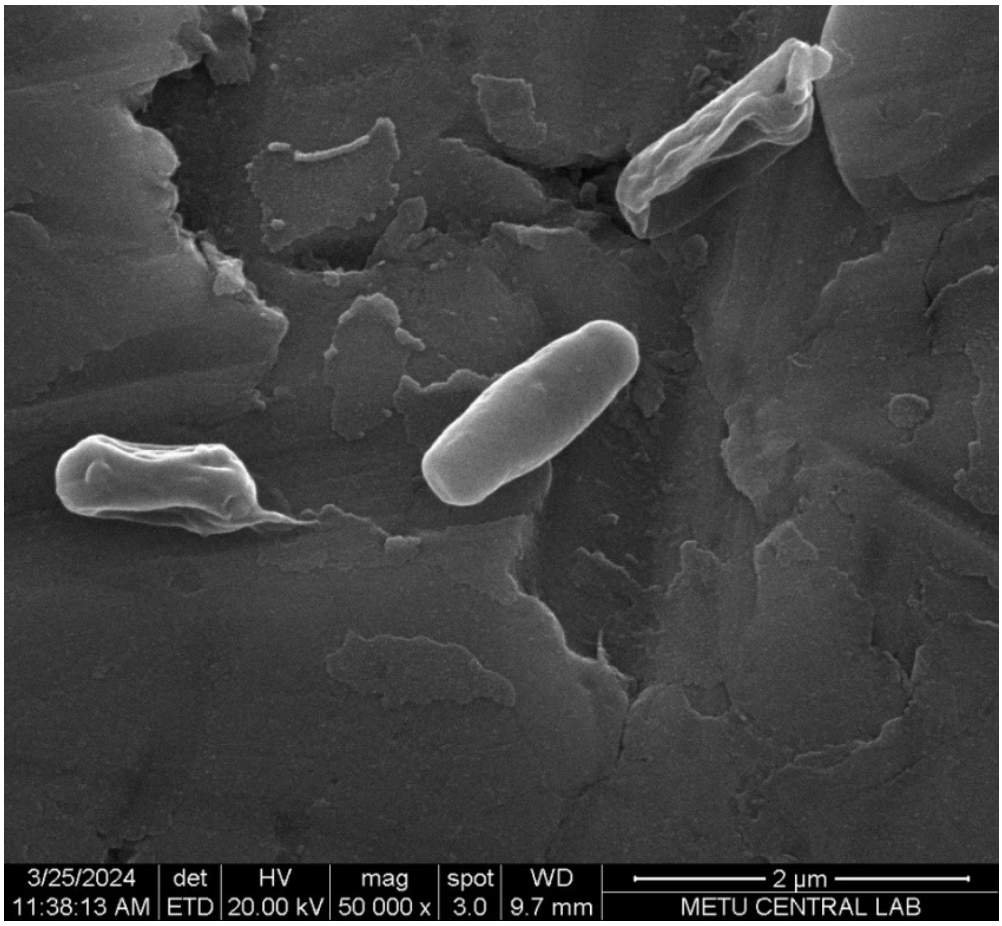

Figure 3.44. *Mycobacterium chimaera* on substrate which is coated with 200 nm DLC thin film.

3.16 The Florescence Microscope Measurements of *Mycobacterium chimaera*

After incubating for 5 days in a liquid environment enriched with Mycobacterium Chimaera, a total of 4 samples, each 8 mm in diameter, were collected for measurement using a fluorescence microscope at the Biological Sciences Department Lab in METU.

These four samples are:

1- The control sample: Bare SS-304 sample without any coating

2- The sample coated with 50 nm DLC on 15 nm TiO_2 coated SS-304 Steel sample
3- The sample coated with 100 nm DLC on 15 nm TiO_2 coated SS-304 Steel sample
4- The sample coated with 200 nm DLC on 15 nm TiO_2 coated SS-304 Steel sample.

We use Acridine Orange which is membrane permeable, green (AO) and Propidium Iodide which is not permeable through the membrane, red (PI) double staining on *Mycobacterium chimaera* to observe under the fluorescent microscope. They are the most used stains for analyses of cell apoptosis. Using a combination of these stains, cells appear orange/red to indicate they are apoptosis, while intact cells appear green. [59].

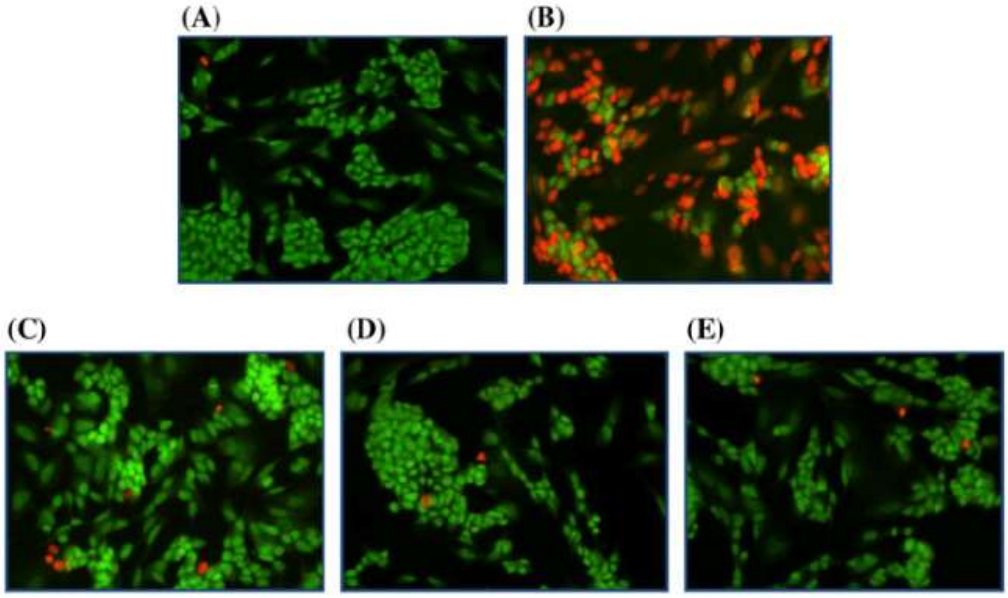

Figure 3.45. Florescent image of mixed (colored as Red & Green) double staining on SH-SY5Y human cells under fluorescent microscope [59]

We obtained clear images after the second trial using the florescent microscope. In the first test, we incubated the samples for 3 days. We only took measurements from the surfaces of DLC coated steel samples. However, the 3-day period was not long

enough to properly observe bacteria, and the surfaces were too rough and scratched to capture clear florescent images. Due to the uneven surface topography with micro level skewness, it was nearly impossible to capture images of most bacteria on the surfaces in a single shot. We believe that the DLC coating was effective in killing bacteria and making it difficult for them to attach to the surface. In the second trial, we extended the incubation period to 5 days and transferred bacteria from the surfaces of the samples between the flat, optically smooth glasses. We increased the total number of samples to be measured, including one steel sample and one smooth lamella sample for each 100 nm DLC coated, 200 nm DLC coated, and uncoated control samples.

The time elapsed between taking the samples from place of the incubation zone to the florescent microscope is less than 1.5 hour including the operation of placing between lamellas. We carry them in proper conditions and packages. Hence, we assure that we kept bacteria as they are.

We could not take proper results from the 50 nm DLC coated samples but the other (especially 200 nm) DLC coated samples give very admirable and good results. Hence, we show and comment on the best results below:

3.16.1 Florescent microscope results for the uncoated steel (Control) sample:

3.16.1.1 Bacteria on Lamella (Agar/Fluid):

Florescent image shown in the Figure 3.46. is taken from fluid which lays over the Control sample. We put the fluid between two lamellas of glass. Thanks to the flatness and optical grade surface smoothness of the lamellas, we could obtain clear and bacteria rich images. Figure 3.46. clearly shows that most of the bacteria are stained as green, in other words they are overwhelmingly alive and some of them are already divided two or more times.

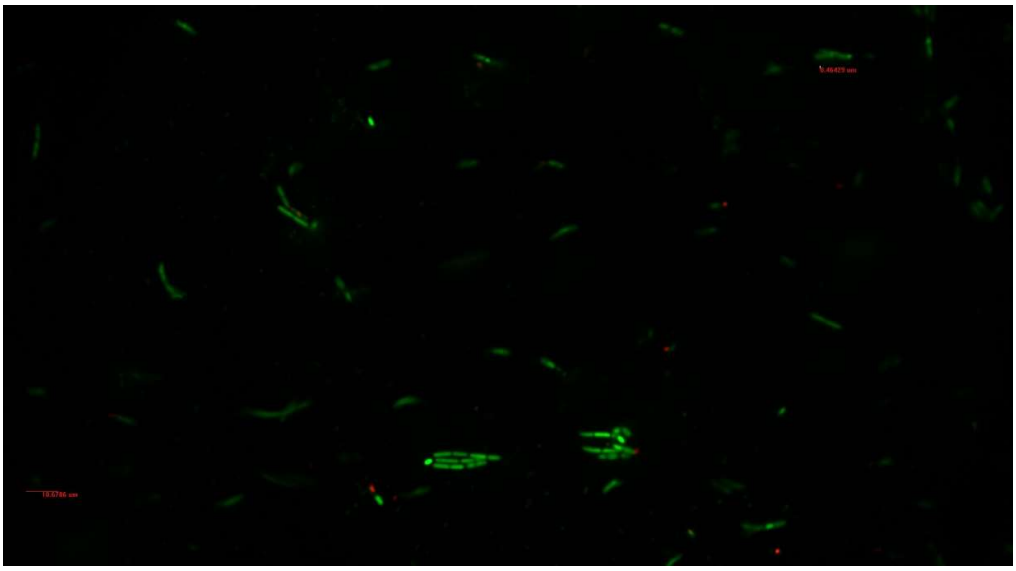

Figure 3.46. Florescent image of mixed (colored as Red & Green) *Mycobacterium chimaera* on lamella which is taken from the uncoated Control sample

3.16.1.2 Bacteria on Sample (on Steel):

As expected, images taken directly on the sample show very rarely populated bacteria, as seen in Figure 3.47. The main reason for this is the surface roughness mentioned above. Furthermore, if we extend the incubation time, we will likely obtain more densely populated bacteria on the surface.

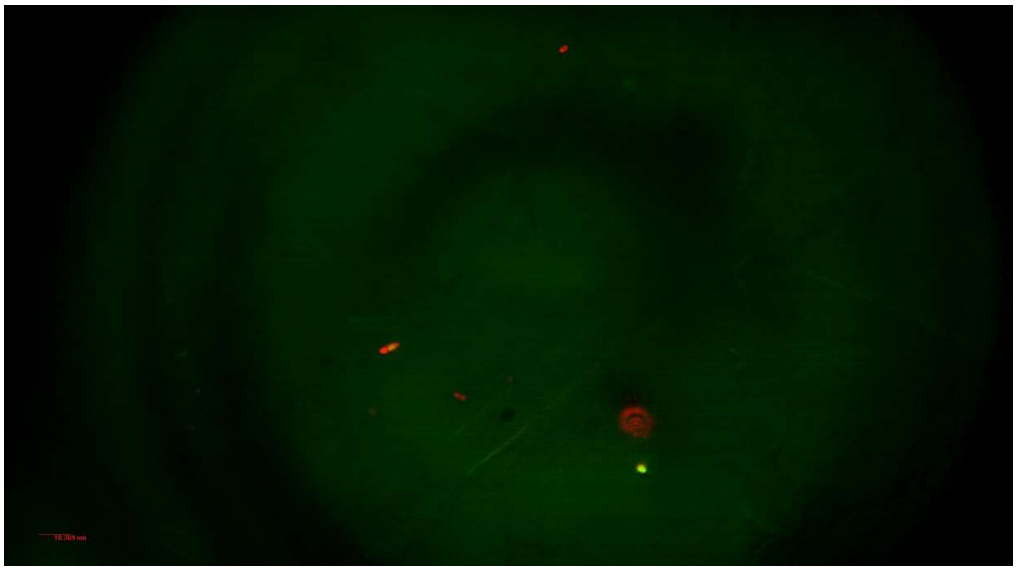

Figure 3.47. Florescent image of mixed (colored as Red & Green) *Mycobacterium chimaera* on substrate which is the uncoated control sample

3.16.2 Florescent microscope results for the 100 nm DLC coated sample:

3.16.2.1 Bacteria on Lamella (Agar/Fluid):

The image shown in Figure 3.48. is for the 100 nm DLC coated sample and as it clearly suggests more than half of the bacteria are killed due to the coating and released in the fluid.

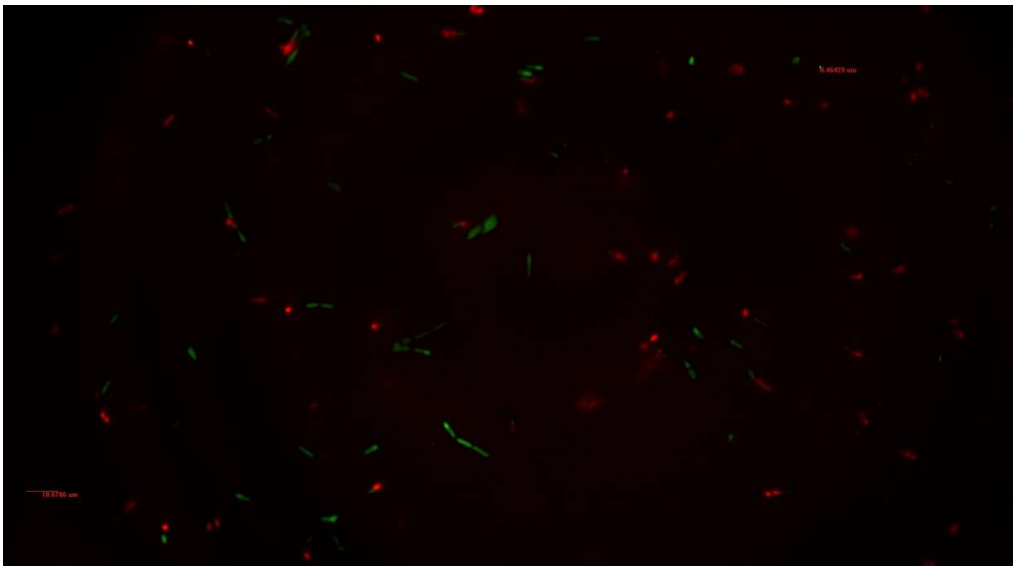

Figure 3.48. Florescent image of live & dead (mixed) *Mycobacterium chimaera* on lamella which is taken from the 100 nm DLC coated sample

3.16.2.2 Bacteria on Sample (DLC on Steel):

As we expected image taken from directly on the sample gives us very rarely populated bacteria as in the Figure 3.49. There is two reason for this we consider, one is that the surface of the sample is too rough to observe at single shoot. The other reason is that 100 nm thick DLC film cannot accommodate the bacteria to attach itself.

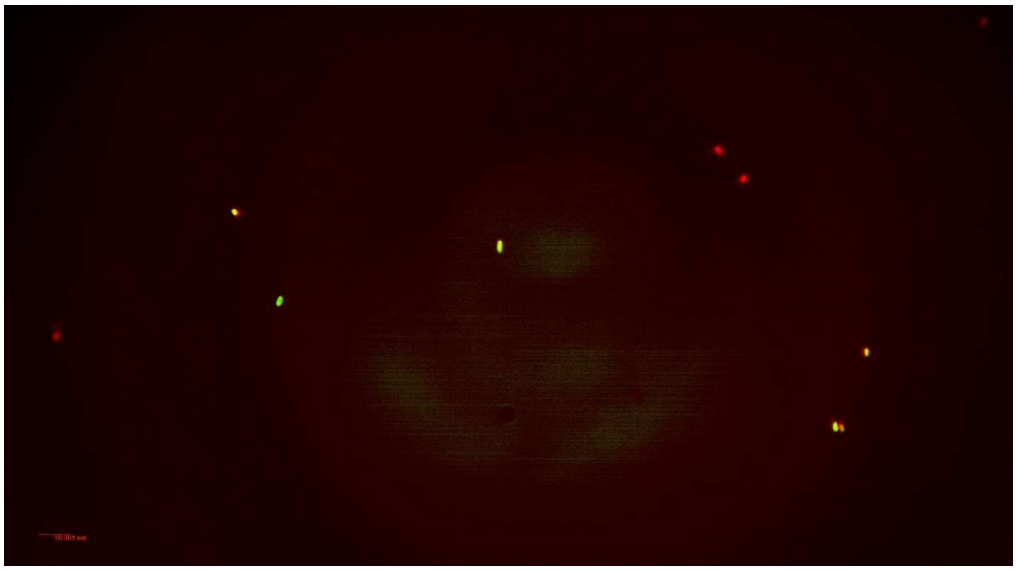

Figure 3.49. Florescent image of live & dead (mixed) *Mycobacterium chimaera* on substrate which is the 100 nm DLC coated sample

3.16.3 Florescent microscope results for the 200 nm DLC coated sample:

3.16.3.1 Bacteria on Agar (Fluid):

The image shown in Figure 3.50. is for the 200 nm DLC coated sample and it is the sharpest and most clear image showing that most of the bacteria are killed due to the 200 nm DLC coating and released in the fluid.

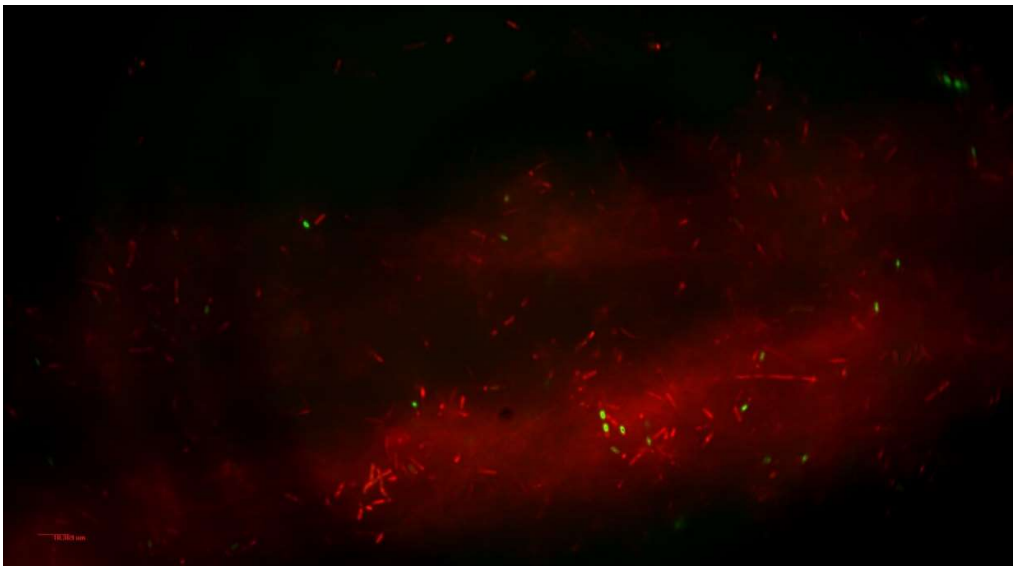

Figure 3.50. Florescent image of live & dead (mixed) *Mycobacterium chimaera* on lamella which is taken from the 200 nm DLC coated sample

3.16.3.2 Bacteria on Sample (DLC on Steel):

Another image showing very rarely populated bacteria as in the Figure 3.51. Again, we thought that the surface of the sample is too rough to observe at single shoot. On the other hand, we observe redder (dead) bacteria on the surface. The reason is that 200 nm thick DLC film killed the bacteria which can barely attached to surface and furthermore most of the bacteria cannot accommodate to attach on 200 nm DLC film.

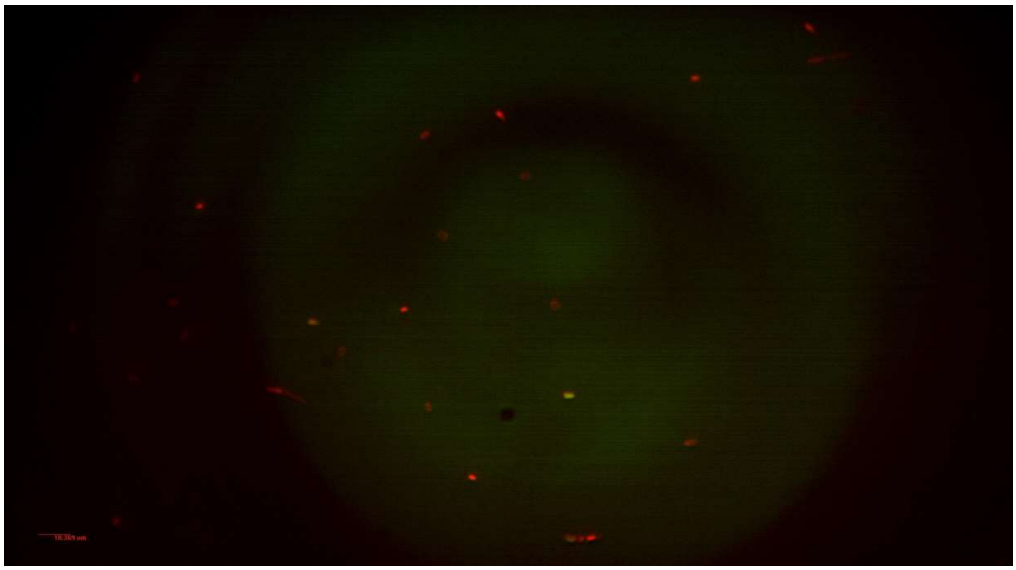

Figure 3.51. Florescent image of live & dead (mixed) *Mycobacterium chimaera* which is taken from the 200 nm DLC coated sample

We count the red (killed) and green (live) bacteria on the images and tabulated the results in Table 3.10. As the table suggests lowest numbers of dead bacteria are for the control (uncoated) samples (about 10%). On the other hand, as the thickness increases, the kill rates are also increasing. The most successful sample is the 200 nm DLC coated steel sample, the kill rates go over 80%.

Table 3.10. number of the red & green stained bacteria for the samples

	Control Steel	Control Fluid	100nm Steel	100nm Fluid	200nm Steel	200nm Fluid
Green	4	77	6	32	3	18
Red	3	9	9	55	20	71
Kill Rate	43%	10%	60%	63%	87%	80%

Furthermore, Figure 3.52. shows a very clear image of how the DLC thin film affects the bacteria on the surfaces. It is obvious that 200 nm DLC coated sample is the most successful one in terms of antibacterial properties.

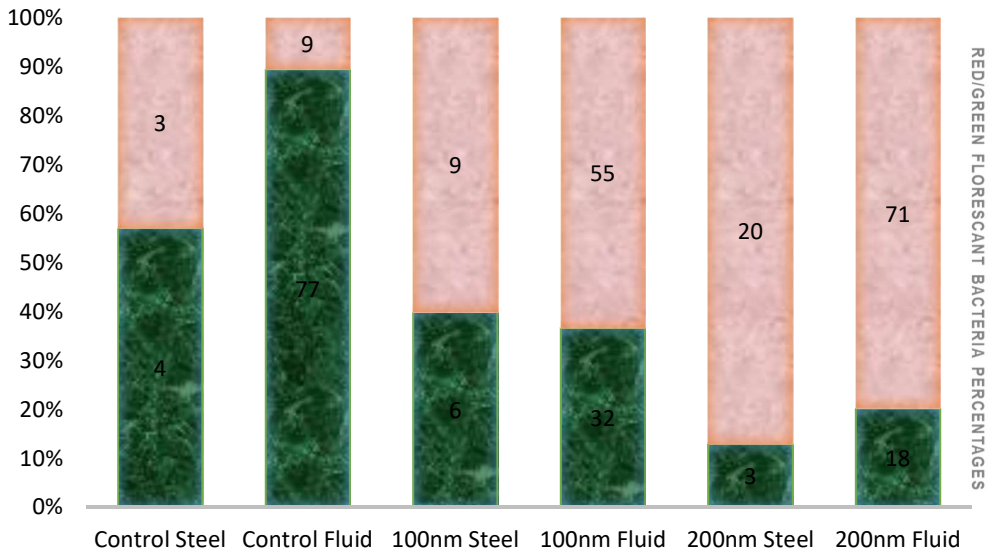

Figure 3.52. The comparative graph for live/dead percentages for each sample

3.17 The FTIR & ATR Measurements of *Mycobacterium chimaera*

Mycobacteria chimaera is a slow-growing NTM species. Furthermore, it has high resistance to antimicrobials. The resistance of mycobacteria chimaera to antimicrobials mostly due to protective biofilm matrix of extracellular polymeric substances (EPS). The biofilm of mycobacteria chimaera on the surfaces starts to form during the first week. However, at least 4 weeks is needed to be enclosed entirely in extracellular matrix [57]. In this study, we waited 6 weeks to develop a complete biofilm to be established safely.

There are different methods to observe or validate biofilms. FTIR is one of the methods. We measure DLC coated steel samples by reflection mode. We made two series measurements for all samples. The first series is done before the incubation and the second series is done after 6 weeks incubation period. We expect to see a difference between two measurements. The characteristic curve for a bacterial biofilm is given in Figure 3.54. [56].

FTIR measures the samples with just one shot, meaning it sends an IR spectrum signal. The signal can either hit the surface and reflect back on the detector, or it can pass through the film or matter and fall on the detector. This limited path through the material or film results in a lack of sufficient data on the material or film. Obtaining a proper graph to identify the material in the film is challenging, but it is possible to observe the film by comparing measurements taken before and after film development. Figure 3.53. displays the results for a specific wavelength interval of 1500-1750 cm-1 in reference to Figure 3.54.

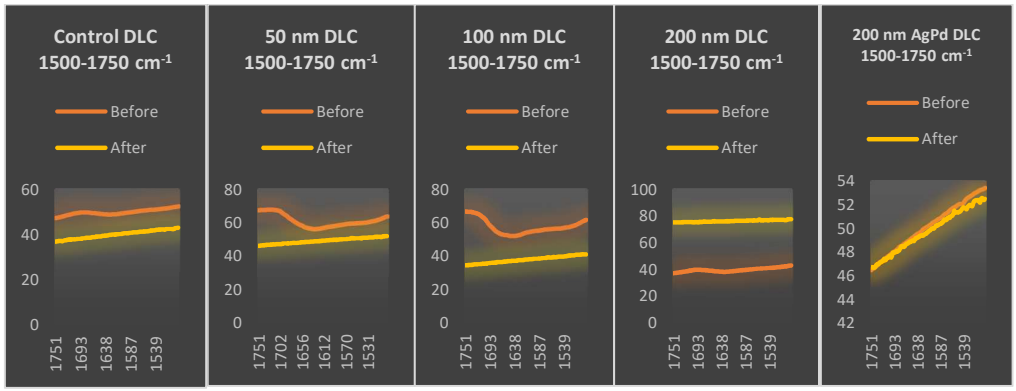

Figure 3.53. FTIR (in reflection mode) measurements before and after the film developed on the samples

Figure 3.53. provides information that AgPd doped DLC has a graph that is nearly identical before and after incubation. This suggests that DLC, when combined with a small amount (3 nm) of AgPd doped layer, demonstrates strong antibacterial properties against *Mycobacterium chimaera*.

Although we have obtained FTIR results on the samples, we should use another measuring technique that can provide more information on the film structure. ATR-FTIR (or ATR) is an appropriate technique for analyzing films and materials. The principle of the ATR-FTIR technique is that emitted infrared wave enters an ATR crystal, which is firmly facing the sample surface or film to be characterized. Then, a series of evanescent waves throughout the sample are collected on the detector.

The total path through the film is longer than in standard FTIR, resulting in more valuable and rich data being collected.

We have samples to measure, specifically: an uncoated and clean SS304 steel, a control sample (uncoated but exposed to bacteria for 6 weeks), 50-100-200 nm DLC coated steel samples, and a 200 nm DLC coated and AgPd seeded sample. The surface of the samples is rough and there are irregularities, causing a mismatch when placing them on the ATR. This results in difficulties during the measurements. The graphs we obtain may not perfectly match the one in Figure 3.54. due to these irregularities, but they show similar patterns, especially for sharp peaks between 1500-1750 cm-1 wavenumbers. Another challenge is that the DLC film has a similar composition to the biofilm we are trying to measure. Both contain carbon and hydrogen elements and bonds. The non-perfect match could also be attributed to the unique composition of the biofilm produced by mycobacteria chimaera, specifically in terms of protein and lipid content.

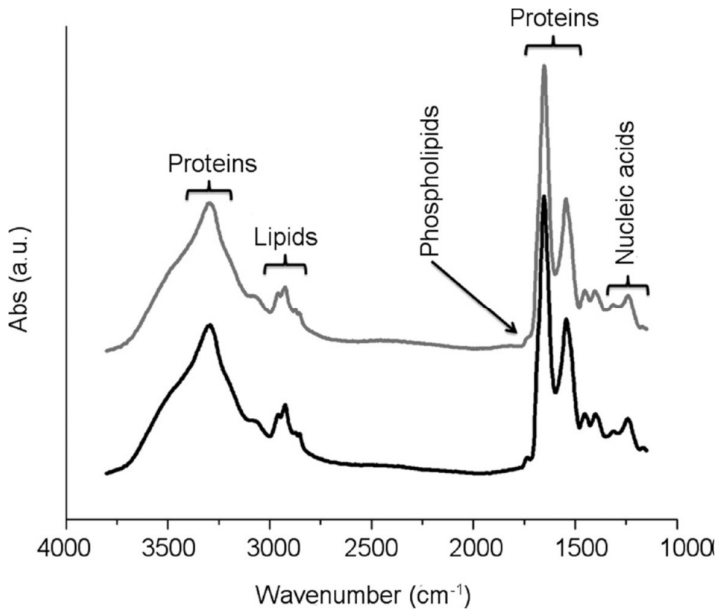

Figure 3.54. Characteristic IR spectra of a biofilm the spectral regions representative for lipids, proteins, nucleic acids, and carbohydrates are shown [56].

3.17.1 The ATR Measurements for the Band of 1500-1750 cm^{-1} wavenumber

The ATR measurement taken on the samples between 1500-1750 cm^{-1} wavenumber is given in the Figure 3.55. As we recognize Control sample has higher protein peak, that means there is thicker biofilm as expected on the surface. On the other hand, 200 nm DLC coated sample shows similar but lower protein peak with the characteristic graph shown in the Figure 3.54. that means 200 nm DLC film inhibits the development of the biofilm.

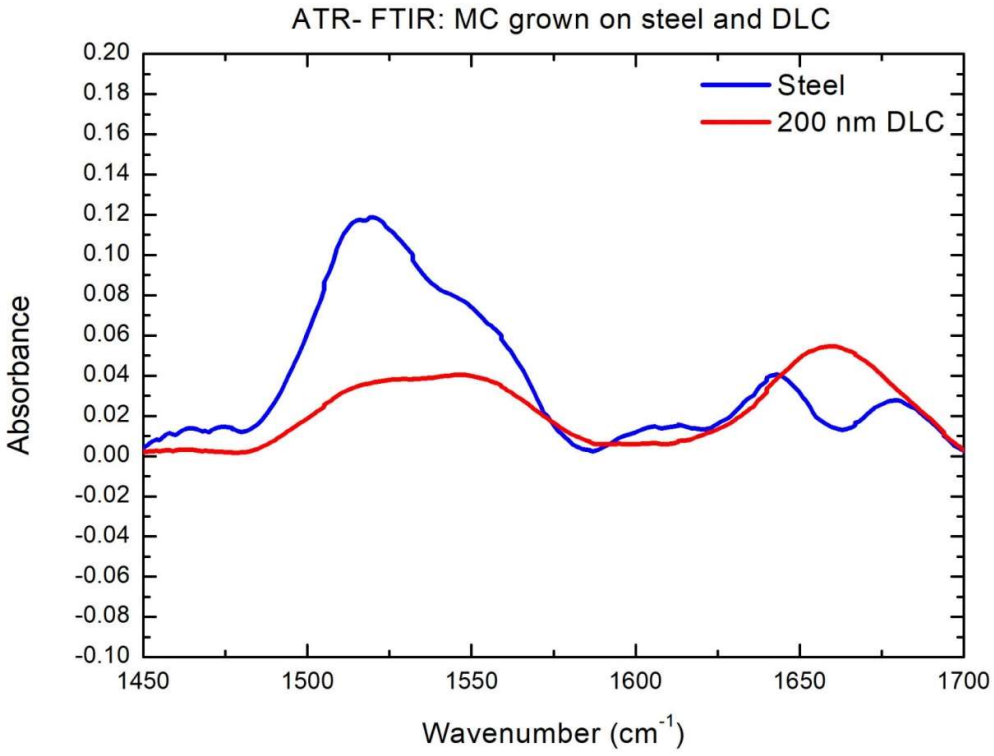

Figure 3.55. The 1500-1750 cm^{-1} wavenumber ATR absorbance results of the samples

CHAPTER 4

CONCLUSION & DISCUSSIONS

Mycobacterium chimaera is commonly found in household water, soil, and even in the air, but typically does not cause illness in healthy individuals during its initial stages of growth without the presence of biofilm. However, it can lead to prolonged complications if introduced into open, deep surgical wounds or directly into the lungs during surgery. Recently, *Mycobacterium chimaera* has been identified as a source of infections specifically linked to Heating Cooling Units (HCU). In this study, we propose the idea that *Mycobacterium chimaera*, like other non-tuberculous mycobacteria (NTM) species, is skilled at forming biofilms on certain materials used in medical devices, particularly those with large surface areas like stainless steel found in HCUs.

In this thesis work, we study SS-304 steel, which is commonly used in HCU units. We coat the SS-304 steel with different DLC thicknesses in nanometer order using a (PE)PCVD machine to observe the relevant effects. The DLC thicknesses used are 50 nm, 100 nm, and 200 nm. Additionally, we apply 1.5-micron DLC films to optical grade Si samples to investigate how thicker films affect anti-bacterial properties. Some of the samples also have a 3 nm Ag-Pd layer added. The literature discusses three main mechanisms, as shown in (Figure 2.12.):

1. Anti-adhesive
2. Contact active
3. Biocide release

After completing all the tests, including adhesion and anti-bacterial tests, as well as measurements such as contact angle, florescence microscope, SEM, and FTIR measurements, we can conclude that DLC, as a hydrophobic film, decreases the

number of *Mycobacterium chimaera* that can adhere to the surface. In other words, it is quite successful in terms of its anti-adhesive properties.

Furthermore, the results suggest that the DLC thin film exhibits contact active characteristics. Although further detailed research is needed, the DLC thin film can be likened to having numerous nano-knives with hard and sharp tips on its surface, which can damage cell membranes and ultimately lead to the death of bacteria.

Silver and its compounds, such as Ag-Pd, are well-known antibacterial materials. We added a very small amount of Ag-Pd to selected samples to observe its impact on the overall antibacterial properties. Figure 2.12. indicates that metals with established antibacterial properties can be incorporated into films to enhance their biocide release and antibacterial capabilities. Thus, we have demonstrated that antibacterial agents can be incorporated into DLC films to improve their effectiveness.

In summary, DLC exhibits promising and effective antibacterial properties against *Mycobacterium chimaera*. Additionally, the antibacterial properties increase as the thickness of DLC increases at the nano-scale.

REFERENCES

[1] C. Donnet, A. Erdemir, “Tribology of diamond-like carbon films: recent progress and future prospects,” Journal of Physıcs D: Applıed Physıcs 39, pp. pp 312-312, 2006.

[2] D. Hofmann, K. Bewilogua ,”History of diamond-like carbon films — From first experiments to worldwide applications,” Surface & Coatings Technology 242, pp. pp 214-215, 2014.

[3] J. A. Byrne, J. McLaughlin, A. Waqar, H. A. Mukhtar, “Study of Human Serum Albumin Adsorption and Conformational Change on DLC and Silicon Doped DLC Using XPS and FTIR Spectroscopy,” Journal of Biomaterials and Nanobiotechnology 4, pp. 194-203, 2013.

[4] H. O. Pierson, Handbook of chemical vapor deposition, New Mexico: Noyes Publications, 1992.

[5] A. Soininen, Studies Of Diamond-Like Carbon And Diamond-Like Carbon Polymer Hybrid Coatings Deposited With Filtered Pulsed Arc Discharge Method For Biomedical Applications., Helsinki: ORTON Research Institute, 2015.

[6] J. Robertson, “Mechanism of sp^3 bond formation in the growth of diamond-like carbon,” Diamond & Related Materials 14 , pp. pp 943-947, 2004.

[7] A. Erdemir, J. Fonatine, C. Donnet, “An Overview of Superlubricity in Diamond-like Carbon Films,” Tribology of Diamond -Like Carbon Films, New York, Springer, pp. 237-262, 2008.

[8] A. Mansour, Structural Analysis of Planar sp^3 and sp^2 Films: Diamond-Like Carbon and Graphene Overlayers, Thuwal: King Abdullah University of Science and Technology, 2011.

[9] Y. Lifshitz, “Diamond-like carbon — present status,” Diamond and Related Materials 8 , p. 1659–1676, 1998.

[10] J. Vlcek, P. Fitl, M. Vrnata, L. Fekete, A. Taylor, F. Fendrych, “UV-laser treatment of nanodiamond seeds—a valuable tool for modification of nanocrystalline diamond films properties,” J. Phys. D: Appl. Phys. 46 , pp. 2-6, 2012.

[11] K. Bewilogua, D. Hofmann, “History of diamond-like carbon films — From first experiments to worldwide applicaitons,” Surface & Coatings Technology 242, pp. pp 215-220, 2014.

[12] S. Pellicori, “Durable Coatings For IR Window Materials,” Durable Coatings For IR Window Materials, 2008.

[13] A. Macleod, Optical Coatings From Design Through Manufacture, Tucson: Thin Film Center Inc, 1999.

[14] A. Erdemir, J. Fonatine, C. Donnet, “Fundamentals of the Tribology of DLC Coatings,” Tribology of Diamond -Like Carbon Films, New York, Springer, pp. 139-154, 2008.

[15] A. Grill, “Electrical and optical properties of diamond-like carbon,” Thin Solid Films 355-356 , pp. 189-193, 1999.

[16] C. Yi-Nan, M. Tian-Bao,Z. Peng-Zhe, Y. Da-Chuan, H. Yuan-Zhong, C. Zhe, W. Hui, “Growth mechanismof hydrogenated amorphous carbon films:Molecular dynamic simulations,” Surface& Coatings Technology 258, pp. 901-907, 2014.

[17] C. Angus, C. Cliff, J. Hayman, “Low-Pressure, Metastable Growth of Diamond and “Diamondlike” Phases,” SCIENCE, VOL. 241, pp. 913-921, 1988.

[18] B. Tian, P.K. Chu, X.M. Cui, H.Q. Zhang, L.H. Li, “Growth and nucleation of diamond-like carbon (DLC) film on aluminum,” Nuclear Instruments and Methods in Physics Research B 206 , p. 691–695, 2003.

[19] G.M. Pharr, Y.J.Park, T.R. Watkins, A.Z. Misra, X. Zhang, C.M. Lepienski, “Factors limiting the measurement of residual stresses in thin films by nanoindentation,” Thin Solid Films 447–448 , p. 251–257, 2004.

[20] Y.Paluleau, “Residual Stresses in DLC Films and Adhesion to Various Substrates,” Tribology of Diamond -Like Carbon Films, Springer, p. 102, 2008.

[21] H. Ronkainen, Tribological properties of hydrogenated and hydrogen-free diamond-like carbon coatings, Espo: VTT Publicaitons, pp. 1-53, 2001.

[22] G.J. KolK, “Wear Resistance of Amorphous DLC and Metal Containing DLC in Industrial Applications,” Tribology of Diamond -Like Carbon Films, New York, Springer, pp. 484-493, 2008.

[23] G. Pagnouxa, S. Fouvryb, M. Peigneyc, B. Delattrea, G. Mermaz-Rolleta, “Influence of scratches on the wear behavior of DLC coatings,” Wear 330-331 , pp. 380-389, 2015.

[24] A. Erdemir, J. Fonatine, C. Donnet, “An Overview of Superlubricity in Diamond-like Carbon Films,” Tribology of Diamond -Like Carbon Films, New York, Springer, pp. 237-262, 2008.

[25] A. Grill, C. Donneta, “Friction control of diamond-like carbon coatings,” Surface and Coatings Technology 94-95, pp. 456-462, 1997.

[26] K.L. Choy, “Chemical vapour deposition of coatings,” Progress in Materials Science 48, p. 57–170, 2003.

[27] C.Jones, M.L. Hitchman, Chemical Vapour Deposition. Precursors, Processes and Applications, Cambridge: Royal Society of Chemistry, 2009.

[28] G. Fedosenkoa, D. Korzeca, A. Schwabedissena, J. Engemanna, E. Bracab, J.M. Kenny, “Comparison of diamond-like carbon films synthesized by 2.45 GHz microwave and 13.56 MHz multi-jet radiofrequency plasma sources,” Diamond and Related Materials 10, pp. 920-926, 2001.

[29] L.Y. Huang, K.W. Xu,J. Lu, B. Guelorget, “Analysis of nano-scratch behavior of diamond-like carbon films,” Surface and Coatings Technology 154, p. 232–236, 2002.

[30] L. Huanga, J. Lub, K. Xua, “Elasto-plastic deformation and fracture mechanism of a diamond-like carbon film deposited on a Ti–6Al–4V substrate in nano-scratch test,” Thin Solid Films 466, pp. 175-182, 2004.

[31] T. Y. Leung, W. F. Man, P.K. Lim, W.C. Chan, F. Gaspari, S. Zukotynski, “Determination of the sp^3/sp^2 ratio of a-C:H by XPS and XAES,” Journal of Non-Crystalline Solids 254 , pp. 156-160, 1999.

[32] X. Lei, J. X. Ma, “Synthesis and Electrochemical Performance of Aluminum Based Composites,” Journal of the Brazilian Chemical Society 21, pp. 209-213, 2009.

[33] M. Cloutier, C. Harnagea, P. Hale, O. Seddiki, F. Rosei, D. Mantovani, “Long-term stability of hydrogenated DLC coatings: Effects of aging on the structural, chemical and mechanical properties,” Diamond & Related Materials 48 , p. 65–72, 2014.

[34] A. K. Gangopadhyay, P. A. Willermet, W. C. Vassell, M. A. Tamor, “Amorphous hydrogenated carbon films for tribological applications II. Films deposited on aluminium alloys and steel,” Tribology International, pp. pp 19-31, 1997.

[35] tydexoptics, “http://www.tydexoptics.com/coatings/DLCcoatings/,” 1994. Available: http://www.tydexoptics.com/. [Retrieved: 10. 06. 2017].

[36] M. Shojiro, I. Junichi, M. Masatoshi, “Dependence ofthefrictiondurabilityofextremelythindiamond-like carbon films on film thickness,” Wear 356-357, p. 66–76, 2016.

[37] Dr Şirin Menekşe, “A report prepared for Kartal Koşuyolu Kalp Damar Cerrahi Hastanesi”, 2021

[38] Murat Günaydın, Keramttin Yanık, Cafer Eroğlu, Ahmet Sanic, İsmail Ceyhan, Zayre Erturan, Rıza Durmaz “Distribution of Nontuberculos Mycobacteria Strains”, 2013

[39] Serap Şimşek-Yavuz “Açık Kalp Cerrahisi Uygulanmış Hastalarda Kontamine Isıtıcı-Soğutucu Cihazlarla İlişkili *Mycobacterium chimaera* İnfeksiyonları: Küresel Bir Salgın” , 2019

[40] Haluk Eraksoy “*Mycobacterium chimaera* ya da Likya’nın Sönmeyen Ateşi”, 2017

[41] Mirko Kaluza1, Gloria Färber, Benjamin May, Ute Dobermann, Mathias W. Pletz, Birgit Edel, Bettina Löffler, Torsten Doenst “Heater–Cooler Devices and Risk of Contamination during Cardiac Surgery”, 2021

[42] F.R. Marciano, L.F. Bonetti, L.V. Santos, N.S. Da-Silva, E.J. Corat, V.J. Trava-Airoldi “Antibacterial activity of DLC and Ag–DLC films produced by PECVD technique” 2009

[43] Tadas Juknius, Modestas Ružauskas, Tomas Tamulevicius, Rita Šiugždiniene, Indre Juknien, Andrius Vasiliauskas, Aušrine Jurkevici , Sigitas Tamulevi “Antimicrobial Properties of Diamond-Like Carbon/Silver Nanocomposite Thin Films Deposited on Textiles: Towards Smart Bandages”, 2016

[44] Rami Sommerstein, Christian Rüegg, Philipp Kohler, Guido Bloemberg, Stefan P Kuster, Hugo Sax “Transmission of *Mycobacterium chimaera* from Heater-Cooler Units during Cardiac Surgery despite an Ultraclean Air Ventilation System” 2016

[45] Archana D. Siddam, Shari J. Zaslow, Yi Wang, K. Scott Phillips, Matthew D. Silverman, Patrick M. Regan and Jayaleka J. Amarasinghe “Characterization of

Biofilm Formation by *Mycobacterium chimaera* on Medical Device Materials", 2021

[46] J.M.Gutiérrez, KatiaConceição,Vitor Martinsde Andradec, V.J.Trava-Airoldi, G.Capotee "High antibacterial properties of DLC film doped with nanodiamond", 2019

[47] Shaun N Robertson, Des Gibson, William G MacKay, Stuart Reid, Craig Williams, Ross Birney "Investigation of the antimicrobial properties of modified multilayer diamond-like carbon coatings on 316 stainless steel", 2017

[48] F.R. Marciano, D.A. Lima-Oliveira, N.S. Da-Silva, E.J. Corat, V.J. Trava-Airoldi "Antibacterial activity of fluorinated diamond-like carbon films produced by PECVD", 2010

[49] https://www.engineeringtoolbox.com/friction-coefficients-d_778.html

[50] Cao, X., Tang, M., Liu, F., Shen, W., & Zhang, W. Surface Functionalization of Polyethersulfone Membrane with Quaternary Ammonium Salts for Contact-Active Antibacterial and Anti-Biofouling Properties. *Journal of Colloid and Interface Science, 589*, 590-601. https://doi.org/10.1016/j.jcis.2020.11.092, 2021

[51] Cheng, Y., Feng, G., Morikawa, A., & Yamamoto, K.. Contact-active antibacterial materials: Mechanisms and applications. *Progress in Materials Science, 105*, 100581. https://doi.org/10.1016/j.pmatsci.2019.100581, 2019

[52] Gittens, R. A., Olivares-Navarrete, R., Tannenbaum, R., Boyan, B. D., & Schwartz, Z.. Electrical polarization enhances the efficacy of the antibacterial properties of bioactive titanium surfaces. *Biomaterials, 32*(30), 7226-7231. https://doi.org/10.1016/j.biomaterials.2011.06.019, 2011

[53] Jiang, J., Pi, Q., Liang, H., & Ren, X. Surface antimicrobial functionalization with polymers: fabrication, mechanisms and applications. *Journal of Materials Chemistry B, 9*(42), 9374-9389. https://doi.org/10.1039/D2TB01555B, 2021

[54] Wang, C.-G., Surat'man, N. E. B., Mah, J. J. Q., Qu, C., & Li, Z. Surface antimicrobial functionalization with polymers: fabrication, mechanisms and applications. *Journal of Materials Chemistry B, 10*(36), 9349-9368. https://doi.org/10.1039/D2TB01555B, . 2022

[55] Yang, L., & Ren, X. Antimicrobial Polymers in Solution and on Surfaces: Overview and Prospects. *Polymer Reviews, 60*(4), 626-671. https://doi.org/10.1080/15583724.2020.1713545, 2020

[56] A Didonna, L Vaccari, A Bek, G Legname. A Infrared microspectroscopy: a multiple-screening platform for investigating single-cell biochemical perturbations upon prion infection CS chemical neuroscience, ACS Publications, 2011

[57] AD Siddam, SJ Zaslow, Y Wang, KS Phillips, MD Silverman, PM Regan, JJ Amarasinghe. Characterization of Biofilm Formation by *Mycobacterium chimaera* on Medical Device Materials. Frontiers in microbiology, 2021

[58] Taburoğlu V.E. "Characterization and Enhancement of IR Optical and Tribological Properties of DLC Films Synthesized by RF-PECVD", MRS Conference Bulletin-Boston/USA, 2017

[59] Zhiping Hou, Maznah Ismail, Rozi Mahmud; Lactoferrin and ovotransferrin contribute toward antioxidative effects of Edible Bird's Nest against hydrogen peroxide-induced oxidative stress in human SH-SY5Y cells; Bioscience Biotechnology and Biochemistry 79(10):1-9, 2015

[60] Aude Cumont,Andrew R. Pitt,Peter A. Lambert,Marco R. Oggioni &Haitao Ye; Properties, mechanism and applications of diamond as an antibacterial material Functional Diamond, 1(1), 1–28, 2021

[61] Tadas Juknius, Modestas Ružauskas, Tomas Tamulevičius, Rita Šiugždinienė, Indrė Juknienė, Andrius Vasiliauskas, Aušrinė Jurkevičiūtė, and Sigitas Tamulevičius ; Antimicrobial Properties of Diamond-Like Carbon/Silver Nanocomposite Thin Films Deposited on Textiles: Towards Smart Bandages, Materials (Basel). 2016 May; 9(5): 371, 2016

[62] Fernanda Marciano, Luis Franscisco Bonetti, J. F. Mangolin, Vladimir Trava-Airoldi. Investigation into the antibacterial property and bacterial adhesion of diamond-like carbon films, Vacuum 85(6):662-666, 2011

APPENDICES

A. Roughness Measurements

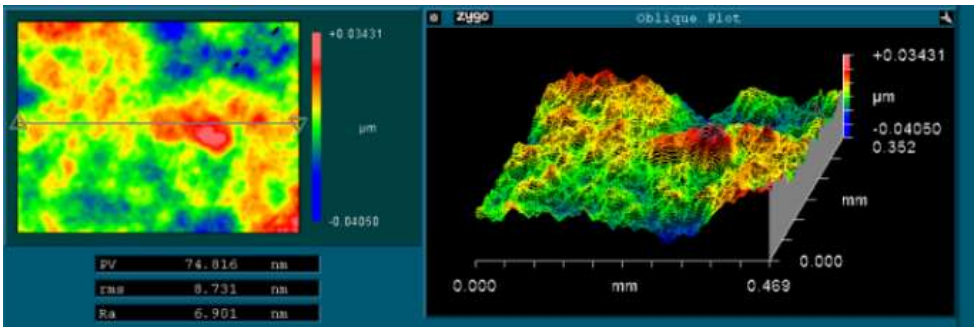

Figure A.1. Roughness Measurement by a Zygo Roughness Measuring Device for Sample #1

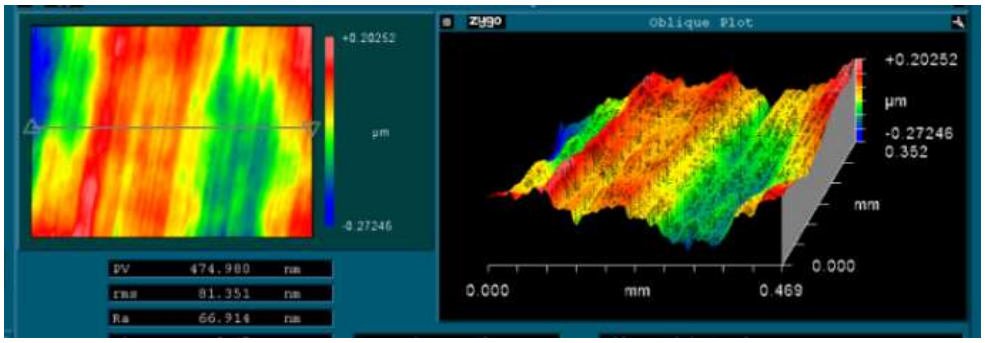

Figure A.2. Roughness Measurement by a Zygo Roughness Measuring Device for Sample #2

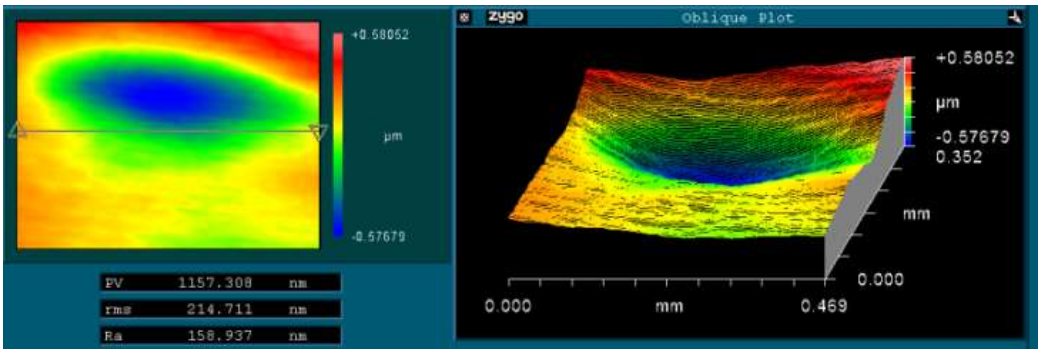

Figure A.3. Roughness Measurement by a Zygo Roughness Measuring Device for Sample #3

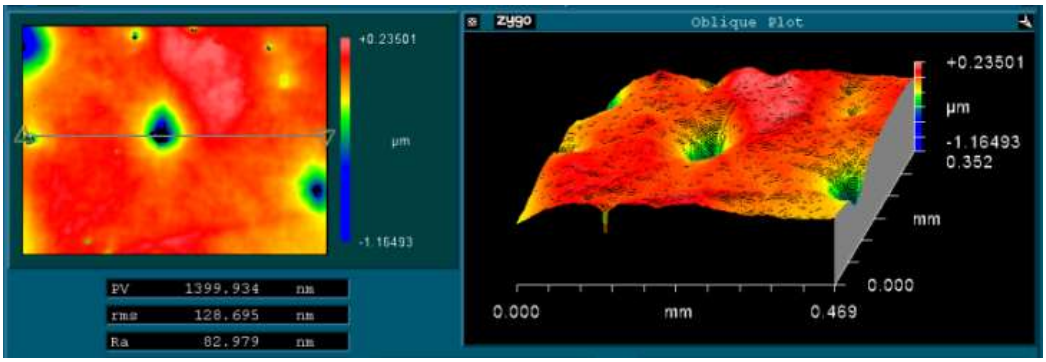

Figure A.4. Roughness Measurement by a Zygo Roughness Measuring Device for Sample #4

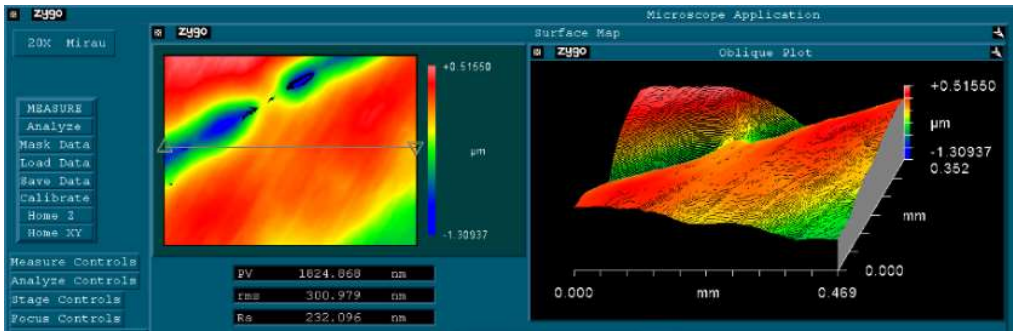

Figure A.5. Roughness Measurement by a Zygo Roughness Measuring Device for Sample #5

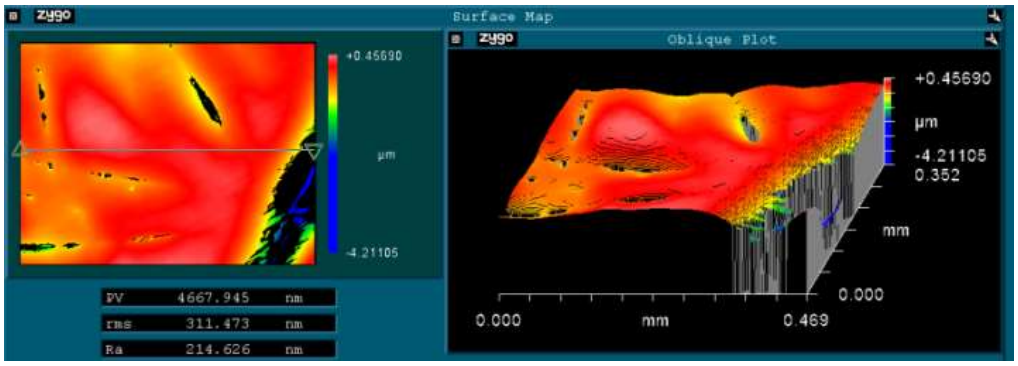

Figure A.6. Roughness Measurement by a Zygo Roughness Measuring Device for Sample #6

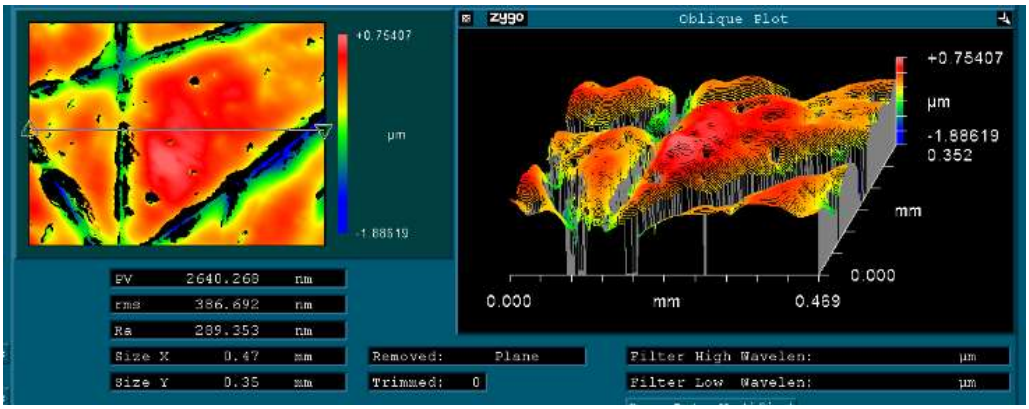

Figure A.7. Roughness Measurement by a Zygo Roughness Measuring Device for Sample #7

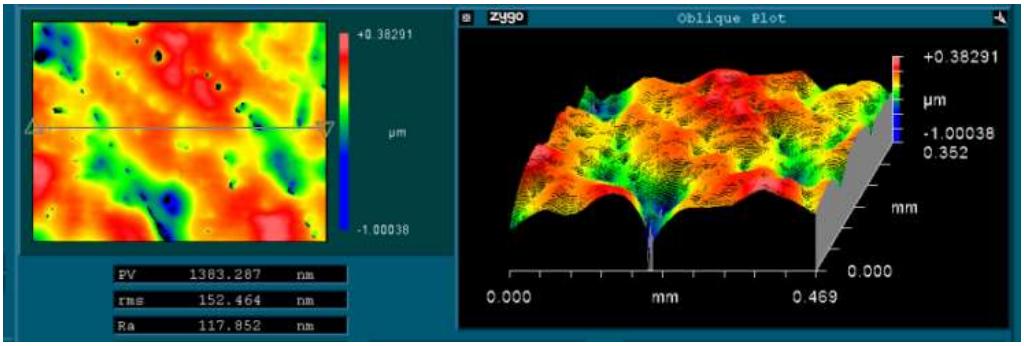

Figure A.8. Roughness Measurement by a Zygo Roughness Measuring Device for Sample #8

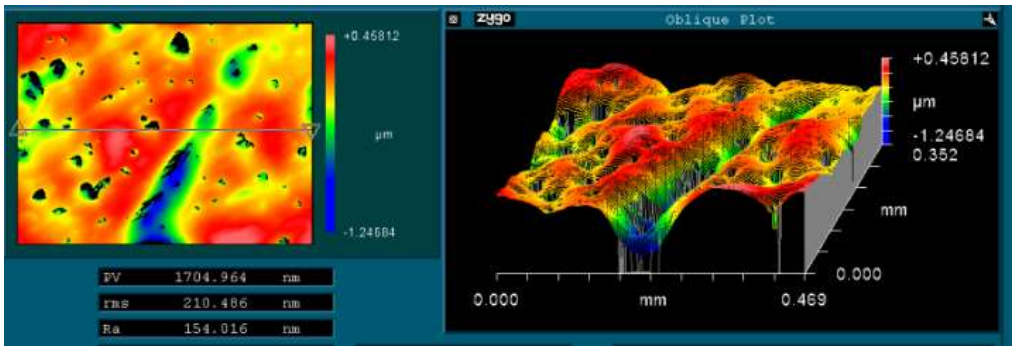

Figure A.9. Roughness Measurement by a Zygo Roughness Measuring Device for Sample #9

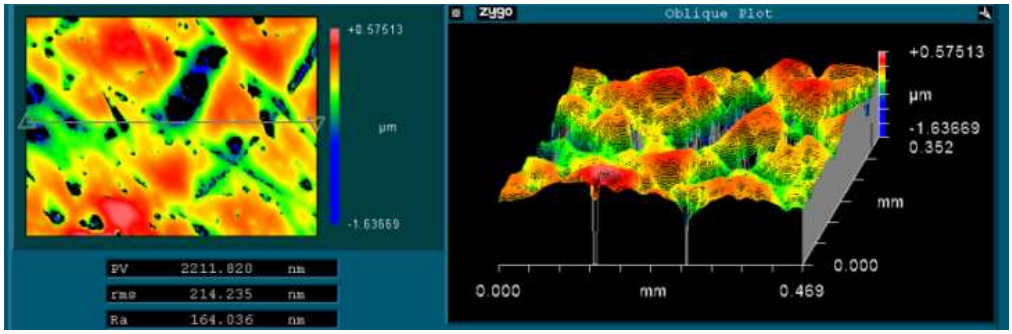

Figure A.10. Roughness Measurement by a Zygo Roughness Measuring Device for Sample #10

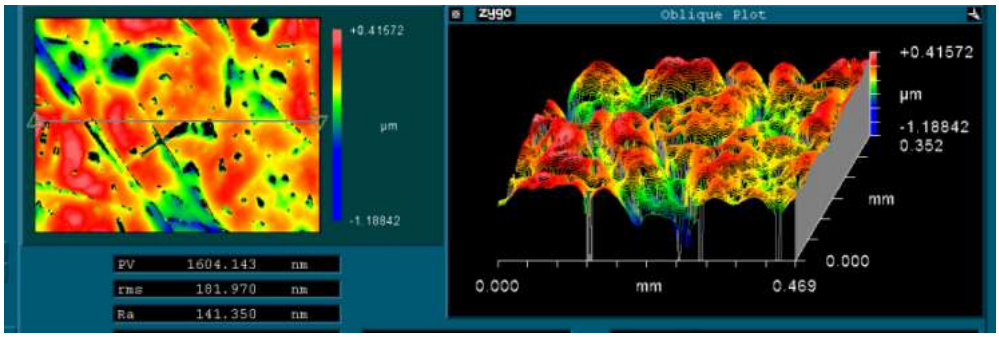

Figure A.11. Roughness Measurement by a Zygo Roughness Measuring Device for Sample #11

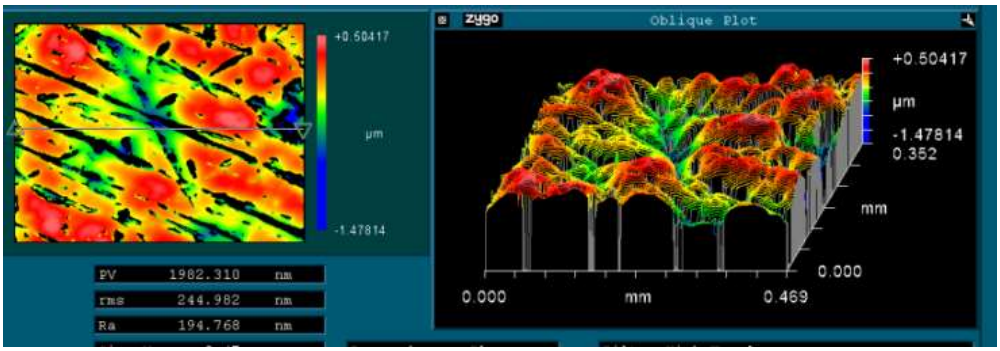

Figure A.12. Roughness Measurement by a Zygo Roughness Measuring Device for Sample #12

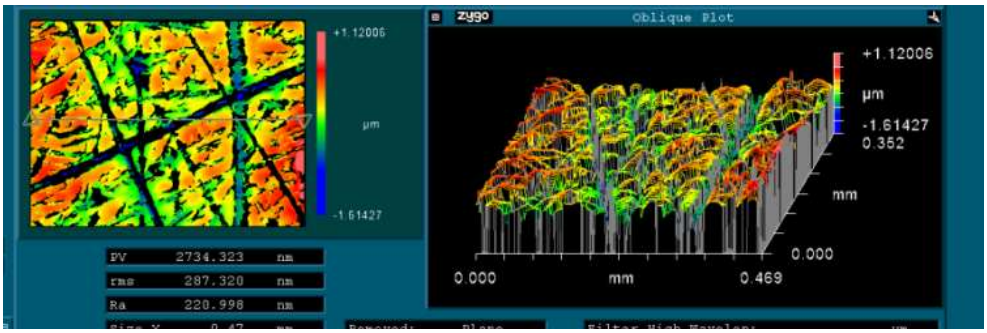

Figure A.13. Roughness Measurement by a Zygo Roughness Measuring Device for Sample #13

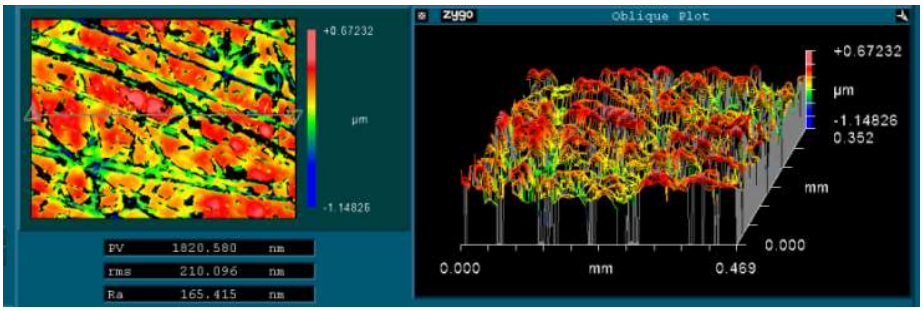

Figure A.14. Roughness Measurement by a Zygo Roughness Measuring Device for Sample #14

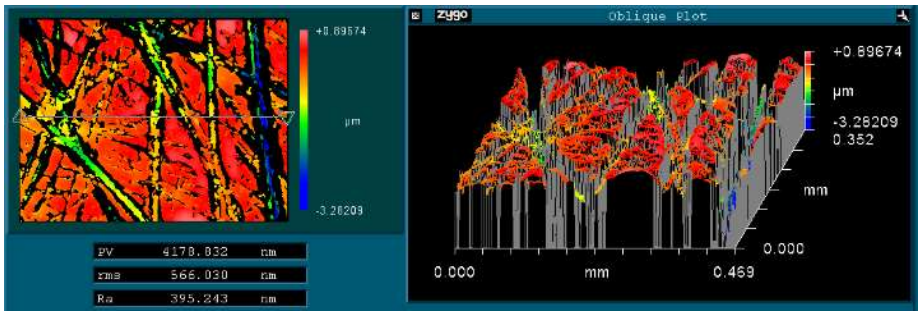

Figure A.15. Roughness Measurement by a Zygo Roughness Measuring Device for Sample #15

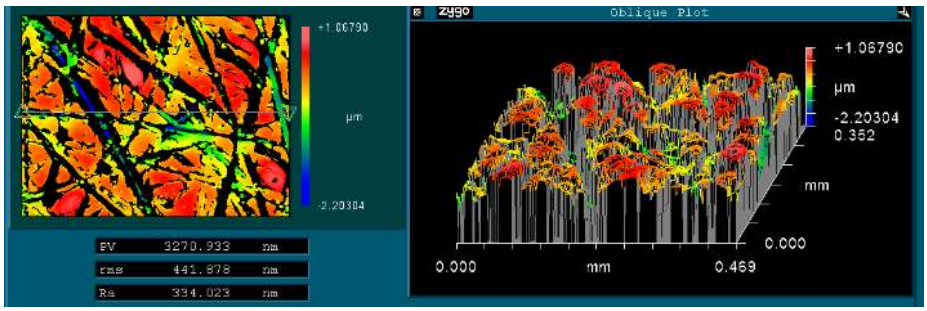

Figure A.16. Roughness Measurement by a Zygo Roughness Measuring Device for Sample #16

B. Friction Measurements

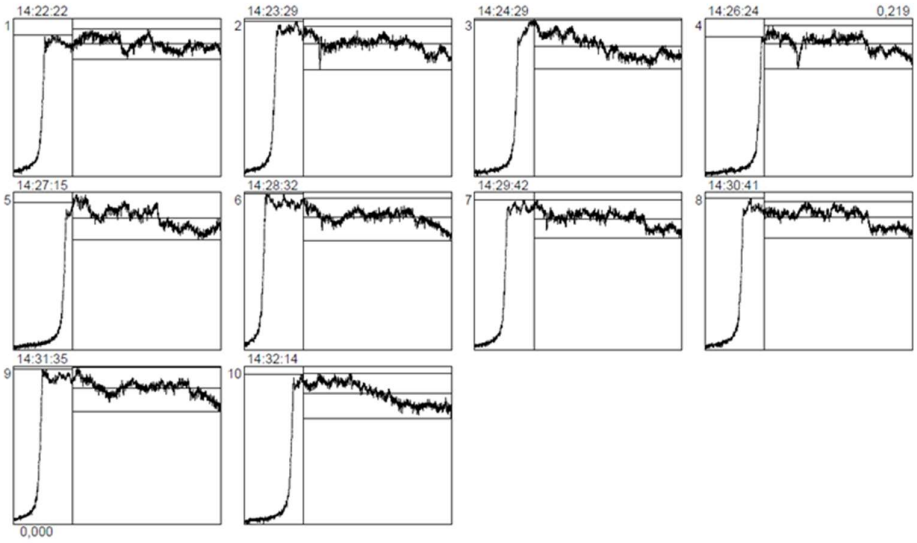

Figure B.17. Friction (Slip) SP-2100 Slip/Peel Test Results for the Sample #30

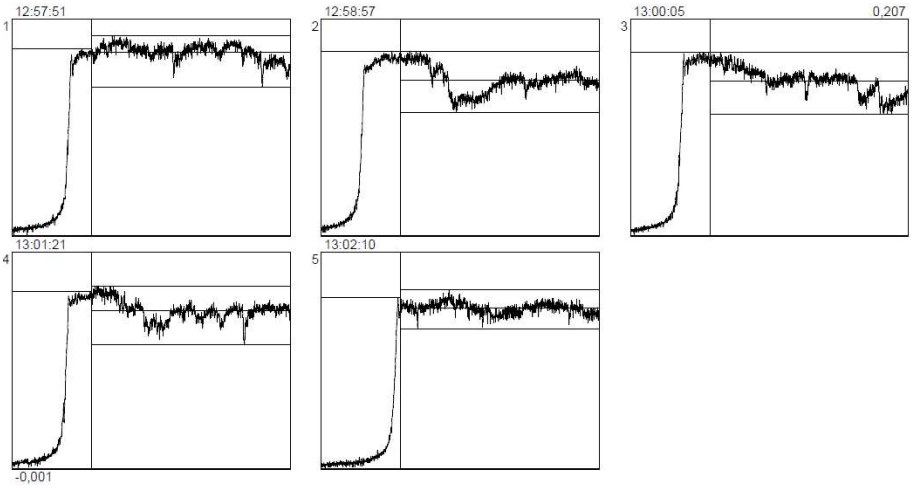

Figure B.18. Friction (Slip) SP-2100 Slip/Peel Test Results for the Sample #5

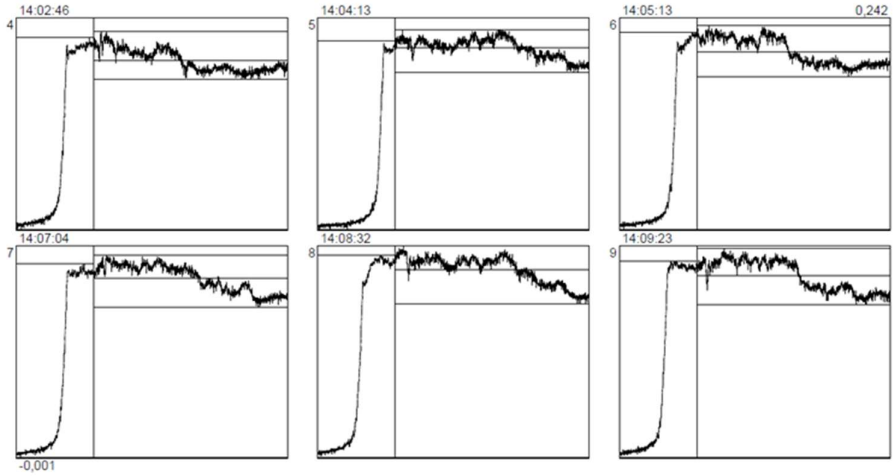

Figure B.19. Friction (Slip) SP-2100 Slip/Peel Test Results for the Sample #7

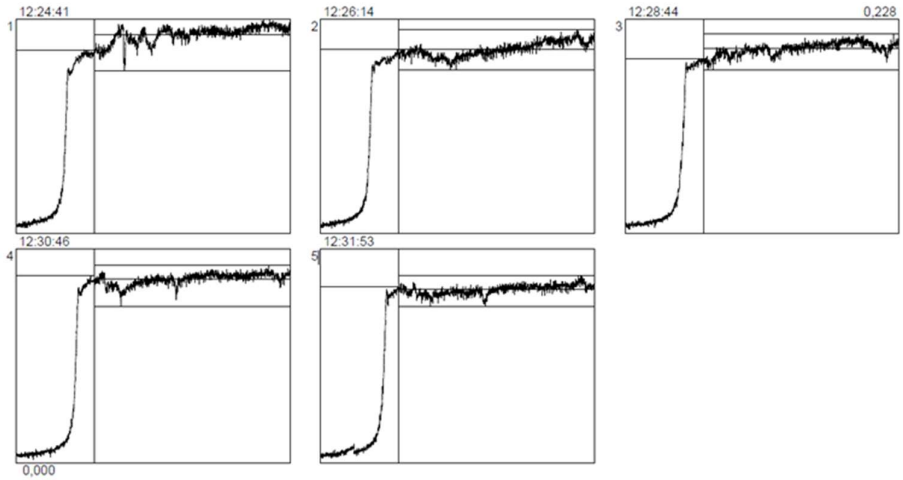

Figure B.20. Friction (Slip) SP-2100 Slip/Peel Test Results for the Sample #23

C. Florescent Microscope Measurement

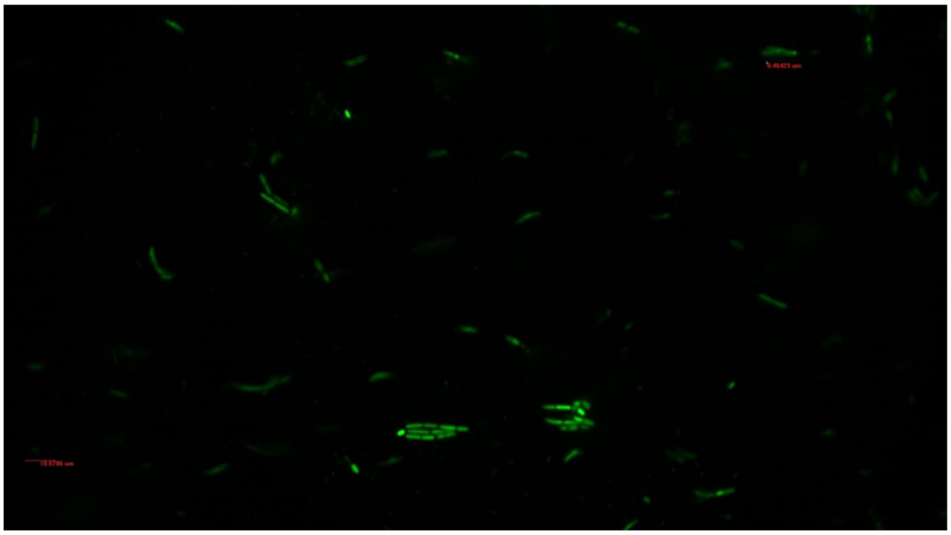

Figure C.21. Florescent image of live *Mycobacterium chimaera* on lamella which is taken from the uncoated control sample

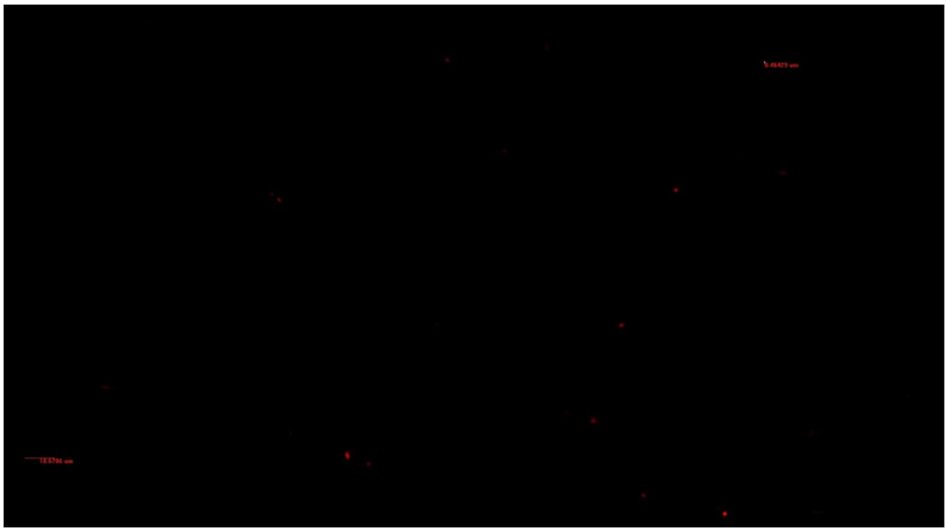

Figure C.22. Florescent image of dead *Mycobacterium chimaera* on lamella which is taken from the uncoated control sample

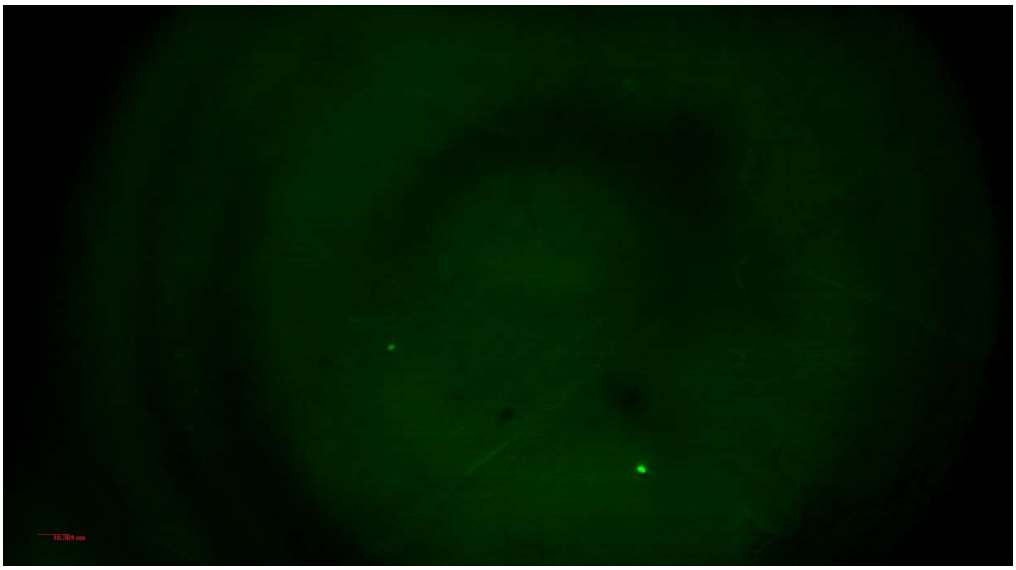

Figure C.23. Florescent image of live *Mycobacterium chimaera* on substrate which is the uncoated control sample

Figure C.24. Florescent image of dead *Mycobacterium chimaera* on substrate which is the uncoated control sample

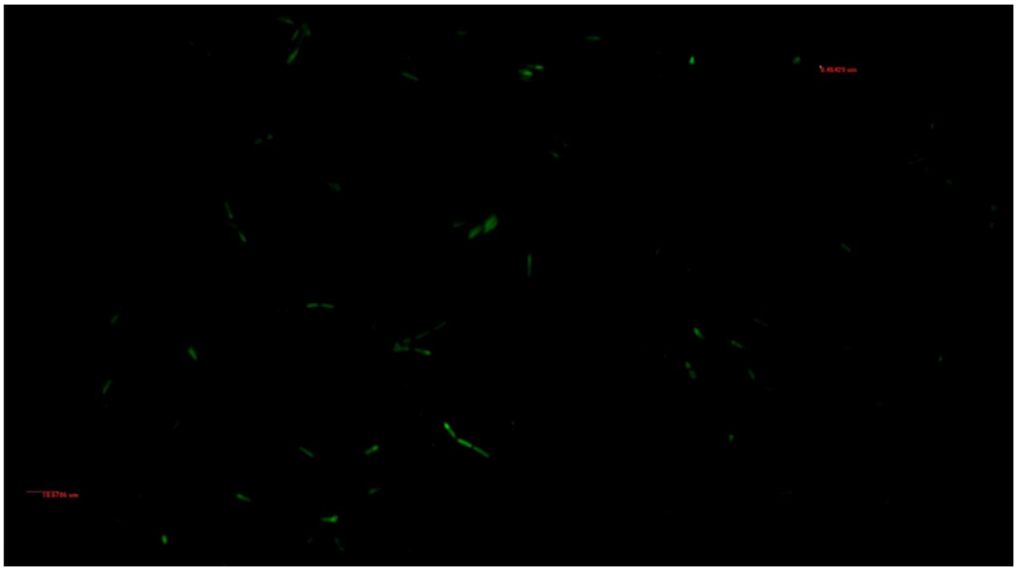

Figure C.25. Florescent image of live *Mycobacterium chimaera* on lamella which is taken from the 100 nm DLC coated sample

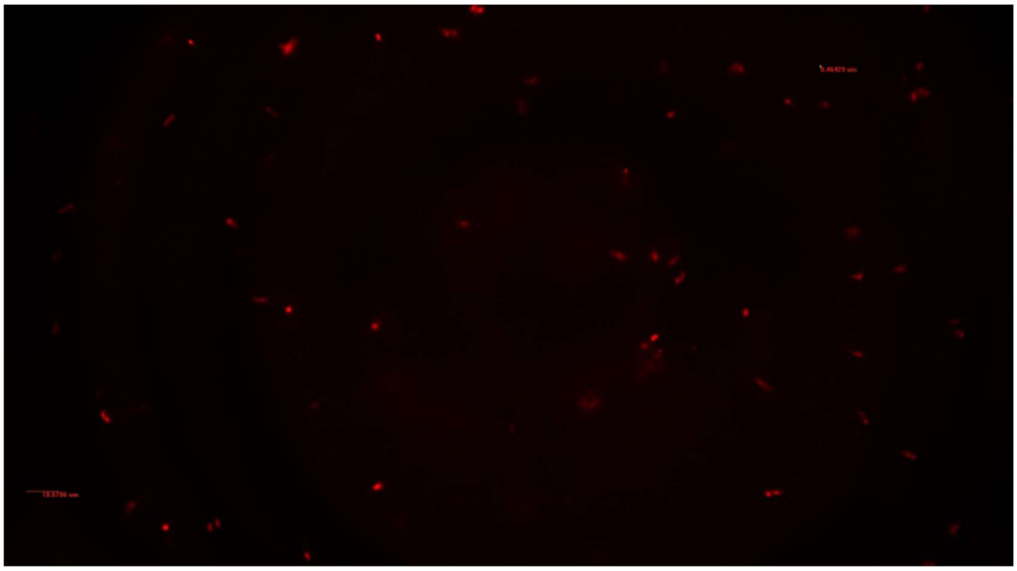

Figure C.26. Florescent image of dead *Mycobacterium chimaera* on lamella which is taken from the 100 nm DLC coated sample

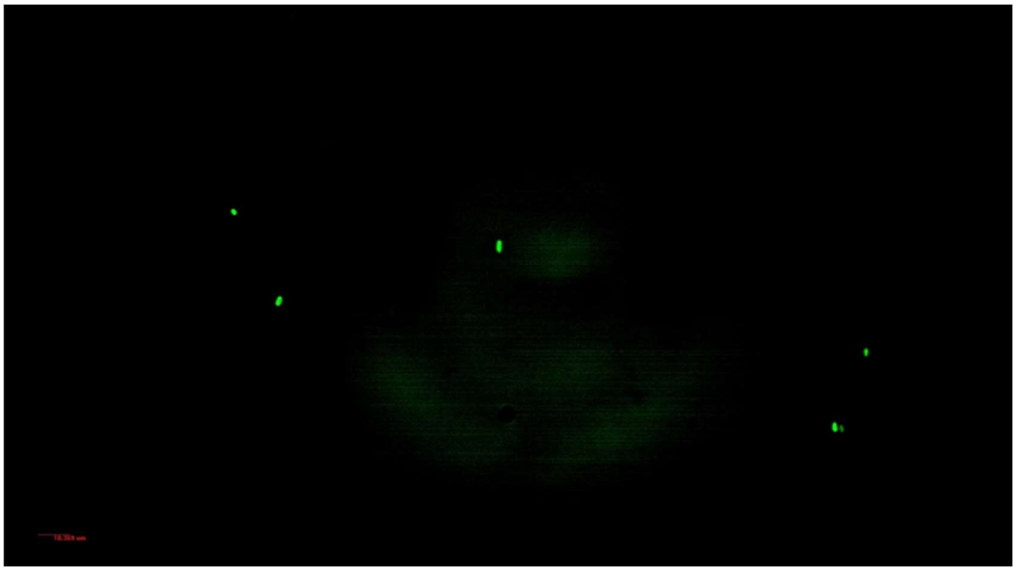

Figure C.27. Florescent image of live *Mycobacterium chimaera* on substrate which is the 100 nm DLC coated sample

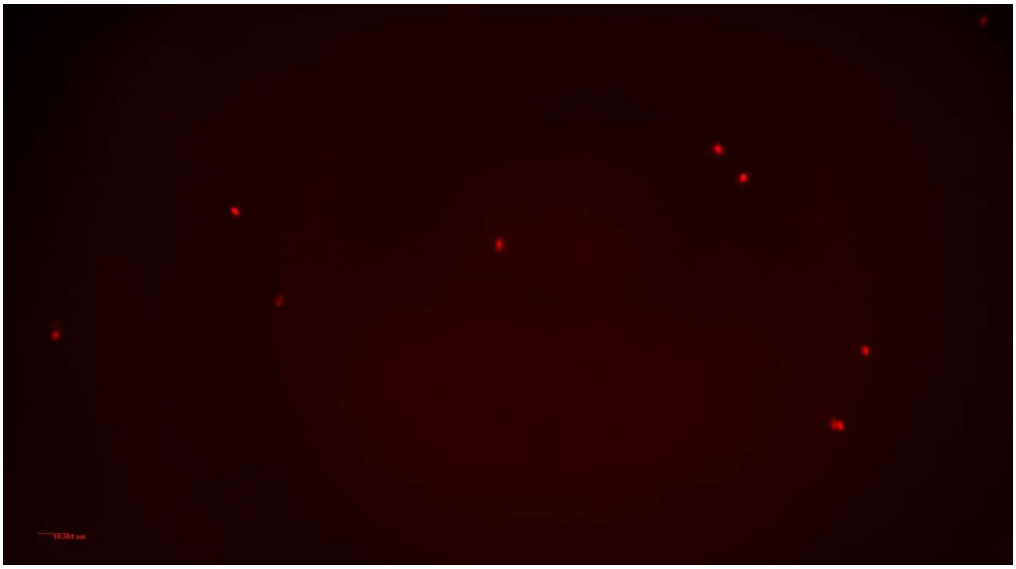

Figure C.28. Florescent image of dead *Mycobacterium chimaera* on substrate which is the 100 nm DLC coated sample

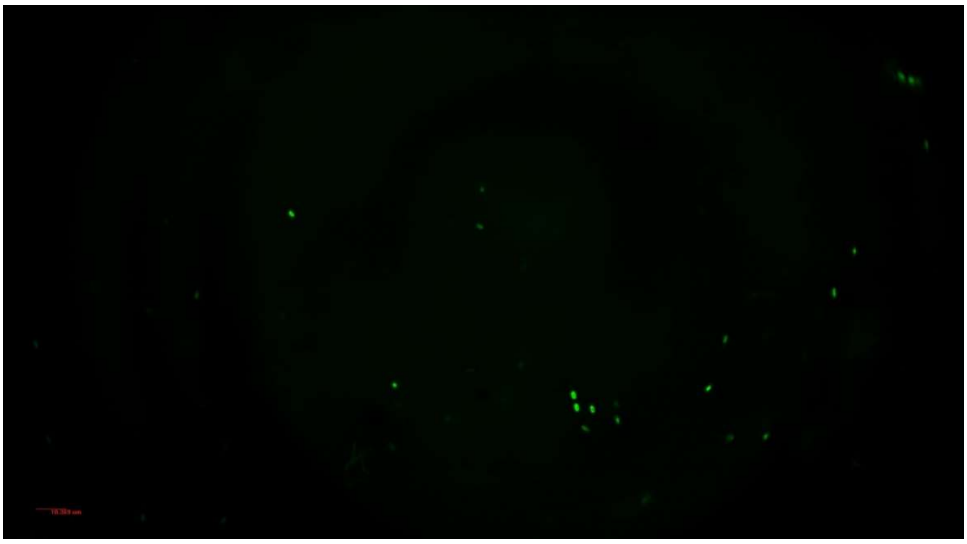

Figure C.29. Florescent image of live *Mycobacterium chimaera* on lamella which is taken from the 200 nm DLC coated sample

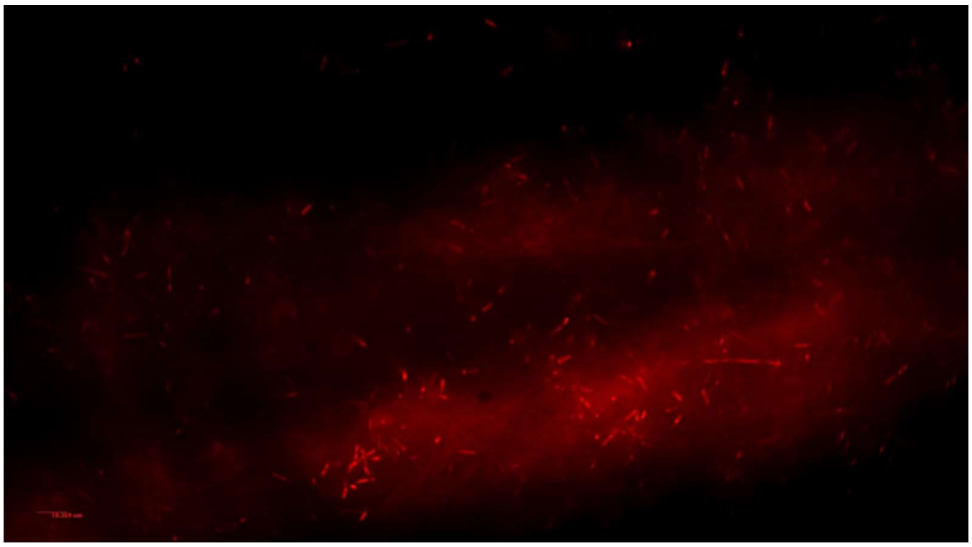

Figure C.30. Florescent image of dead *Mycobacterium chimaera* on lamella which is taken from the 200 nm DLC coated sample

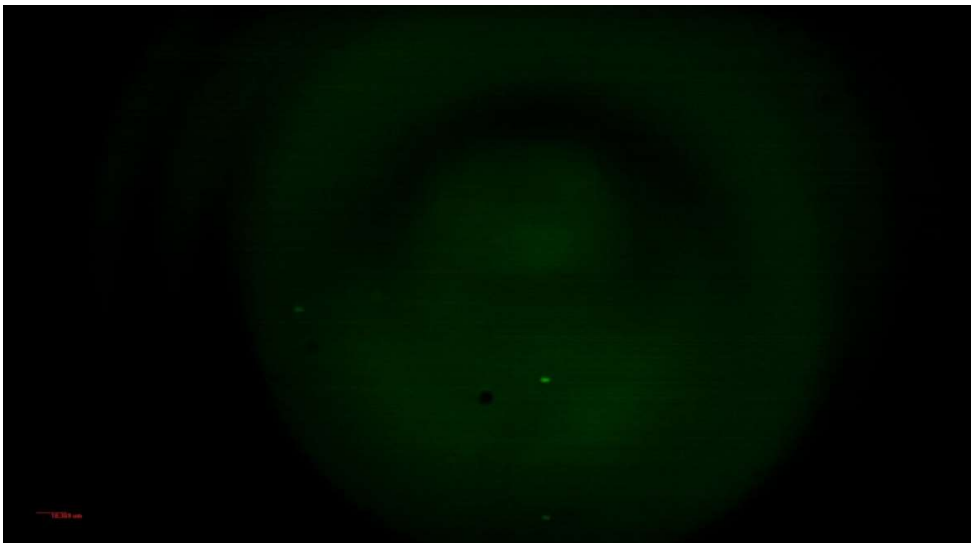

Figure C.31. Florescent image of live *Mycobacterium chimaera* which is taken from the 200 nm DLC coated sample

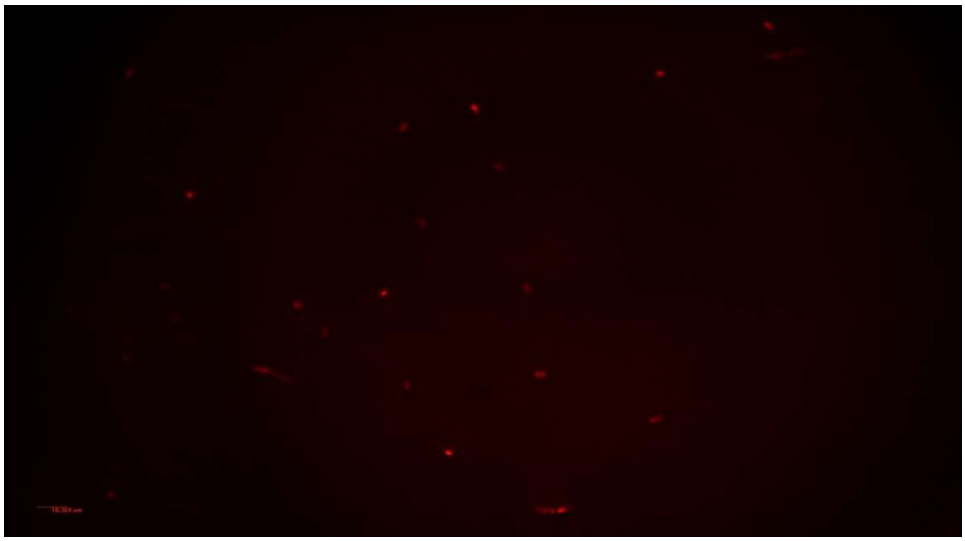

Figure C.32. Florescent image of dead *Mycobacterium chimaera* which is taken from the 200 nm DLC coated sample

D. FESEM Measurements

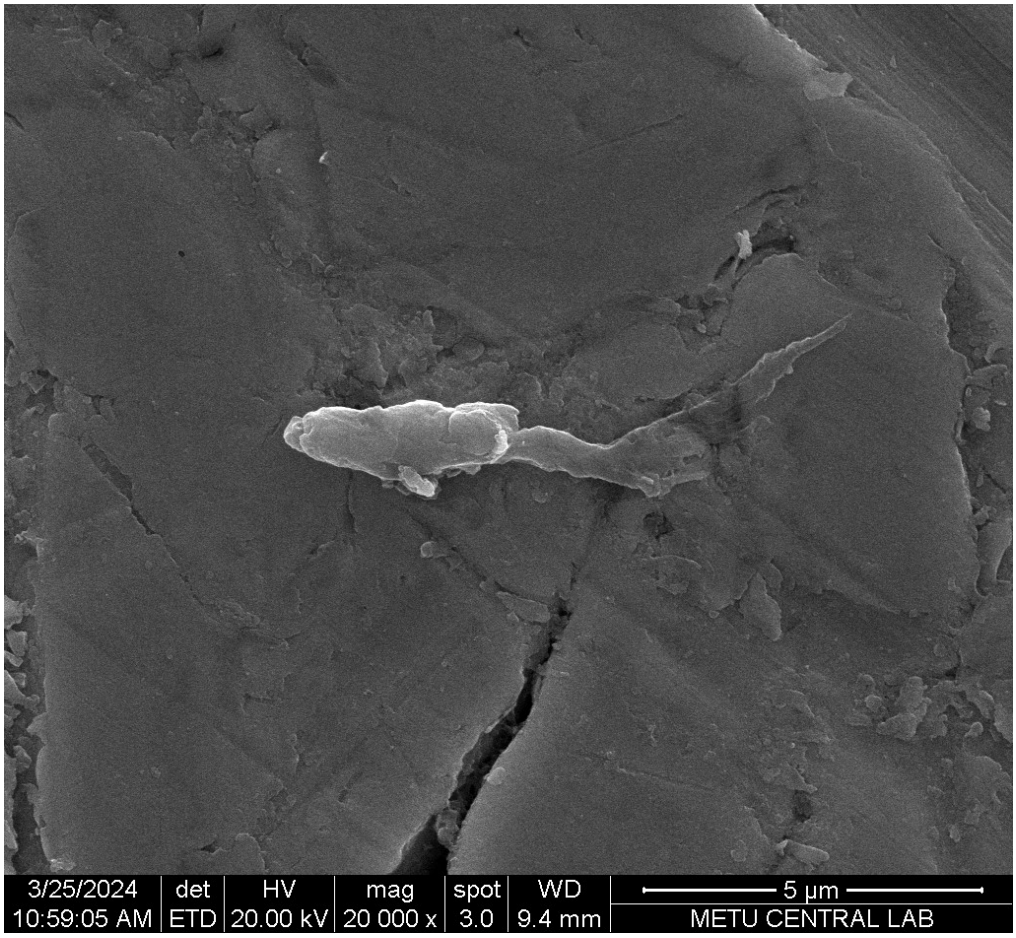

Figure D.33. FESEM image of *Mycobacterium chimaera* which is taken from the Control sample

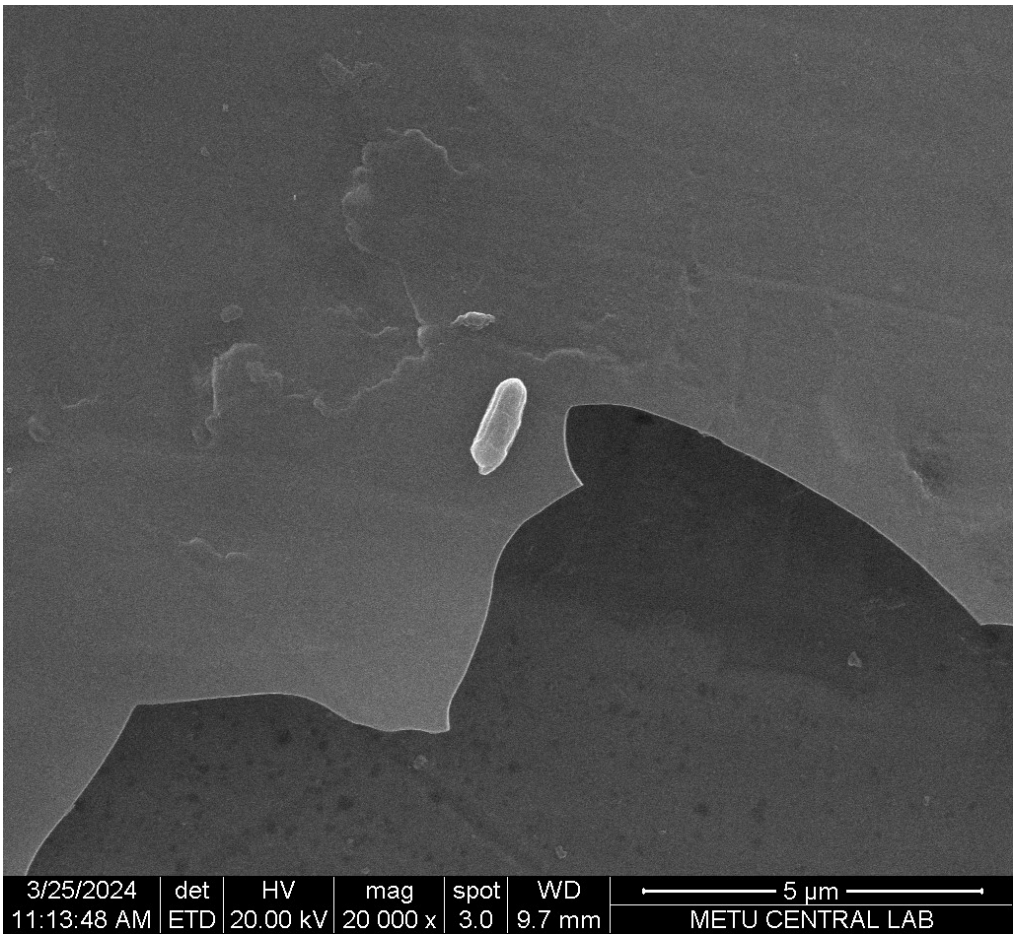

Figure D.34. FESEM image of *Mycobacterium chimaera* which is taken from the 100 nm DLC coated sample

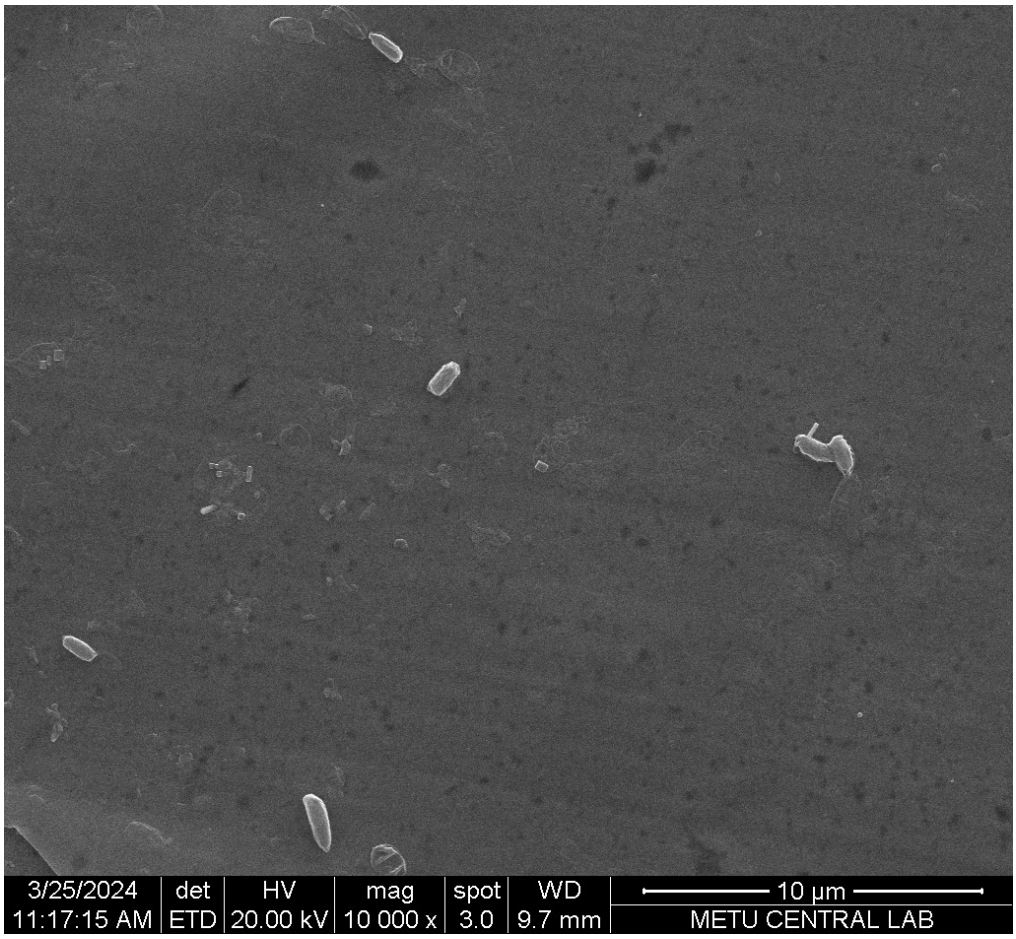

Figure D.35. FESEM image of *Mycobacterium chimaera* which is taken from the 100 nm DLC coated sample

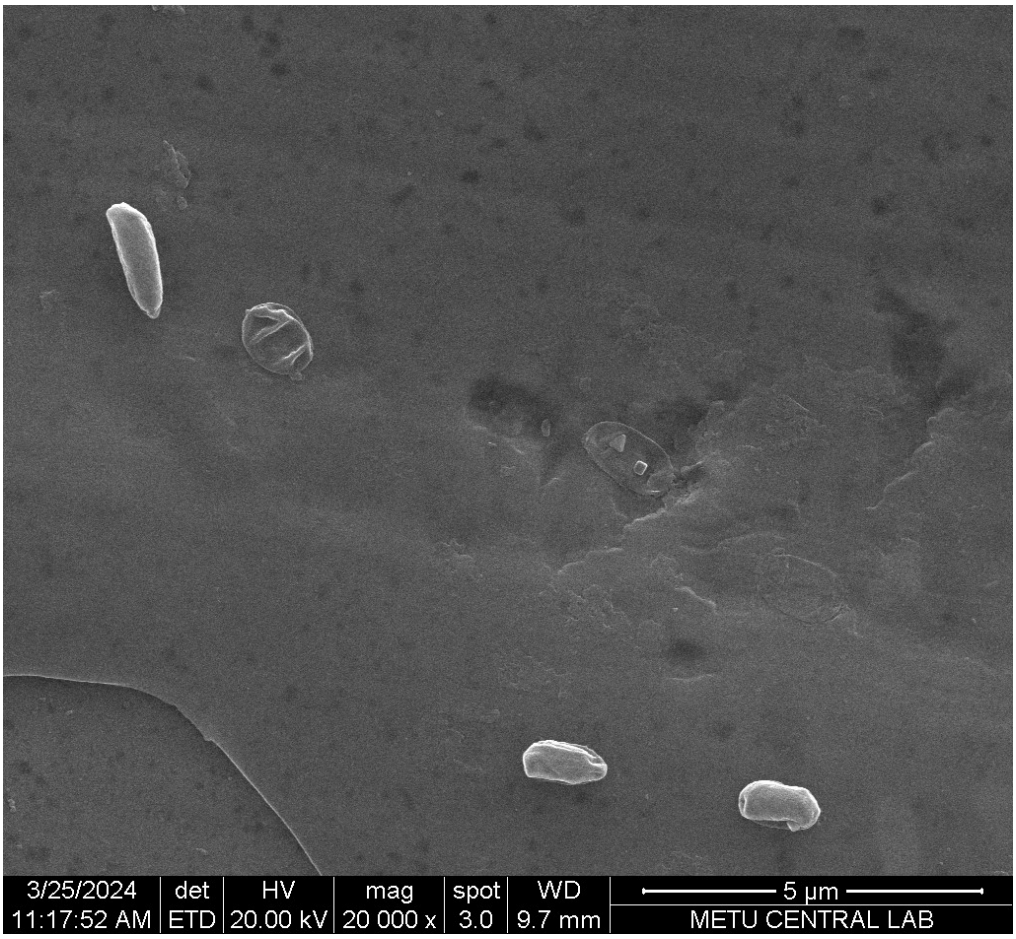

Figure D.36. FESEM image of *Mycobacterium chimaera* which is taken from the 100 nm DLC coated sample

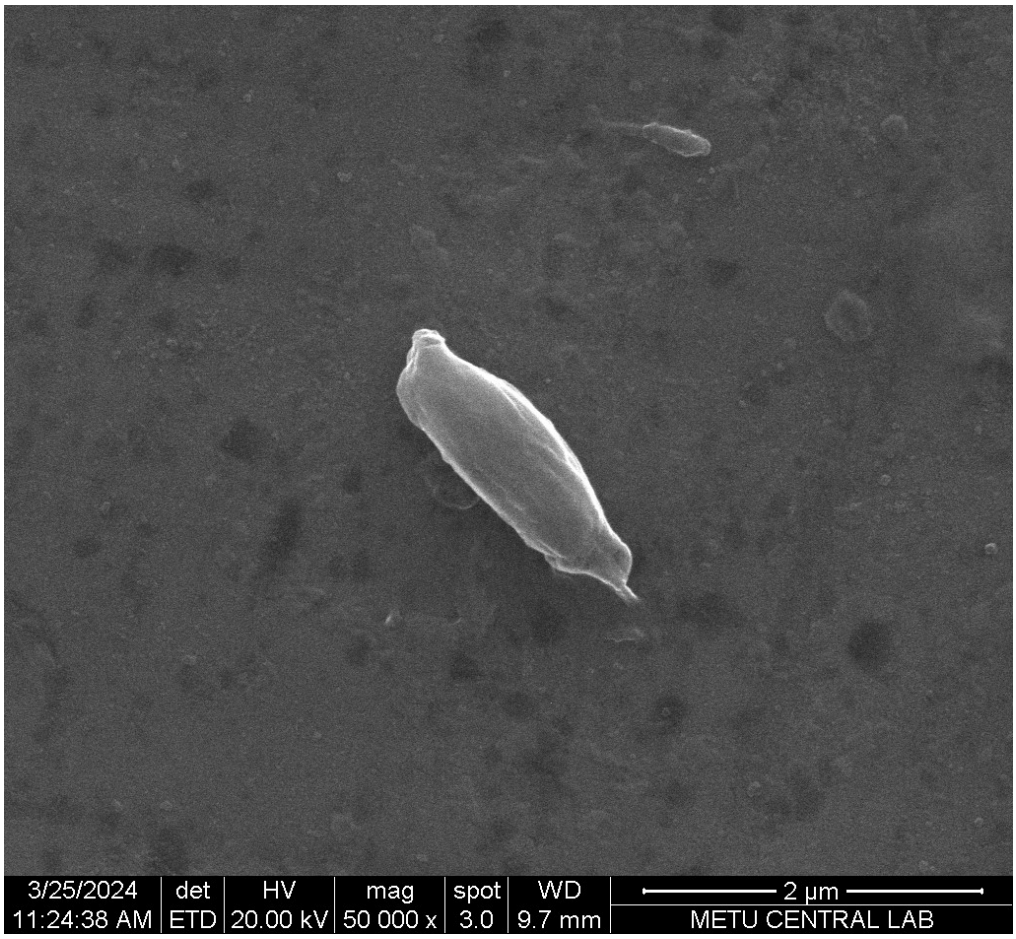

Figure D.37. FESEM image of *Mycobacterium chimaera* which is taken from the 100 nm DLC coated sample

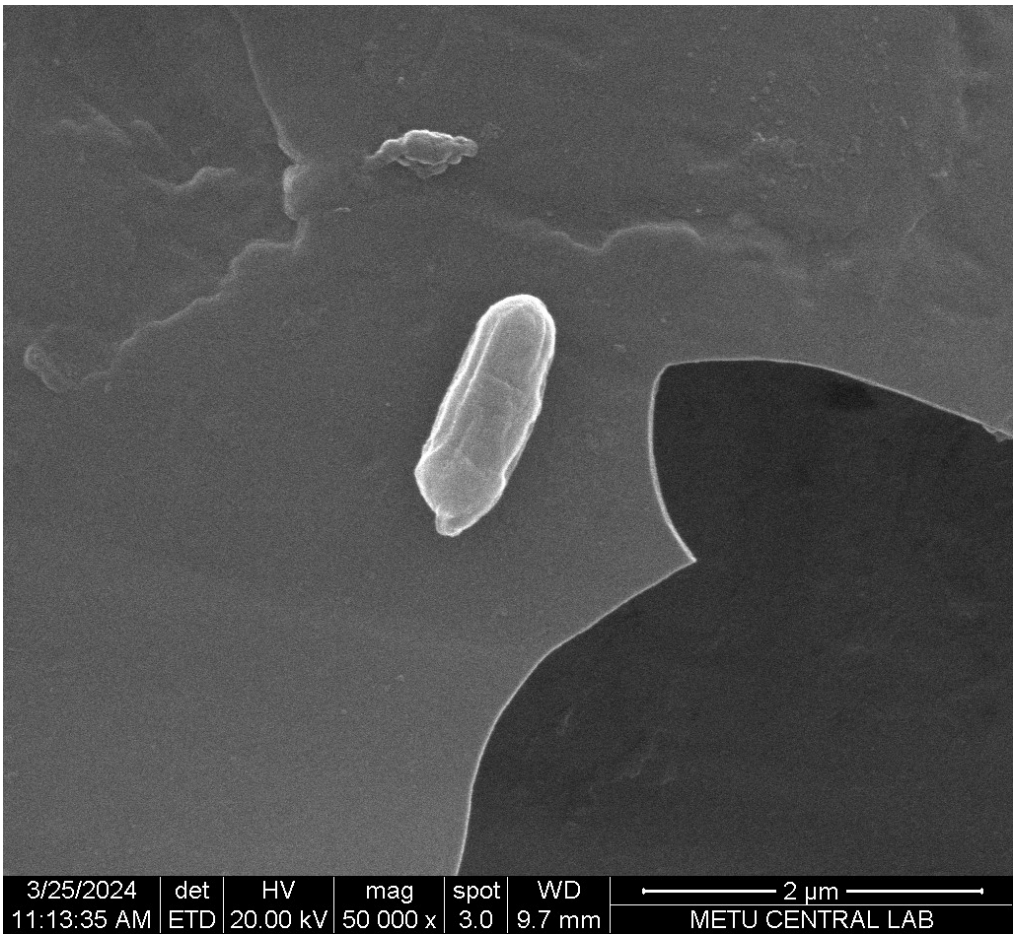

Figure D.38. FESEM image of *Mycobacterium chimaera* which is taken from the 100 nm DLC coated sample

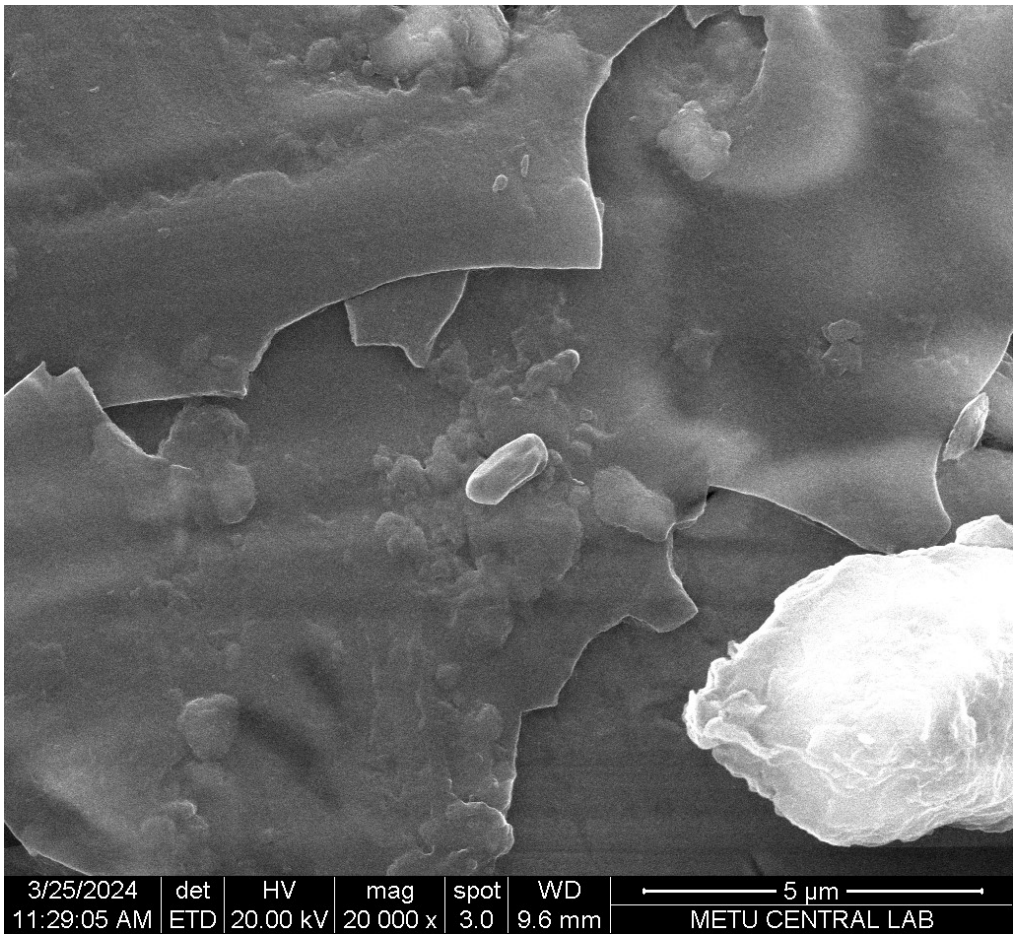

Figure D.39. FESEM image of *Mycobacterium chimaera* which is taken from the 200 nm DLC coated sample

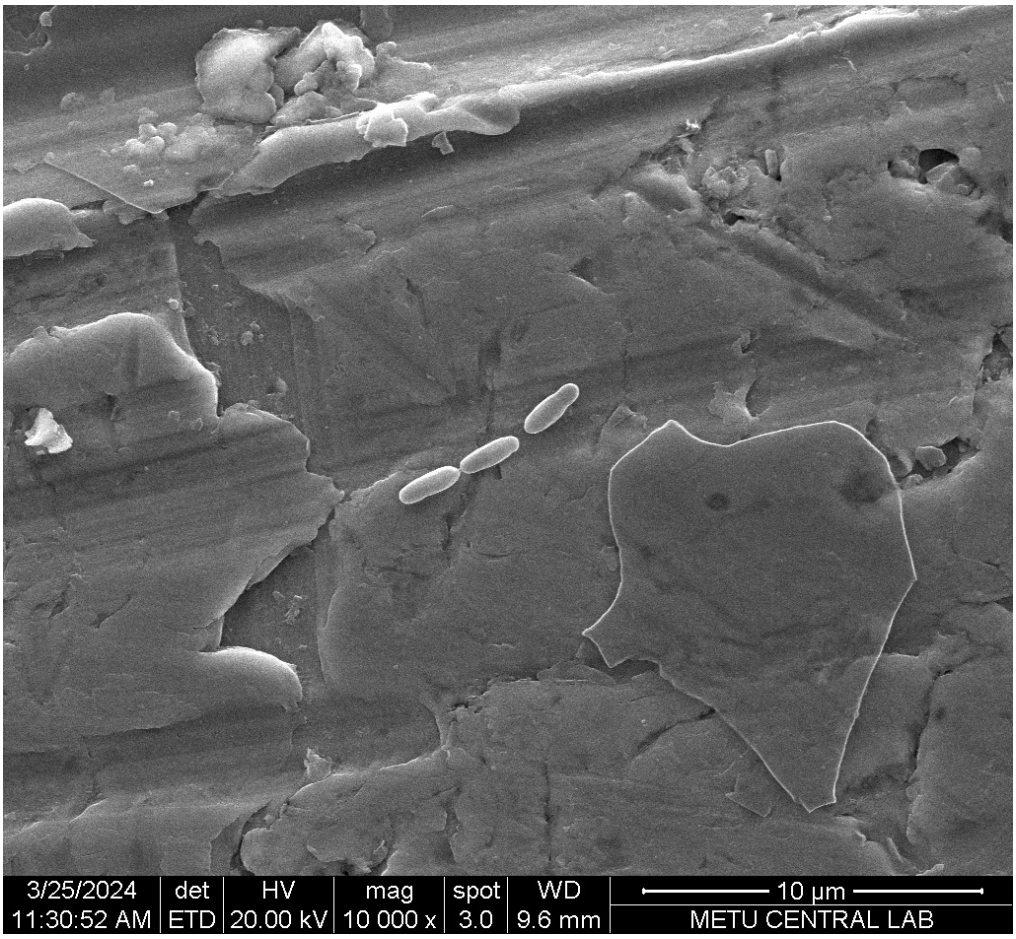

Figure D.40. FESEM image of *Mycobacterium chimaera* which is taken from the 200 nm DLC coated sample

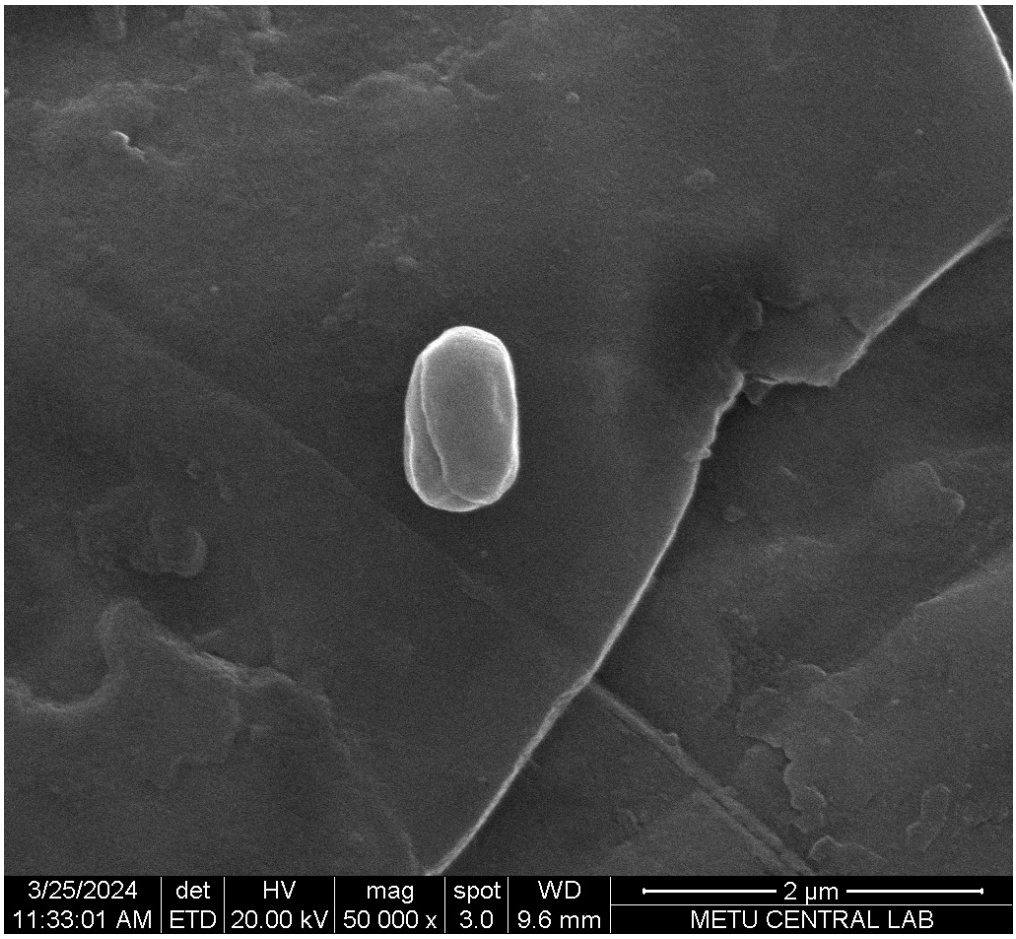

Figure D.41. FESEM image of *Mycobacterium chimaera* which is taken from the 200 nm DLC coated sample

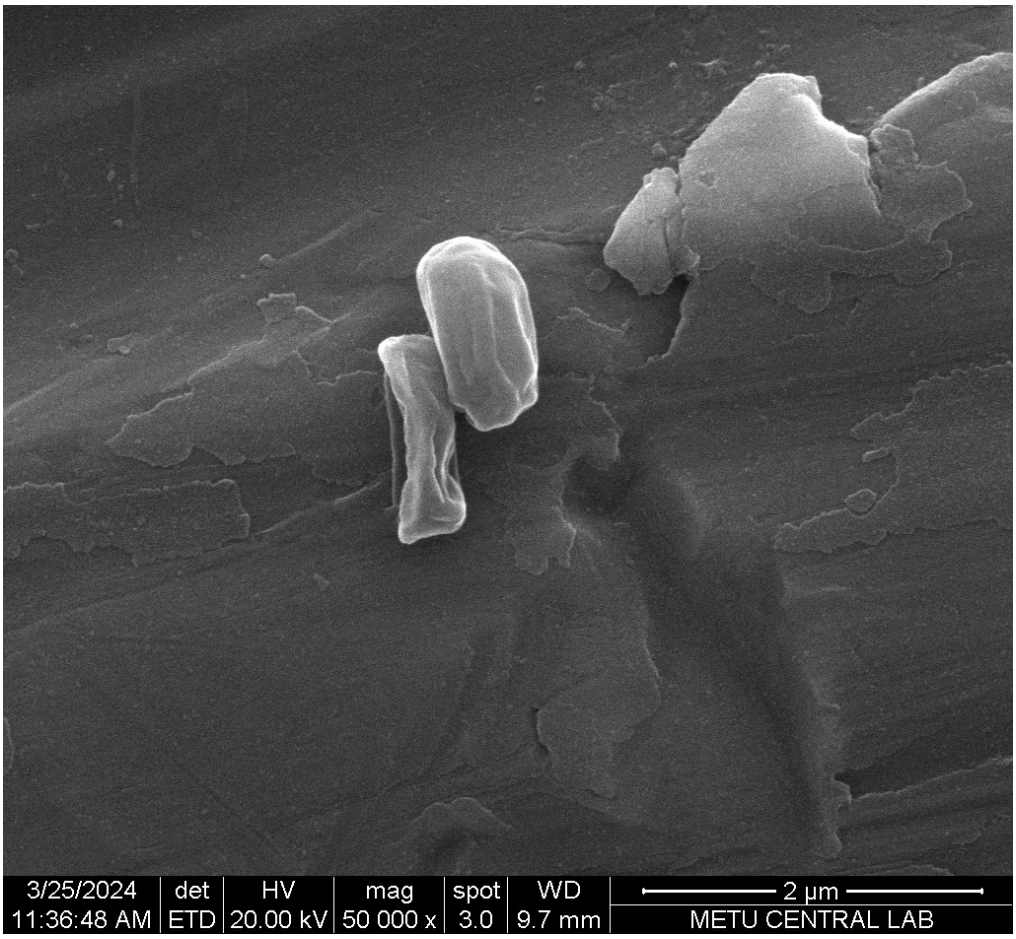

Figure D.42. FESEM image of *Mycobacterium chimaera* which is taken from the 200 nm DLC coated sample

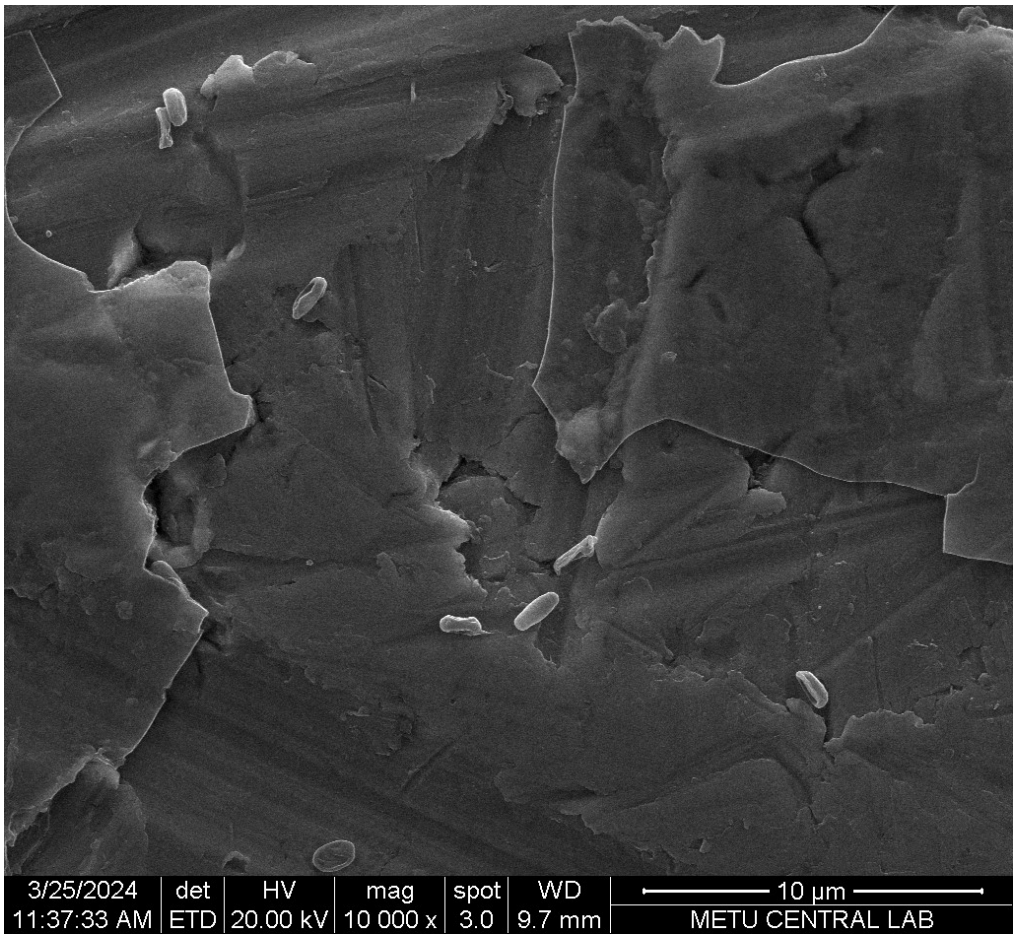

Figure D.43. FESEM image of *Mycobacterium chimaera* which is taken from the 200 nm DLC coated sample

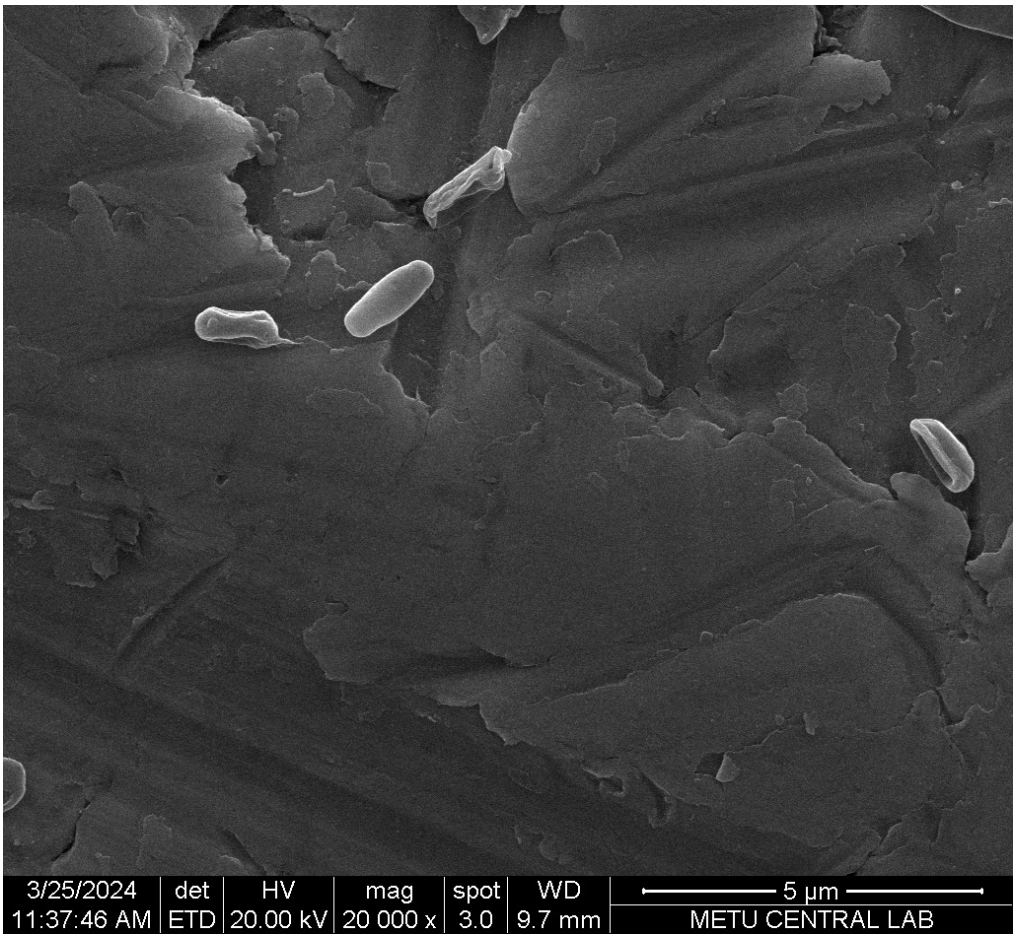

Figure D.44. FESEM image of *Mycobacterium chimaera* which is taken from the 200 nm DLC coated sample

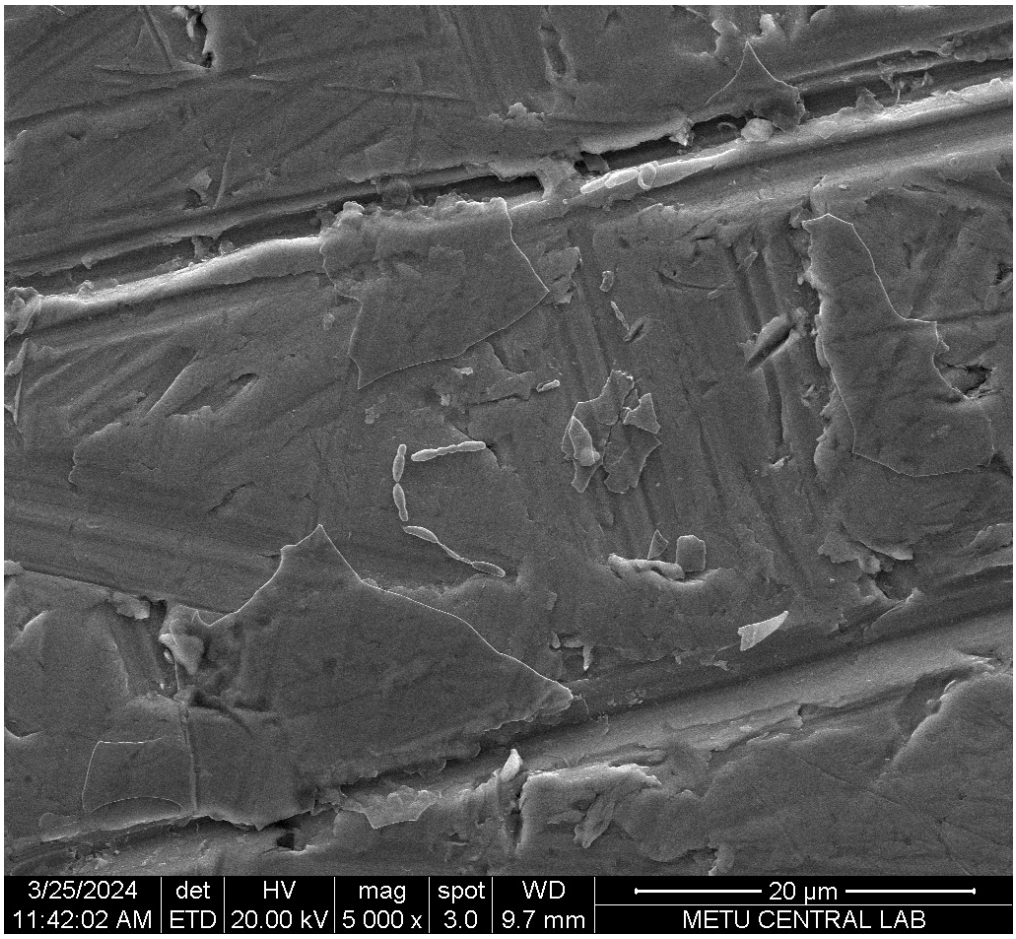

Figure D.45. FESEM image of *Mycobacterium chimaera* which is taken from the 200 nm DLC coated sample

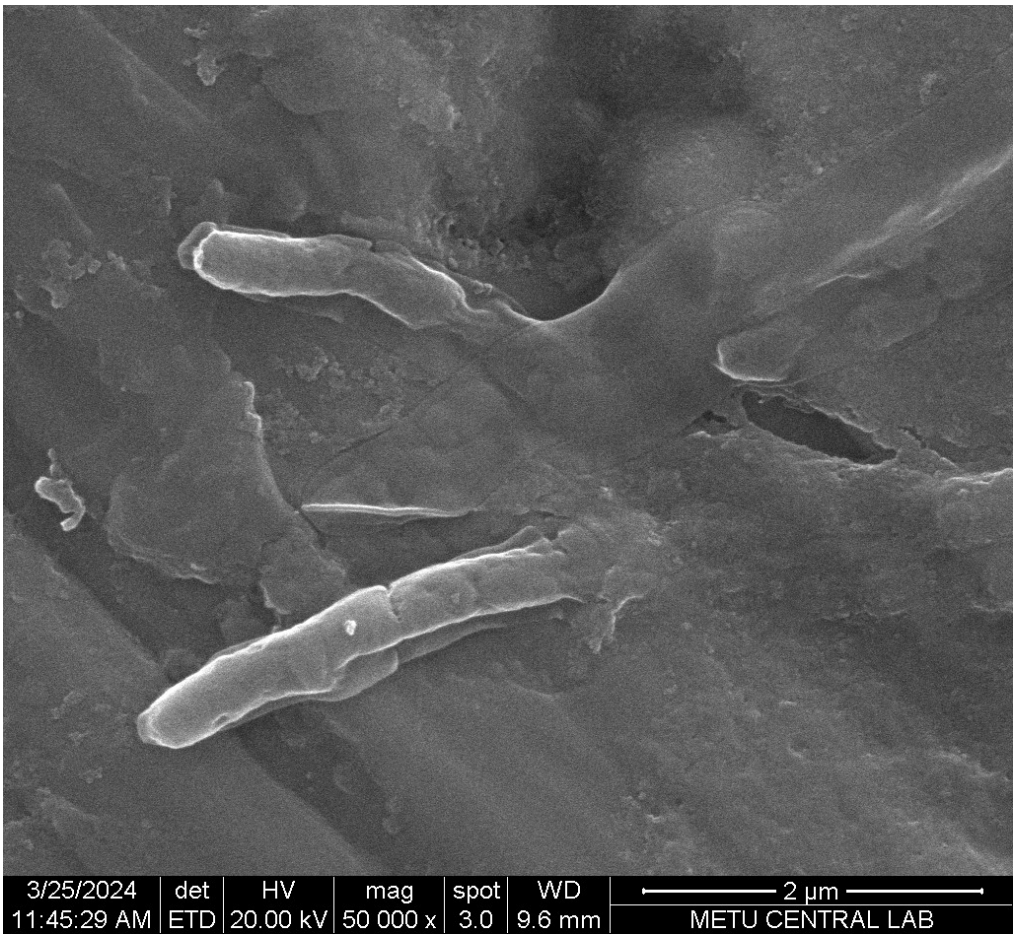

Figure D.46. FESEM image of *Mycobacterium chimaera* which is taken from the 200 nm DLC coated sample

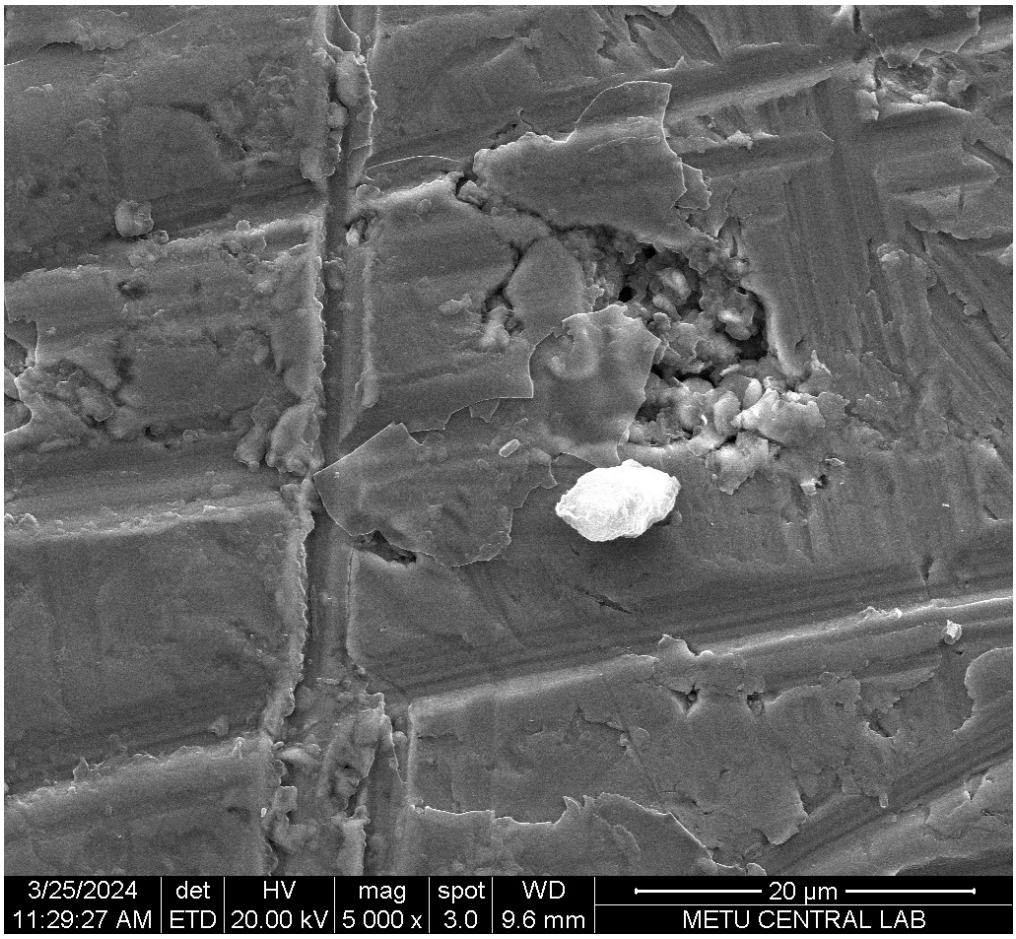

Figure D.47. FESEM image of *Mycobacterium chimaera* which is taken from the 200 nm DLC coated sample

CURRICULUM VITAE

Surname, Name: Taburoğlu, Vahit Eren

EDUCATION

Degree	Institution	Year of Graduation
MS	METU Micro and Nanotechnology	2017
BS	METU Mechanical Engineering	2005
High School	Kırşehir Lisesi, Kırşehir	1998

FOREIGN LANGUAGES

Advanced English

PUBLICATIONS

1. Taburoğlu V.E. “Characterization and Enhancement of IR Optical and Tribological Properties of DLC Films Synthesized by RF-PECVD”, MRS Conference Bulletin-Boston/USA, (2017)